NANOMECHANICS SCIENCE AND TECHNOLOGY
An International Journal

VOLUME 1 / ISSUE 1 2010

International Journal of Nanomechanics. Science and Technology 1(1), 1–29 (2010)

QUANTUM-MECHANICAL STUDIES OF DEFORMATION OF CARBON NANOTUBES

Yu. G. Yanovsky,[1] E. A. Nikitina,[1] S. M. Nikitin,[2] & Yu. N. Karnet[1]*

[1]*Institute of Applied Mechanics, Russian Academy of Sciences, Moscow*

[2]*Peoples' Friendship University of Russia, Moscow, Russia*

Address all correspondence to Yu. N. Karnet E-mail: iam@ipsun.ras.ru

The microscopic mechanisms and characteristics of deformation and destruction in uniaxial tension of carbon nanotubes (CNT) of different diameters and chirality have been investigated within the framework of the quantum-mechanical approach. CNTs with the "armchair" (4, 4) and (5, 5) and "zigzag" (8, 0) configurations were considered under different conditions of loading. The results of calculation of the Young modulus have shown that CNTs with a larger diameter have a higher strength (E = 1.2 TPa) than CNTs with a smaller diameter (E = 0.76 TPa). CNTs with the "armchair" configuration are stronger (E = 1.2 TPa) than CNTs with the "zigzag" configuration (E = 0.825 TPa). Thus, a computer experiment has shown both qualitative and quantitative agreement with the experimental data known from the literature and with the available theoretical calculations.

KEY WORDS: *quantum-mechanical calculations, carbon nanotubes, structure, mechanical properties, moduli, strength*

1. INTRODUCTION

Since their discovery and obtaining, carbon nanotubes (CNT) have aroused considerable interest in scientific circles. CNTs are distinguished by a special regular atomic structure that makes them different from isotropic materials. An uncommon combination of linear dimensions, specific weight, deformation and strength characteristics is inherent in CNT, therefore they have found a wide utility in engineering and medicine.

1947-5748/10/35.00

Recently, the microstructure and mechanical properties of carbon nanotubes have become the object of comprehensive scientific studies; however, direct natural experiments require huge material and time expenditures, since high-precision, rare, and expensive equipment is used. By virtue of difficulties in conducting the experiments and inapplicability of general analytical approaches of continuum to the analysis of the mechanical behavior of nanotubes, their characteristics and special features of the microscopic mechanism of deformation have been studied inadequately.

Under these conditions, computational approaches that allow virtual investigation of the microscopic structure, properties, and mechanical behavior of carbon nanotubes, depending on the atomic structure, as well as consideration of the microscopic mechanisms of their deformation and destruction have acquired great significance. Theoretical and numerical simulation become an alternative method of study that makes it possible to solve new problems and conduct computational investigations, thus leaving behind natural experiments.

Most of computational methods known from the literature and presently used in the mechanics of carbon nanotubes are based on the approaches where a solid body is treated as a continuum. A stress-strain state is modeled, in particular, by the finite element methods with a step-by-step integration where the integration step is not related to the molecular structure of the material. To solve the corresponding equations one has to introduce many parameters that take into account a chemical nature of nanotubes. However, it is seen proceeding from the nature of any substance that there exists a natural limit of its numerical division into small components. Atoms that constitute this substance and carry information on its chemical properties make such a limit. By virtue of this, it is quite natural to consider microscopic mechanical characteristics of carbon nanotubes with account for their microscopic structure. An approach in which an atomic structure of nanoobjects makes explicitly one of the first principles is represented by quantum-mechanical modeling within the framework of which the studies of the present work have been conducted.

A combination of nanoscopic and macroscopic approaches is a specific feature of the present theoretical modeling. A spatial structure of nanotubes, their energy and force of deformation were calculated at the nanoscopic level within the framework of quantum-mechanical approximation. In this case, deformations and destructions were described as mechanical-chemical responses where the forces of deformation were calculated as energy gradients along these coordinates. Then, using these forces, the characteristics of deformation and destruction of nanotubes were calculated within the framework of the macroscopic approach on the basis of the relationships of the linear elasticity theory. Although here the forces of deformation clearly have a nanoscopic

character, this approach has acquired a good reputation in studying a wide range of nanoobjects [1–5].

In the present work, microscopic mechanisms and characteristics of deformation and destruction in uniaxial deformation of carbon nanotubes of different diameters and chirality were investigated. CNTs with the "armchair" (4, 4) and (5, 5) and "zigzag" (8, 0) configurations were considered under different conditions of loading. Calculations were conducted within the framework of the software NDDO/sp-spd within which calculations by the semi-empirical method NDDO with the AM1 parametrization in cluster approximation were realized. A specific feature of this modeling of deformation and destruction of molecular systems where the rupture of interatomic bonds occurs is the use of the unrestricted Hartree–Fock (UHF) method. The following deformation and strength characteristics have been calculated: dependence of force and energy of deformation on elongation of a nanotube; dependence of mechanical stress on relative deformation; deformation work and energy of the rupture of bonds; the elasticity (Young) modulus and the coefficient of rigidity; critical force, stress, and relative deformation in destruction (strength characteristics).

2. GENERAL INFORMATION ON CARBON NANOTUBES

2.1 Discovery of Carbon Nanotubes and Special Features of Their Chemical Structure

In 1991, a Japanese scientist Iijima was the first to discover nanotubes in an electronic microscope [6]. This discovery marked the beginning of a new trend in carbon studies. Nanotubes formed on carbon electrodes in an electric discharge in helium at a high pressure and a temperature of 3000^{o}C. The achievements in the technology of synthesis allow one to obtain rather uniform nanotubes in an amount of grams. With a diameter of about a nanometer a length of the obtained nanotubes reaches 1 μm and more. Figure 1 gives the exterior view of a carbon nanotube.

An ideal nanotube is a cylinder obtained in rolling-up of a plane hexagonal lattice of graphite (graphene plane) without seams. All atoms of carbon in carbon nanotubes have sp^2 hybridization (see Fig. 2), i.e., one *s* orbital and two *p* orbitals of the peripheral electronic level hybridize thus giving three sp^2 orbitals that lie in the same plane at an angle of 120o and form σ-bonds with neighboring atoms of carbon. Thus, graphene sheets from which carbon nanotubes are formed are plane. Nonhybridized *p*-orbitals are perpendicular to this plane and are overlapped pairwise forming a single electron cloud that unites hexamerous (benzene) cycles that are the

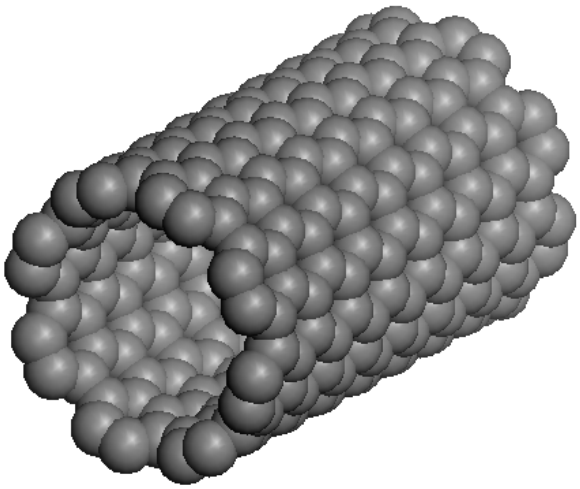

FIG. 1: An exterior view of a carbon nanotube

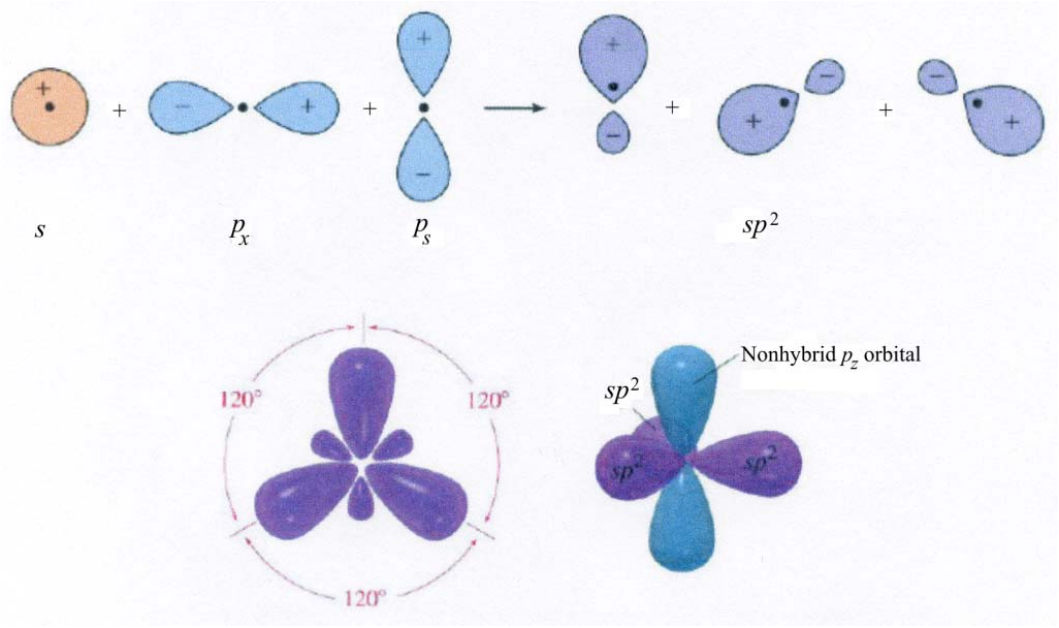

FIG. 2: Schematic of formation of sp^2 hybridization of carbon atoms

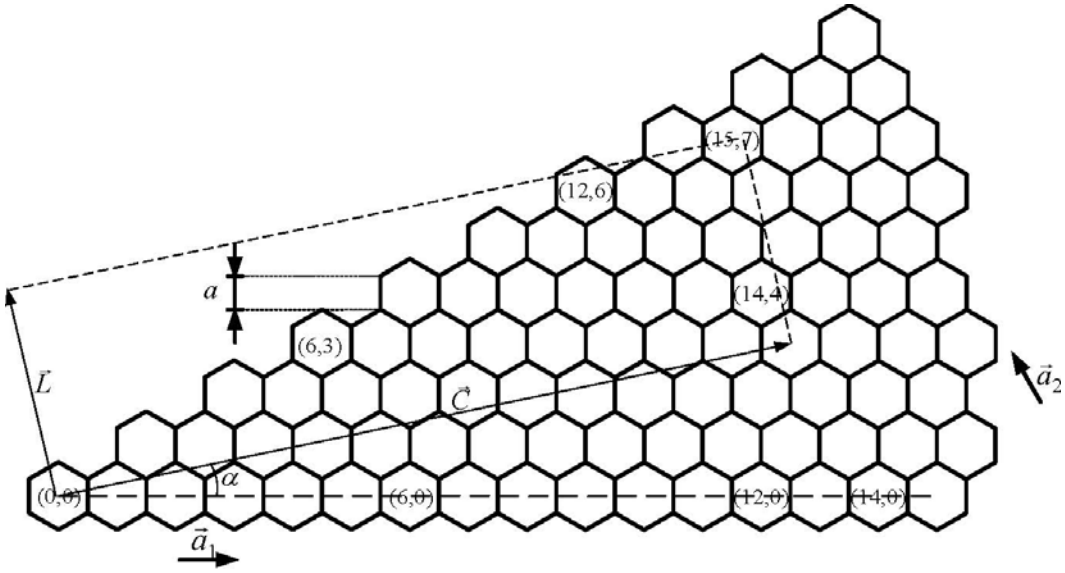

FIG. 3: Schematic of rolling-up of a hexagonal graphene grid in formation of single-wall nanotubes with different chirality

structural basis of nanotubes. Such a system possesses high stability and is called an aromatic electronic system. Thus, free electrons of a hexagonal plane produce a nonzero density of electron clouds on both sides of the plane. This is a π-electronic plane.

Mutual orientation of the hexagonal lattice of graphite and the longitudinal axis of a nanotube determines a very important structural characteristic of a nanotube, which has come to be known as chirality.

Chirality is characterized by two integer numbers (*m*, *n*) that indicate the position of that hexagon of the lattice, which, as a result of rolling-up, must coincide with the hexagon lying in the origin of coordinates. The said above is illustrated in Fig. 3 that shows a part of the hexagonal graphene grid the rolling-up of which to a cylinder leads to formation of single-wall nanotubes with different chirality. Nanotube chirality also can be uniquely determined by an angle α formed by the direction of nanotube rolling-up and the direction where the neighboring hexagons have a common side. Two indices of chirality, *m* and *n*, and a nanotube length (in units of length of interatomic distances) fully determine an ideal nanotube.

Chirality may affect the degree of anisotropy of physical and mechanical properties of a nanotube. By a value of the parameters (n, m) we distinguish direct (achiral) nanotubes of the "armchair" ($n = m$) and "zigzag" ($m = 0$ or $n = 0$) configurations and spiral (chiral) nanotubes.

With mirror reflection a nanotube (n, m) changes over to a nanotube (m, n), therefore a tube of a general form is mirror asymmetric. Direct nanotubes either change over to themselves in mirror reflection ("armchair" configuration) or change over to themselves with an accuracy of a turn.

Depending on the chirality, nanotubes can possess both metallic conduction and semiconductor properties. Metallic nanotubes conduct electric current at absolute zero whereas conductivity of semiconductor tubes is zero at absolute zero and increases with the temperature. Semiconductor properties manifest themselves in a tube due to a slit at the Fermi level. The tube is metallic if (n–m) being divided by 3 gives an integer number. In particular, all tubes of the "armchair" type are metallic.

Carbon nanotubes can be single-wall and multiwall. Multiwall nanotubes consist of concentric graphite cylinders with both ends closed. End roundings possess, in addition to hexagons, a finite number of pentagons. Similar to graphite, the layers in such a nanotube are spaced by a distance of 0.34 nm (for nanotubes with a diameter smaller than 10 nm this distance increases, e.g., it is 0.39 nm for a diameter of about 2 nm).

According to the estimation made, the world-longest cable, 42,000 km — the distance from the space station to the Earth, can be made from a nanotube not producing high load at the expenses of its own weight and length.

2.2 Application of Carbon Nanotubes

Despite a relatively recent discovery, carbon nanotubes have acquired wide application in different branches of science, technology [7], and chemistry [8]. In what follows, we list the main, currently known from the literature, trends of application of carbon nanotubes:

- mechanics: ultrastrong fibers, composites, nanoscales;
- microelectronics: transistors, nanowires, transparent conducting surfaces, fuel elements;
- biology: connections between biological neurons and electronic devices in the up-to-the-minute neurocomputer developments;
- physics: capsules for active molecules, storage of metals and gases, nanopipettes;
- optics: displays, light-emitting diodes (LED);

– space technologies: cables for a space elevator;
– medicine: at the stage of active development;
– different engineering applications: single-wall nanotubes (individual, in small assemblies or networks) are miniature sensors for detection of molecules in the gaseous medium or in solutions with ultra-high sensitivity (electric resistance of a nanotube in adsorption of molecules on its surface and characteristics of a nanotransistor may change); such nanosensors can be used in monitoring of the environment and for military, medicine, and biotechnological purposes, and others.

Thus, we can state that unique properties of carbon nanotubes find application, e.g., in small-scale electronics — electric resistance of a nanotube can change due to deformation and nanotubes can serve as sensors of deformations or vibrations. In probe microscopy nanotubes can be used as a needle with a nanotube diameter (due to high strength and the ability to bend this needle possesses, in addition to an increased resolving power, an increased reliability). These needles are used in nanolithography.

The most important aspect of application of nanotubes, that is based on the unique mechanical properties of them, is creation of strengthened composite materials on their basis. Despite the fact that manufacture of composites with nanotubes as a filler is an obvious field of their application, a number of successive experiments reflecting the advantages of using nanotubes as a filler over ordinary carbon fibers is scanty. The main problem is in obtaining high adhesion between nanotubes and a composite matrix in order to attain good transfer of load from the matrix to nanotubes in deformation. Nanotubes are atomically smooth and have almost the same diameters and length/diameter ratios as polymer chains (the most wide-spread composite matrix). In this case, they are almost always organized in aggregate structures perceiving the load in cooperation.

To achieve a maximum effect of strengthening, the nanocomposite nanotubes should be distributed over the matrix volume. Strengthening of the composite in filling the matrix by nanotubes is achieved due to absorption of energy in increasing the flexibility and elasticity of it. (A 25% increase of tensile strength was observed in a nanocomposite with 5 wt.% of nanotubes.) Filling by nanotubes also increases the electric conductivity of the material and improves the behavior of the nanocomposite in compression loads compared with an ordinary carbon fiber.

The said above explains an increased interest to the study of mechanical properties of carbon nanotubes.

2.3 Experimental Study of Mechanical Properties of Carbon Nanotubes

Nanotubes have the highest parameters of mechanical characteristics among carbon fibers. A traditional carbon fiber is about 50-fold stronger than steel (by the strength/density ratio) and is widely used in strengthening of composites; however, development of even stronger composites based on nanotubes is undoubtedly under demand. Recent experiments on single nanotubes confirmed that they are one of most rigid materials. A covalent carbon–carbon bond is one of the strongest in nature and a regular structure of these bonds along the axis of a nanotube should provide an extremely high strength of material.

The known experimental data demonstrate almost the same deformation characteristics of carbon nanotubes, namely, the Young modulus E = 0.8–1.2 TPa (with an average value of 1.0 TPa), critical stress σ_{cr} = 100–120 GPa, critical relative deformation ε_{cr} = 0.17–0.25 [9, 10]. In this case, absolutely different experimental methods and approaches were used to obtain these data. The Young moduli of nanotubes were determined from observation of thermal oscillations in an electronic microscope. The needles of atomic power microscopes in a scanning electronic microscope were used for the same purpose. Nanotubes were studied on electronic substrates in compression by a needle of a scanning power microscope. Finally, Pan et al. [11] speak of direct measurement of the Young modulus of carbon nanotubes in tensile tests of ropes of very long aligned multiwall parallel nanotubes, though in this case they state lower moduli — from 0.2 to 0.8 TPa.

It is seen from the literature that experimental values of deformation characteristics of carbon nanotubes strongly depend on their chirality, diameter, and the number of walls and defects [10, 12].

2.4 Theoretical Investigations of Mechanical Properties of Carbon Nanotubes

According to theoretical estimates, the Young modulus of single-wall nanotubes reaches 1 TPa [13] which corresponds to the same values for graphite in the direction of base planes. We are aware of a small number of theoretical investigations where the continuum approach to the study of nanotubes was used, though it was assumed that the continuum mechanics is inapplicable to the atomic or nanometer scale. In [14], the applicability of the continuum beam theory to the description of deformation of carbon nanotubes was studied. The ranges of the parameters of nanotubes where modeling of them in the form of shells or rod is possible have been distinguished.

A number of works on investigation of the Young modulus of nanotubes, which are based on the atomic-molecular approach, are known. The main method of modeling of the behavior of nanoscopic systems is the method of molecular dynamics [15]. In this method, the values of coordinates and velocities are calculated by the algorithms of integration of the equations of motion with the specified conditions, which are based on the Werle scheme. A set of interaction potentials and their parameters that depend on the type of interacting atoms is determining in this case.

Quantum methods of molecular dynamics where different effective potentials are introduced have been developed separately. Among them are the density functional method, method and theory of pseudopotential, iterative diagonalization method, and supercell method. These methods serve for the purpose of reducing the multiparticle problem of motion of all atomic electrons in the field of ions to the problem of motion of a valence electron in the effective field of the ion core and internal electrons. Although the enumerated quantum methods allow investigation of a number of properties of nanoobjects, they are rather resource consuming and complex in realization. By virtue of this, semiempirical quantum mechanical approaches which allow one, within the framework of the unrestricted Hartree–Fock method, to model deformation and rupture of rather lengthy carbon nanotubes in cluster approximation in a reasonable computation time, are especially topical.

3. METHODS OF MODELING

As the main quantum-mechanical method, within the framework of which the structure and mechanical properties of carbon nanotubes have been modeled in the present work, we took the semiempirical NDDO method with the AM1 parametrization [16]. This method is realized within the framework of an original NDDO/sp-spd package. The applied method is intended for calculation of the reference structural and energy characteristics of polyatomic nano-sized clusters in the basic electronic state. In the method used, an error in calculation of bond lengths is on the average 0.01 Å, valence angles are calculated with an accuracy of several degrees, and generation heat is calculated to better than 0.5–1.0 kcal/mol [16]. These values have the same order of magnitude as typical errors in the data obtained experimentally. Thus, the method applied represents experimental geometric and energy characteristics of molecular systems rather well, it is highly competitive with nonempirical calculations in accuracy in considering geometric and energy characteristics, and greatly benefits from the rate of calculation.

The computational experiment was conducted in cluster approximation [17] where carbon nanotubes were modeled by clusters of a rather large size (with a length of several tens of nanometers and up to a hundred of atoms).

3.1 Package of Programs CLUSTER-Z1

The package of programs NDDO/sp-spd provides fulfillment of semiempirical quantum-mechanical calculations in *sp*- and *spd*-bases of structural, electronic, energy, deformation, spectroscopic characteristics of atomic-molecular systems up to 999 atoms. In this case, different semiempirical methods are realized. These methods are conceptually most close to *ab initio* methods and are somewhat exceeded by them in accuracy of calculations; however, they are superior to the above methods in the time of calculation and possible dimensions of the considered molecular systems. Such methods are based on the NDDO (Neglect of Diatomic Differential Overlap) approximation. Semiempirical methods and the corresponding programs MNDO, AM1, and PM3 are realized in the present package. These methods are intended for calculation of polyatomic systems in the *sp*-basis. The necessity to expand quantum-mechanical calculations by including the *spd*-basis has caused substantial modification of the above-mentioned methods in the form of the NDDO-BM methods that is well parametrized and theoretically substantiated especially for calculation of large molecular systems in the *spd*-basis. The method of weighting factors (MWF) that is also realized in the program is based on introduction of weighting factors that scale the integrals of Coulomb scattering into calculation. These weighting factors are the parameters of the MWF; they substitute one-centered integrals that are the parameters of the AM1 and PM3 methods. The developed program of MWF parametrization gave the parameters of the required set of atoms that allow consideration of problems with accuracy approaching to the accuracy of nonempirical computation techniques.

The use of the improved optimization methods, e.g., Fletcher algorithm (VA09A), Broyden, Fletcher, Goldstein, and Shanno (BFGS) algorithm, the modified Newton–Raphson (NRAF) algorithm, that are applicable to both exact localization of minimum and determination of the saddle point in studying the response coordinate, makes it possible to greatly reduce the expenditures for calculation (time and computer) and to calculate complex-composition molecular systems including up to a thousand of atoms, i.e., to several tens of nanometers, with complete optimization of a spatial structure in a reasonable time.

The program complex NDDO/sp-spd includes the possibility of calculation of the ground state of a molecular system by the restricted Hartree–Fock (RHF) and unre-

stricted Hartree–Fock (UFH) methods suitable for molecular systems of closed and open electron shells. In doing so, the package of programs allows optimization of the spatial structure of molecular systems; calculation of heats of formation, dipole moments, ionization potentials, polarizability of molecules, quadrupole moments, distribution of charges by atoms, distribution of electron density, electrostatic potentials of molecules, Vaiberg indices that characterize the degree of cohesion of atoms, and frequencies of harmonic oscillations of atoms; oscillation analysis in a harmonic approximation; and calculation of the position and intensity of IR and Raman scattering bands and the response coordinate. The package of programs envisages calculation of molecular systems in an electrostatic field, both linear and produced by a system of point charges. Moreover, using the method of mechanical-chemical coordinate of deformation that is realized in the package of programs in the form of internal (microscopic compression-tension) and outer (microscopic friction) modes, it is possible to calculate microscopic deformation and strength characteristics of molecular systems.

3.2 Approximation of Mechanical-Chemical Coordinate of Deformation

To model restructuring of carbon nanotubes with an increase in deformation and to analyze microscopic characteristics of deformation of molecular systems, the computational experiment is built, by analogy with natural mechanical tests, in the mode of active loading. However, in such experiments an active load is applied to the specimen (deformation force and pressure are set) and then the change in the shape is analyzed and elongation of the specimen is determined. In the computer experiment, by virtue of the specifics of modeling, initially elongations of a molecular system are specified step-by-step and the deformation force is calculated.

In what follows we give the description of the scheme of the computational experiment. First, a microscopic model of a molecular system is constructed and quantum-mechanical minimization of it is performed. Then, a mechanical-chemical coordinate of deformation (MCD), a change of which allows description of the required sequence of deformation states, is selected. The microscopic coordinate of deformation is specified by two groups of atoms determining the planes of application of the "deforming" force, direction, and type of deformation. The computational experiment consists in consistent step-by-step deformation of a molecular system from the stable initial state to rupture of bonds and destruction along MCD. Complete optimization of the spatial structure of a molecular system is performed at each step of quantum-chemical calculation. The atoms determining MCD are excluded from the

optimization process. The deformation force F_i obtained for the i-th MCD is determined as the gradient of the total energy of the system along this coordinate.

3.3 Calculation of Deformation and Rapture of Bonds in Open Shells

The main state of a carbon nanotube is a singlet one, which seemingly should lead to the use of ordinary quantum-chemical schemes of calculation based on approximation of closed shells. However, due to the presence of weakly interacting redundant electrons in a nanotube, in calculating the state of a nanotube one should take into account spins of electrons as a result of which electronic properties must be calculated in approximation of open shells. The term "redundant electrons" is introduced to emphasize the fact that a number of valence electrons of each of the carbon atoms of a nanotube exceed by unity a number of atoms attached to it. Moreover, it is expedient to model rupture of valence bonds, which, in the general case, can be both homolythic (leads to formation of ions) and heterolythic, within the framework of the method of open shells. As a consequence, the unrestricted Hartree–Fock (UFH) method is used in practice.

3.4 Calculation of Deformation and Strength Characteristics

The energies (or heat of system formation ΔH) and forces F_i that are obtained in nanoscopic quantum-mechanical calculation are used for calculation of the characteristics of deformation, strength, and destruction of carbon tubes. To do this, a traditional macroscopic approach based on the relationships of the linear elasticity theory is used.

In this case, such quantities as the total force of deformation of a molecular system $F = \Sigma F_i$, initial length of a nanotube L_0, nanotube diameter D, pitch of elongation δL, nanotube elongation $\Delta L = L - L_0$ (in particular, critical elongation $\Delta L_{cr} = L_{cr} - L_0$, i.e., elongation of a nanotube in rupture of bonds), area of loading, i.e., the area of the nanotube "end" to which the force of deformation is applied $S = \pi hD$ (where h is the parameter that characterizes a carbon tube thickness and is usually taken equal to 0.335 nm, an experimentally measured thickness of a graphite plate [21]).

The desired deformation and strength characteristics are calculated on the basis of the Hooke law $F = \frac{ES}{L_0}\Delta L = k\Delta L$. The following quantities are calculated:

1) stress applied to the object $\sigma = \frac{F}{S} = \frac{\sum_i F_i}{S}$;

2) a relative elongation of a nanotube $\varepsilon = \frac{\Delta L}{L_0}$;

3) the Young modulus $E = \frac{F}{S}\frac{L_0}{\Delta L} = \frac{\sigma}{\varepsilon}$;

4) the coefficient of rigidity $k = \frac{S}{L_0}E$;

5) deformation work $A_{\text{rupt}} = \sum \Delta F_i \, \Delta L_i \, A$.

Moreover, rupture of bonds in a nanotube is characterized by the critical quantities: ΔH_{cr}, σ_{cr}, and ε_{cr} that are the heat of formation, stress, and deformation at a critical (maximum) value of the deformation force F_{cr}, respectively, as well as by a value of the energy of rupture of one C–C bond in a nanotube $\Delta H_{\text{b}} = \frac{\Delta H_{\text{cr}} - \Delta H_0}{N}$, where N – is number of C–C bonds in the direction of CNT deformation.

4. CALCULATION OF DEFORMATION AND DESTRUCTION OF CARBON NANOTUBES OF DIFFERENT CHIRALITY AND DIAMETER

The experimental works showed that deformation characteristics of carbon nanotubes depend on their chirality and diameter, the number of walls and defects [10, 12]. To confirm this proposition and to study microscopic mechanisms of deformation in each specific case, in the present work we took the following models: one nanotube of the "zigzag" (8, 0) configuration and two nanotubes with the "armchair" configuration with different diameters (4, 4) and (5, 5). The computational experiment was conducted in different regimes of loading for tension and compression and for different points of application of the deformation force, i.e., mechanical-chemical deformation was determined by the atoms of next to last carbon layers ("end deformation" mode) and the atoms of the neighboring, second and third, carbon layers ("neighboring deformation" mode or "deformation of valence C–C bonds").

4.1 Deformation of a (4, 4) Carbon Nanotube, "End Deformation" Mode

A cluster model of a (4, 4) nanotube comprised of 88 carbon atoms was obtained in quantum-mechanical calculation. In this case, the position of all atoms of the nanotube was optimized. Such a model of a (4, 4) nanotube had a diameter D = 5.7 Å

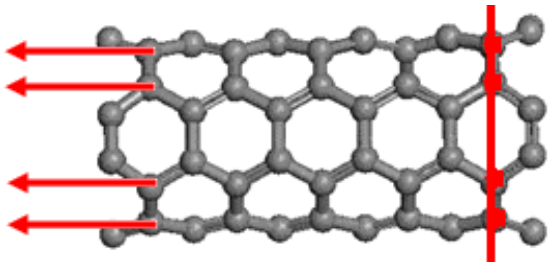

FIG. 4: An optimized structure of the cluster model of a (4, 4) nanotube and a scheme of introduction of the coordinate of mechanical-chemical deformation in the "end deformation" mode

and an initial length L_0 = 12.1 Å. Figure 4 gives an optimized structure of this model and the scheme of introduction of the coordinate of mechanical-chemical deformation (MCD) for it in the "end deformation" mode.

For quantum-mechanical calculation of deformation forces and successive calculation of deformation characteristics, atoms of the first and second layers were fixed (their coordinates were excluded from the process of optimization). The position of the atoms of the last but one layer in space was determined in terms of the atoms of the first and second layers in internal coordinates. Thus, rather long mechanical-chemical coordinates of deformation were obtained. The lengths of these coordinates were increased with a step of 0.1 Å, i.e., the atoms of the last but one layer step-by-step moved away from the atoms of the second layer. The positions in space of the atoms of all other layers were optimized completely. At each step of deformation the energy of the system and the forces of deformation of all bonds between the atoms of the second and last but one layers F_i were calculated as gradients of the total energy of the system by the selected coordinates of deformation. The total force of deformation of the molecular system is calculated as $F = \sum F_i$.

Figure 5 presents several deformed structures of tubes and the corresponding elongation of MCD. The last structure corresponds to the rupture of bonds in a tube.

It is seen that in deformation a tube becomes flat and longer. The final rupture of the tube corresponds to a maximum of deformation forces F_{cr}. On rupture a tube is divided into two parts: in our case, into a carbene chain and a shortened part of the tube where the distances between the atoms are normalized. Figure 6 shows side views of the both sides of the tube after destruction.

Based on the calculation results we constructed the dependences of the heat of system formation and deformation forces of each MCD on MCD elongation and the de-

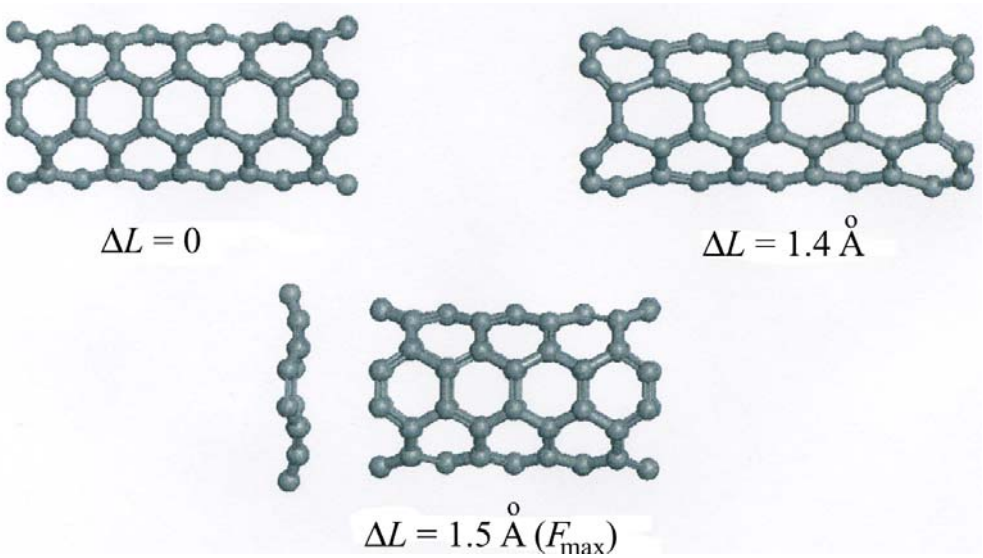

FIG. 5: Structure of a (4, 4) tube at several stages of deformation and the corresponding elongations of the coordinate of mechanical-chemical deformation

pendences of the total force of deformation and stresses on relative elongation (see Figs. 7–10.

For the molecular system under consideration, we analyzed two modes of loading — tension and compression. The corresponding curves of the dependences of the heat of formation and deformation force on elongation are presented in Fig. 11a,b. Curves 1 belong to tension whereas curves 2 — to compression. The graphs show hysteresis (i.e., the trend of the curves in both directions is not repeated) which indicates dissipation or energy release in reloadings.

Mechanical characteristics calculated for a (4, 4) tube are given in Table 1.

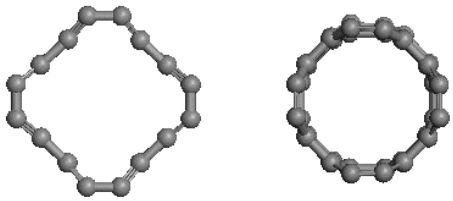

FIG. 6: Side view for a (4, 4) tube destructed at both ends

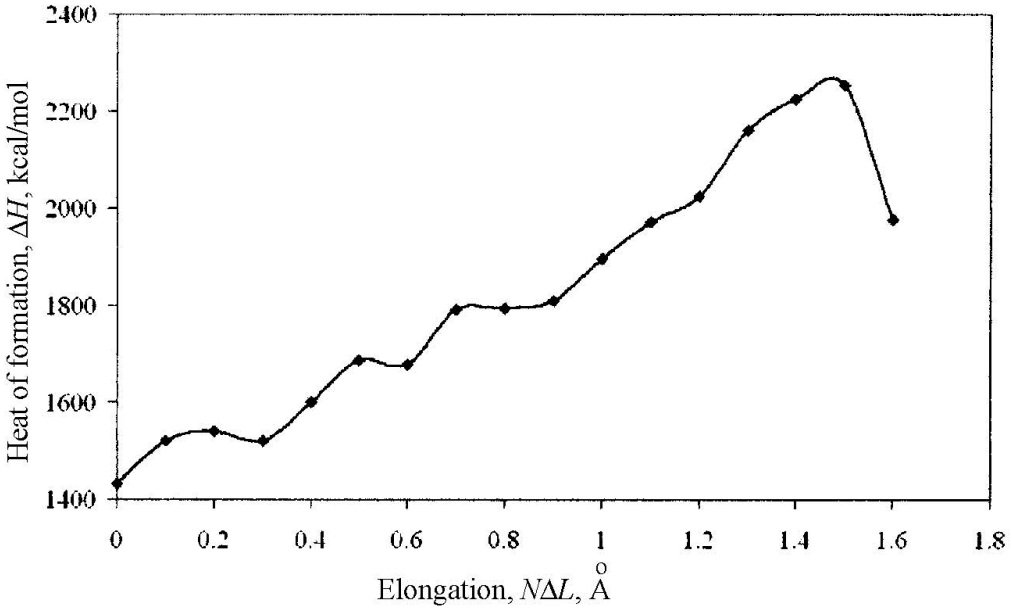

FIG. 7: Dependence of the heat of (4, 4) CNT formation on elongation

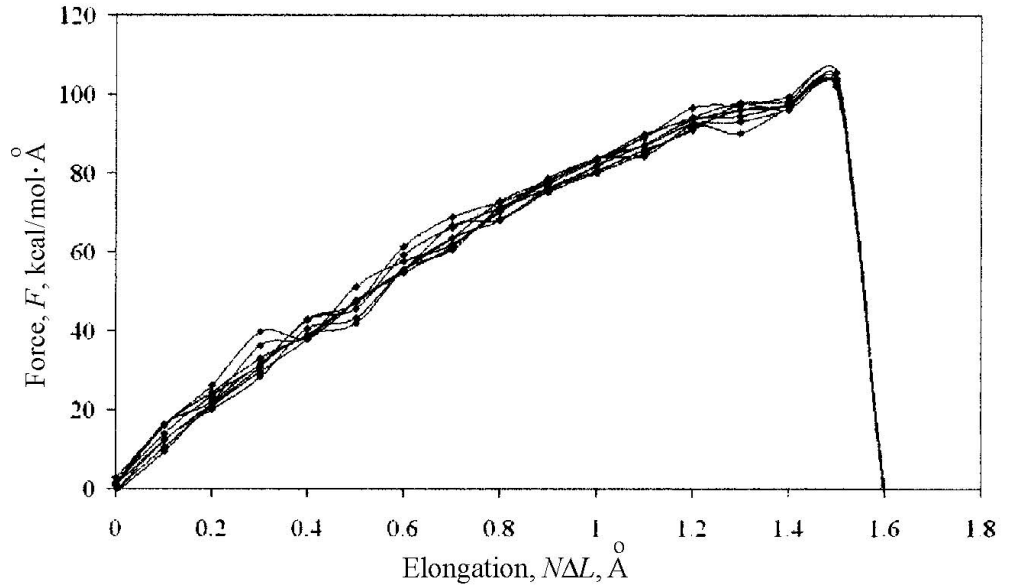

FIG. 8: Dependence of deformation forces on elongation for each coordinate of mechanical-chemical deformation for a (4, 4) CNT

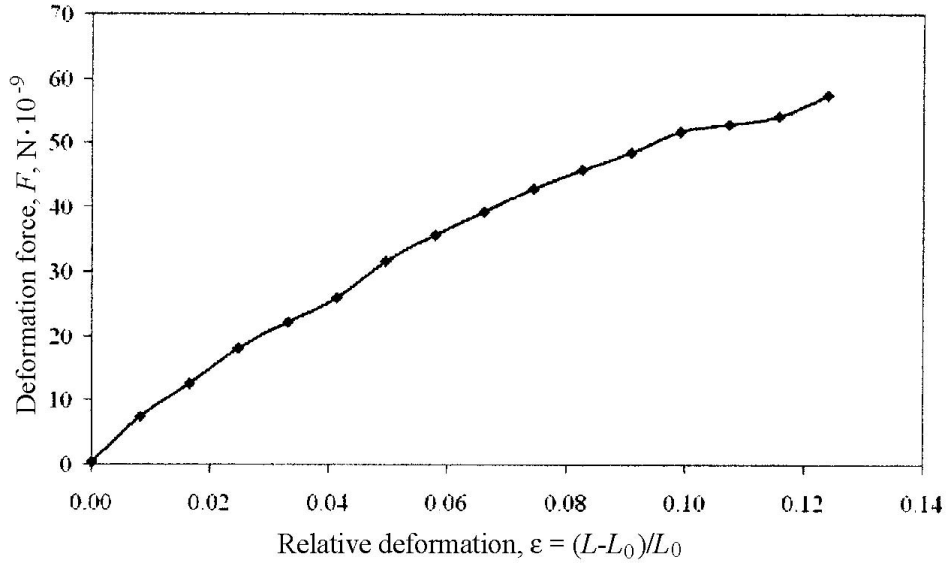

FIG. 9: Dependence of the total force of deformation on relative deformation for a (4, 4) CNT

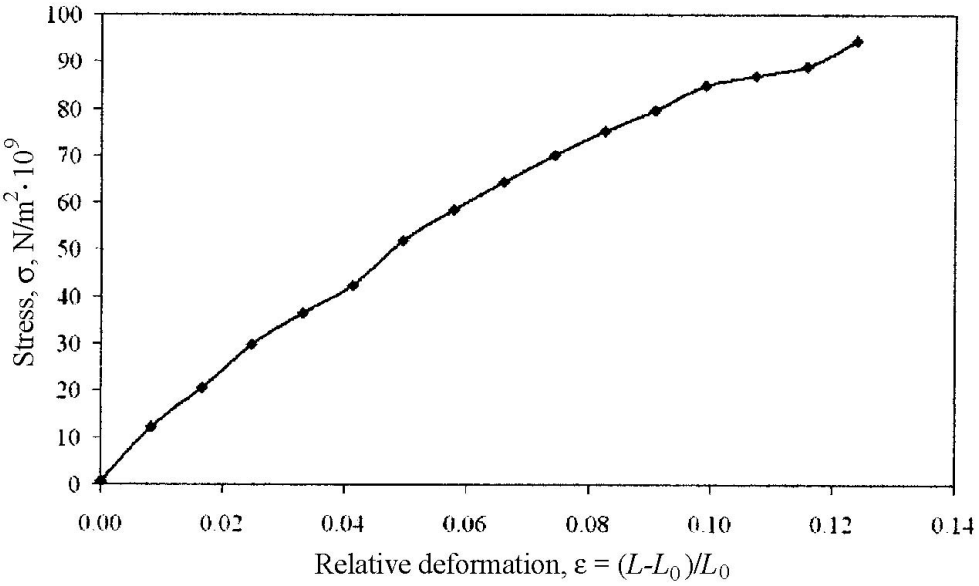

FIG. 10: Dependence of strain stress on relative deformation for a (4, 4) CNT

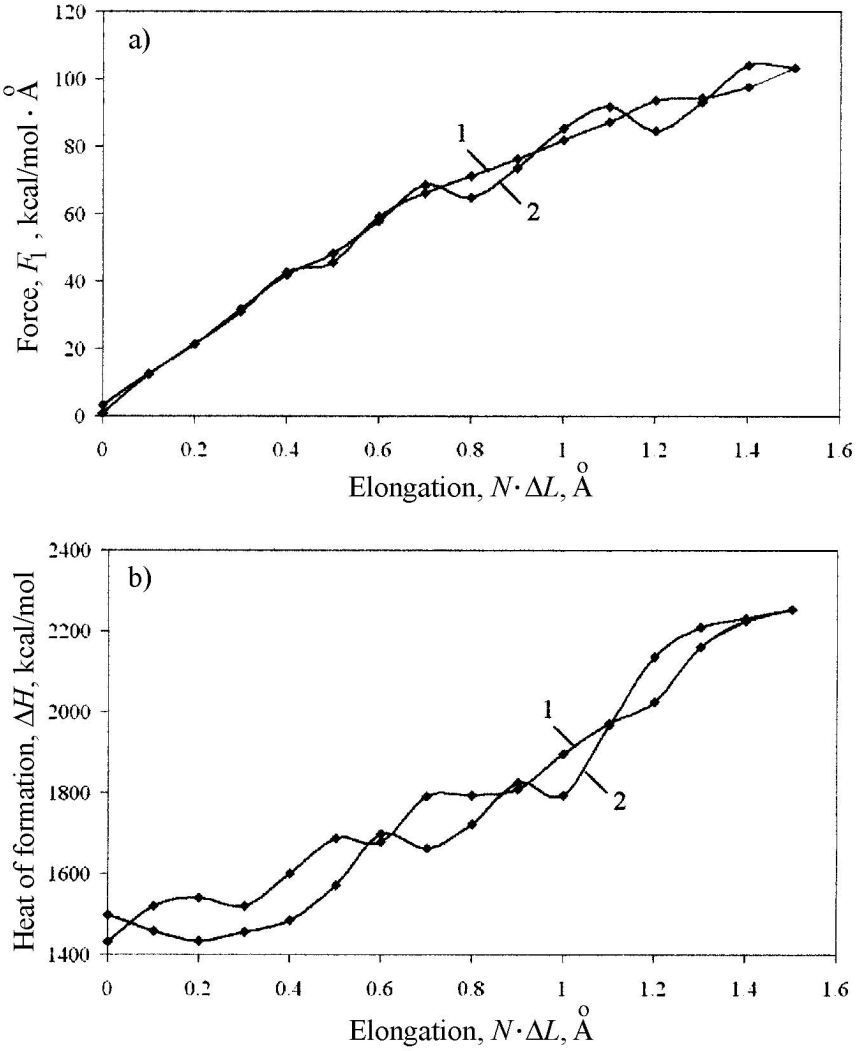

FIG. 11: Dependence of the force of deformation (a) and heat of formation (b) on elongation in tension (curves 1) and compression (curves 2) for a (4, 4) CNT

4.2 Deformation of a (4, 4) Carbon Nanotube, "Deformation of Valence C–C Bonds" Mode

To model another version of loading, we took the same (4, 4) CNT model as was discussed in the previous section. However, in this case, in order to consider deformation and rupture of valence C–C bonds in a nanotube we selected MCD in another

TABLE 1: Mechanical characteristics calculated for a (4, 4) carbon nanotube in "end deformation"

Critical relative deformation, ε_{cr}	**Critical stress, ε_{cr}, GPa·10^{-9}**	**Critical deformation force, F_{cr}, N·10^{-9}**	**Critical heat of formation, ΔH_{cr}, kJ/mol**	**Destruction work, A_{rupt}, kJ/mol**	**Energy of rupture of one bond, ΔH_b, kJ/mol**	**Young modulus, E, TPa**	**Coefficient of rigidity, K, N/m**
0.124	94.5	57.5	9433.7	3072.1	430.2	0.762	383

way. Figure 12 presents the scheme of introduction of the mechanical-chemical coordinate of deformation for the given case.

To calculate deformation characteristics, atoms of the first and second layers were fixed (their coordinates were excluded from the optimization process). The positions in space of atoms of the third row were determined in the internal coordinates via the positions of atoms of the first and second layers. The length of bonds between atoms of the first and second layers was increased by 0.1 Å at each step. Thus, atoms of the third layer step-by-step moved away from atoms of the second row. The positions in space of atoms of all the remaining layers were fully optimized. Heat of formation and deformation forces of all MCD between atoms of the second and third layers were calculated at each step of deformation. In the case described, we analyzed deformation and rupture of covalent bonds in CNT. The results of modeling for the case under consideration are given in Figs. 13 and 14 (cf. Figs. 5–10).

Table 2 summarizes all deformation and strength characteristics obtained for the given case of CNT deformation.

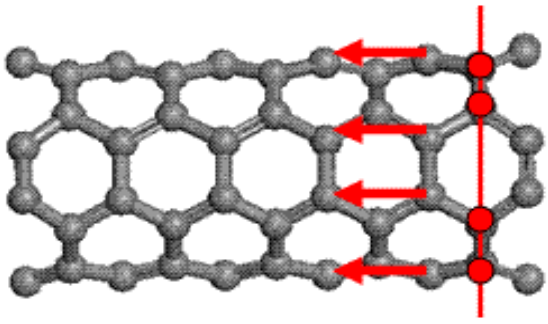

FIG. 12: Schematic of introduction of the coordinate of mechanical-chemical deformation in the "deformation of valence C–C bonds" mode for a cluster model of a (4, 4) nanotube

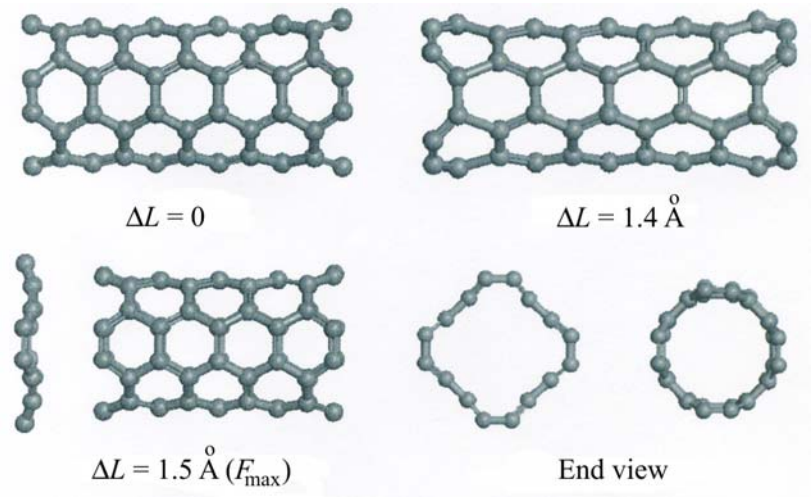

FIG. 13: Structures of clusters of a (4, 4) carbon nanotube at several stages of deformation and corresponding elongations of the coordinate of mechanical-chemical deformation

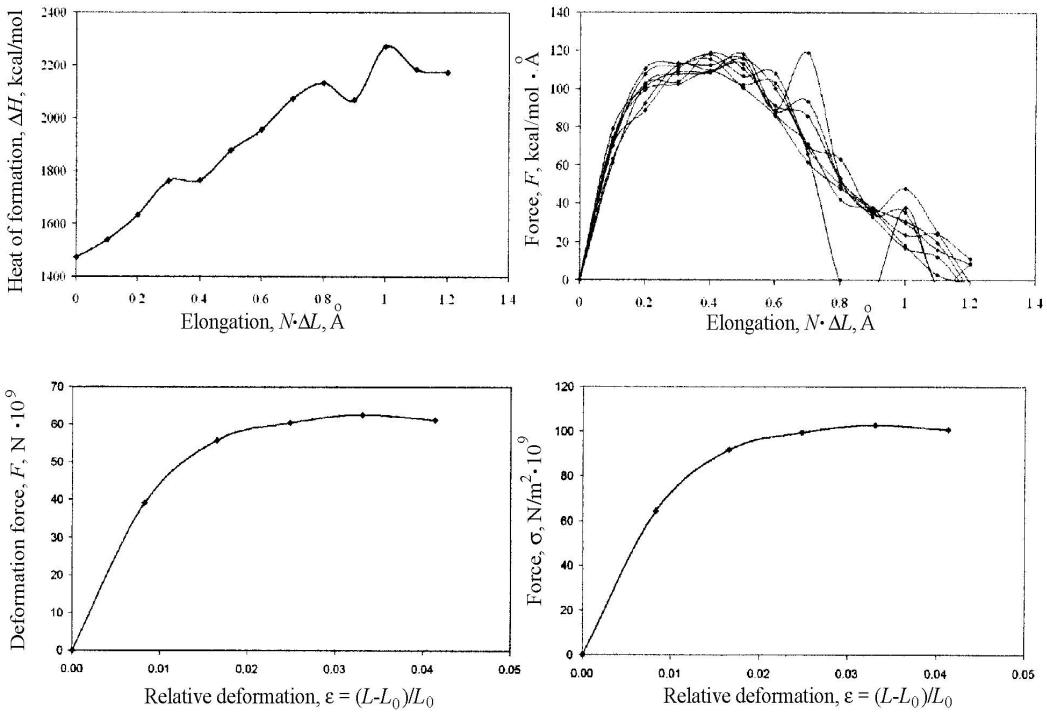

FIG. 14: Deformation characteristics of a (4, 4) CNT for the "deformation of valence C–C bonds" mode

TABLE 2: Mechanical characteristics calculated for a (4, 4) carbon nanotube in "deformation of valence C–C bonds"

Critical relative deformation, ε_{cr}	Critical stress, ε_{cr}, GPa·10^{-9}	Critical deformation force, F_{cr}, N·10^{-9}	Critical heat of formation, ΔH_{cr}, kJ/mol	Destruction work, A_{rupt}, kJ/mol	Energy of rupture of one bond, ΔH_b, kJ/mol	Young modulus, E, TPa	Coefficient of rigidity, K, N/m
0.033	102.9	62.6	7383.5	1125.0	152.5	3.113	1565.5

4.3 Deformation of a (5, 5) Carbon Nanotube, "End Deformation" Mode

The model of a (5, 5) carbon nanotube had 100 atoms of carbon, $L_0 = 9.8$ Å, D = 6.9 Å.

Figure 15 presents an optimized structure of this model and the scheme of introduction of the coordinate of mechanical-chemical deformation (MCD) for it in the "end deformation" mode. The scheme of introduction and calculation of MCD are described in Section 4.1.

Figure 16 shows successive stages of deformation and destruction of a (5, 5) CNT by an example of the structure of clusters of a (5, 5) carbon nanotube at several stages of deformation and corresponding MCD elongation.

It is seen from the results of calculation of critical (maximum) deformation forces (and from the figures) that rupture of this tube, as well as in the case of the model of a (4, 4) tube, occurred at the 15-th step.

Figures 17–20 show the dependences similar to those presented in Figs. 7–10. Table 3 gives the calculated deformation characteristics.

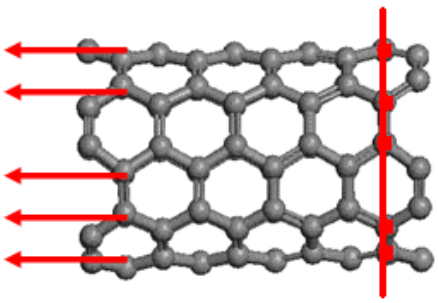

FIG. 15: An optimized structure of the cluster model of a (5, 5) carbon nanotube and a scheme of introduction of the coordinate of mechanical-chemical deformation for it in the "end deformation" mode

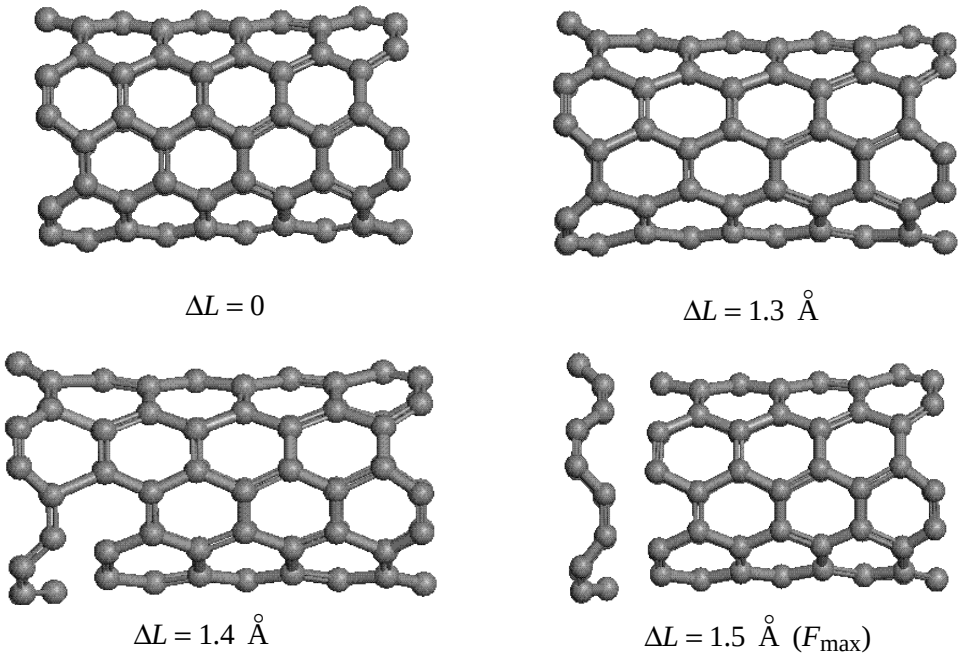

FIG. 16: Structures of clusters of a (5, 5) tube at several stages of deformation and the corresponding elongations of the coordinate of mechanical-chemical deformation

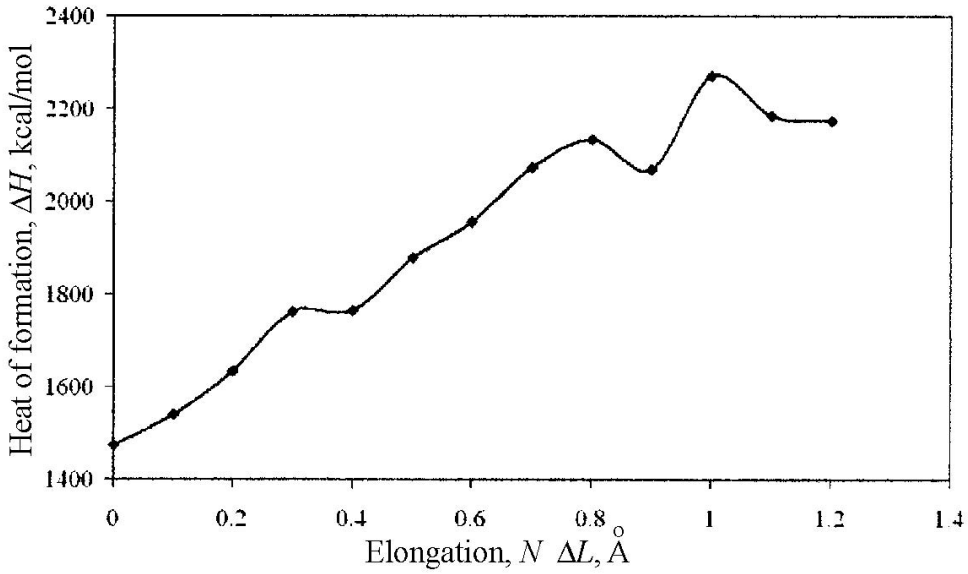

FIG. 17: Dependence of the heat of (5, 5) CNT formation on elongation

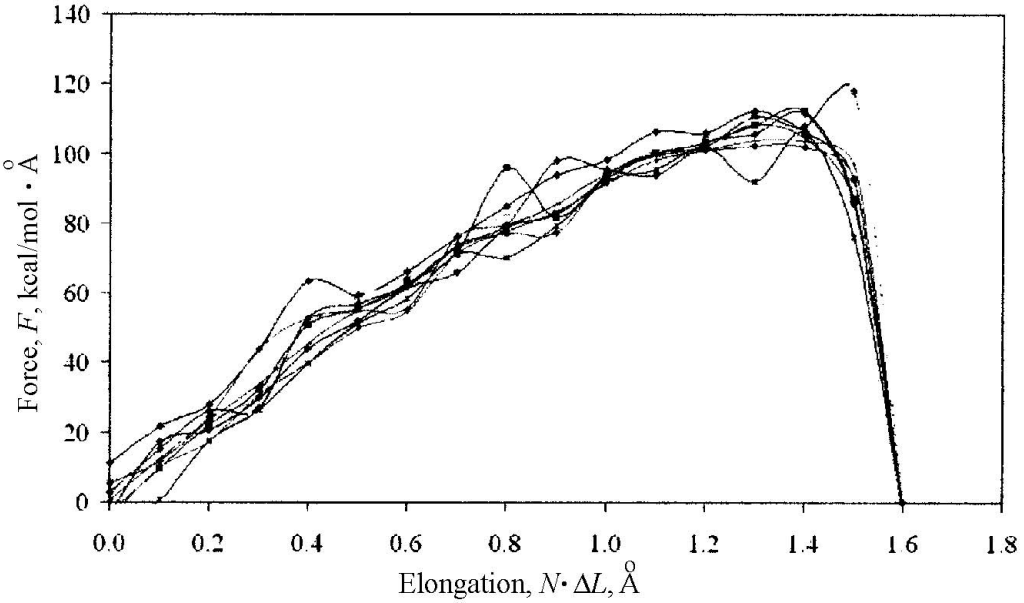

FIG. 18: Dependence of the deformation force of bonds on elongation for a (5, 5) CNT

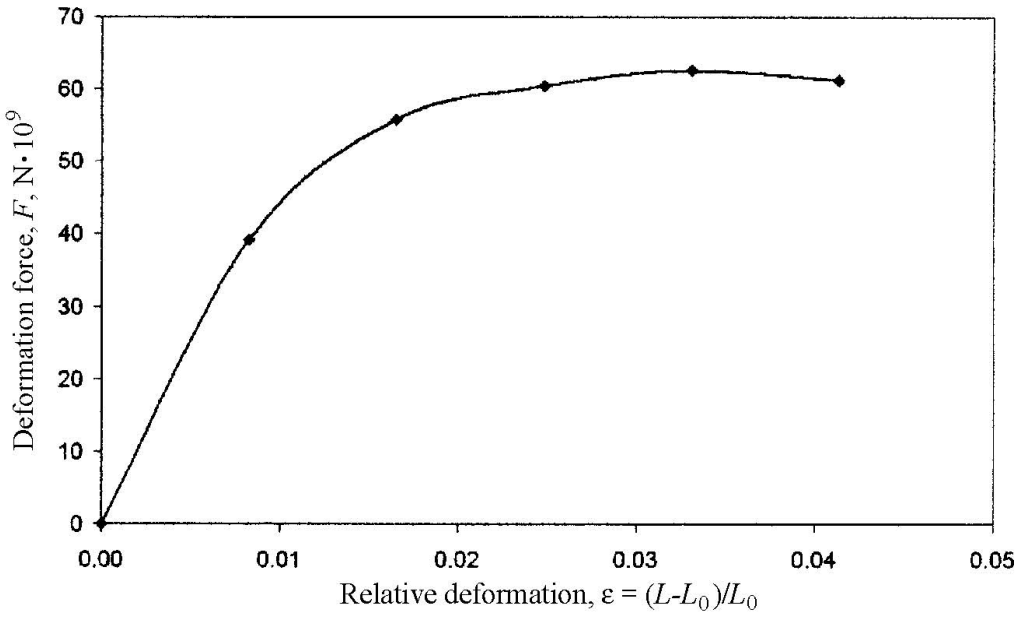

FIG. 19: Dependence of the total force on deformation for a (5, 5) CNT

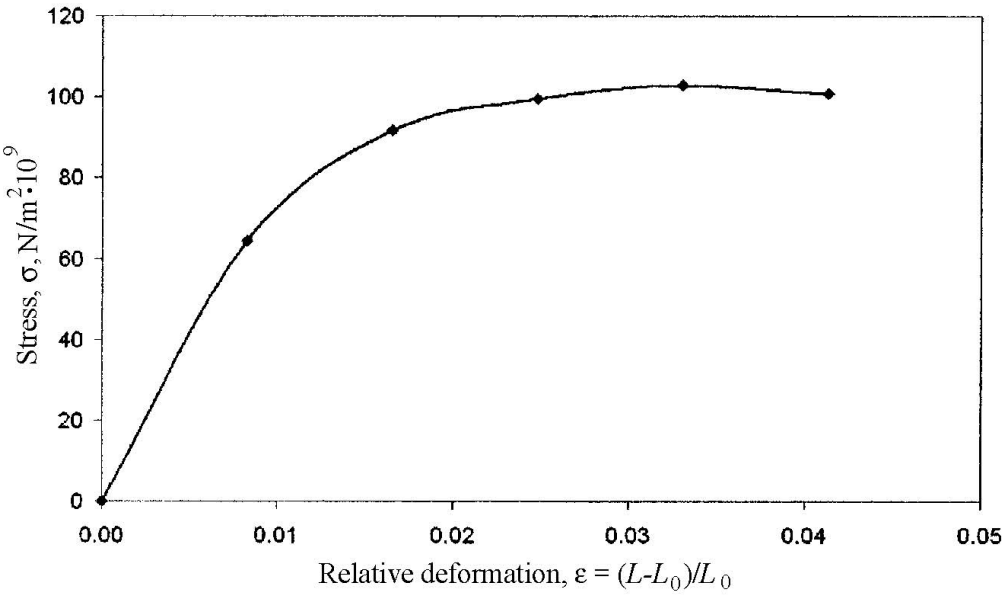

FIG. 20: Dependence of stress on deformation for a (5, 5) CNT

TABLE 3: Mechanical characteristics calculated for a (5, 5) carbon nanotube in "end deformation"

Critical relative deformation, ε_{cr}	**Critical stress, ε_{cr}, GPa·10^{-9}**	**Critical deformation force, F_{cr}, N·10^{-9}**	**Critical heat of formation, ΔH_{cr}, kJ/mol**	**Destruction work, A_{rupt}, kJ/mol**	**Energy of rupture of one bond, ΔH_b, kJ/mol**	**Young modulus, E, TPa**	**Coefficient of rigidity, K, N/m**
0.143	158.9	58.5	10930.7	3370.9	933.9	1.113	418.2

4.4 Deformation of a (8, 0) Carbon Nanotube, "End Deformation" Mode

The model of a (8, 0) carbon nanotube had 96 atoms of carbon, $L_0 = 10.0$ Å, D = 6.3 Å.

Figure 21 presents an optimized structure of this model and the scheme of introduction of the coordinate of mechanical-chemical deformation (MCD) in the "end deformation" mode. The scheme of introduction and calculation of MCD are similar to those described in Section 4.1

Figure 22 shows successive stages of deformation and destruction of a (8, 0) CNT.

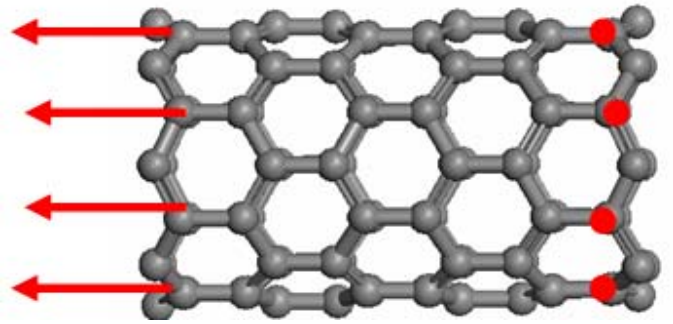

FIG. 21: An optimized structure of the cluster model of a (8, 0) nanotube and a scheme of introduction of the coordinate of mechanical-chemical deformation in the "end deformation" mode

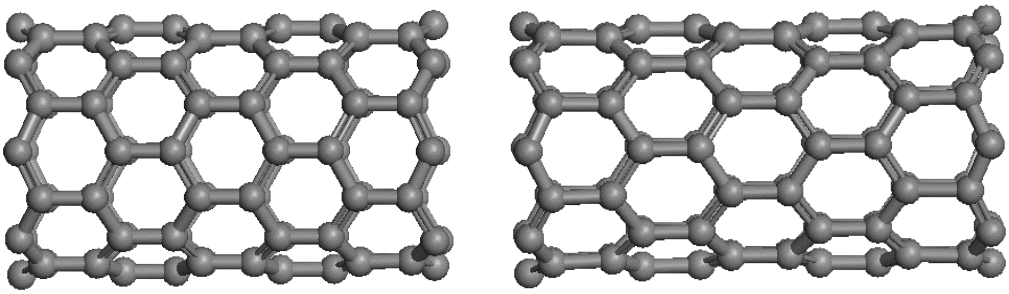

$\Delta L = 0$ $\Delta L = 1.0$ Å

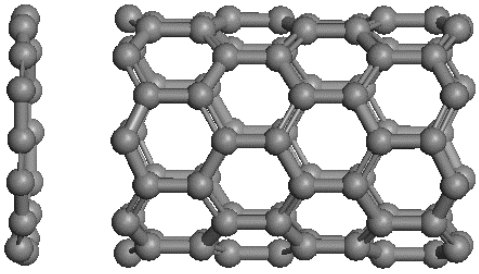

$\Delta L = 1.1$ Å $(F_{\max})$

FIG. 22: Structures of clusters of a (8, 0) carbon nanotube at several stages of deformation and the corresponding elongations of the coordinate of mechanical-chemical deformation

It is seen from the results of calculation of critical (maximum) deformation forces (and from the figures) that rupture of this tube, as well as in the case of the model of a (4, 4) tube, occurred at the 11-th step. The calculated value of the Young modulus is E = 0.737 TPa.

5. DISCUSSION OF THE RESULTS

As is seen from the above-given material, in the work we studied a microstructure and mechanical properties of carbon nanotubes. Here, the geometry, energy, and forces of deformation of nanotubes were calculated at the nanoscopic level using quantum-mechanical methods; then these forces were used for calculation of mechanical characteristics at the macroscopic level using the relationships of the elasticity theory.

Approximations of the mechanical-chemical coordinate of deformation, a semiempirical NDDO method with the AM1 parametrization, unrestricted Hartree–Fock (UHF) method, and cluster approximation (all realized within the package of programs NDDO/sp-spd) were introduced.

Deformation and strength characteristics for tubes of different diameters and chirality were studied. Different versions of loading were considered. It is found that the Young modulus increases with an increase in the CNT radius (for the "armchair' configuration it is higher than for the "zigzag" configuration).

A high calculated strength of an individual C–C bond in CNT is commensurable with the strength of bonds in benzene. Microscopic mechanisms of deformation are revealed. The calculated macroscopic mechanical characteristics of CNT are in good agreement with the experimental data in both value and the presence of the dependence of deformation on chirality and geometric parameters of single-wall CNTs.

All the results obtained are tabulated in Table 4 where the calculated deformation and strength characteristics for all models of loading of carbon nanotubes are given.

The results of calculation of the Young modulus for carbon nanotubes show that

- CNTs with a large diameter (E = 1.2 TPa) are stronger than CNTs with a smaller diameter (E = 0.76 TPa);
- CNTs with the "armchair" configuration are stronger than tubes of the same diameter but with the "zigzag" configuration.

The calculation revealed an extreme strength of bonds between the neighboring atoms of carbon in nanotubes (E = 3.1 TPa) which is in good agreement with analogous results obtained in benzene (E = 3.3 TPa) [23].

TABLE 4: Deformation and Strength Characteristics for Carbon NanoTubes by Different Deformation Modes

Sistem	Critical relative deformation, ε_{cr}	Critical stress, ε_{cr}, GPa·10^9	Critical deformation force, F_{cr}, N·10^{-9}	Critical heat of formation, ΔH_{cr}, kJ/mol	Destruction work, A_{rupt}, kJ/mol	Energy of rupture of one bond, ΔH_b, kJ/mol	Young modulus, E, TPa	Coefficient of rigidity, K, N/m
(4, 4) CNT, end deformation	0.124	94.5	57.5	9433.7	3072.1	430.2	0.762	383
(4, 4) CNT, deformation by neighboring rows	0.033	102.9	62.6	7383.5	1125.0	152.5	3.113	1565.5
(5, 5) CNT, end deformation	0.143	158.9	58.5	10930.7	3370.9	933.9	1.113	418.2
(8, 0) CNT, end deformation	0.123	90.5	48.0	3250.2	1270.6	405.6	0.737	342.8

Thus, we should emphasize that both qualitative and quantitative agreement with the experiments and the available theoretical calculations was obtained in computer experiments.

6. CONCLUSIONS

In the present work, mechanical characteristics of carbon nanotubes are studied by the methods of quantum mechanics. The experimental data known from the literature and available theoretical calculations of structural, energy, and mechanical properties of carbon nanotubes are analyzed. Complex quantum-mechanical modeling of the mechanical behavior of carbon nanotubes was performed in approximation of the mechanical-chemical coordinate of deformation. In this case, deformation forces were calculated within the framework of quantum-mechanical approximation as a response to deformation of the system. These quantities were used for calculation of macroscopic characteristics determining mechanical and strength properties of carbon nanotubes. By virtue of the fact that carbon nanotubes are nanoobjects in themselves, the suggested description of the process of CNT deformation was as much as possible adapted to the scheme of a natural experiment.

As a result, a rather good agreement with the experiment (both quantitative and qualitative) was obtained in the present calculations. It is known from the literature that deformation characteristics and, first of all, the Young moduli for carbon nanotubes depend on the diameter and chirality of tubes. Actually, it was shown in the calculations that the Young modulus increases with an increase in the diameter of nanotubes. It is also found that the Young moduli for nanotubes with the "armchair" configuration are somewhat higher than those for nanotubes in the "zigzag" configuration. And finally, in the present work we obtained good quantitative results on calculations of the Young moduli, which virtually coincide with the experimental data.

The work was carried out with financial support of the Russian Foundation for Basic Research (grant No. 08-01-00390a).

REFERENCES

1. Khavryutchenko, V., Nikitina, E., Malkin, A., and Sheka, E., Mechanics of nanoobjects. Computational mechanochemistry, *Phys. Low-Dimens. Struct.*, 6:65–84, 1995.
2. Nikitina, E. A., Khavryutchenko, V. D., Sheka, E. F., Barthel, H., and Weis, J., Deformation of poly(dimethylsiloxane) oligomers under uniaxial tension, Quantum-chemical view, *J. Phys. Chem. A*, 103:11355–11365, 1999.
3. Yanovsky, Yu. G., Nikitina, E. A., Karnet, Yu. N., Valiev, Kh. Kh., and Lushchekina, S. A., Molecular modeling of mesoscopic composite systems. Structure and micromechanical properties, *Fiz. Mezomekh.*, 8(5):61–76, 2005.
4. Kozlov, G. V., Malamatov, A. Kh., Yanovsky, Yu. G., and Nikitina, E. A., Some aspects of the mechanism of reinforcement of polymer/organoclay nanocomposites, *Mekh. Kompozit. Mater. Konstr.*, 12(2):181–188, 2006.
5. Yanovsky, Yu. G., Vlasov, A. N., Nikitina, E. A., and Karnet, Yu. N., Analysis of theoretical strength of interphase layers of adsorption complexes of polymer composite media, *Mekh. Kompozit. Mater. Konstr.*, 13(1):33–41, 2007.
6. Iijima, S., Helical microtubules of graphitic carbon, *Nature*, 354:56–58, 1991.
7. Ajayan, P. M. and Zhou, O. Z., Applications of carbon nanotubes, *Carbon Nanotubes Topics Appl. Phys.*, 80:391–425, 2001.
8. Kang, S., Pinault, M., Pfefferle, L. D., and Elimelech, M., Single-walled carbon nanotubes exhibiting strong antimicrobial activity, *Langmuir*, 23:8670–8673, 2007.
9. Zhang, P., Huang, Y., Geubelle, P. H., Klein, P. A., and Hwang, K. C., The elastic modulus of singlewall carbon nanotubes: a continuum analysis incorporating interatomic potentials, *Int. J. Solids Struct.*, 39(13–14), 3893–3906, 2002.
10. Liu, F., Ming, P., and Li, J., *Ab initio* calculation of ideal strength and phonon instability of graphene under tension, *Phys. Rev. B*, 76:064120–064126, 2007.
11. Pan, Z. W., Xie, S. S., Lu, L., Chang, B. H., Sun, L. F., Zhou, W. Y., Wang, G., and Zhang, D. L., Tensile tests of ropes of very long aligned multiwall carbon nanotubes, *Appl. Phys. Lett.*, 74:3152–3154, 1999.

12. Hernr'andez, E., Goze, C., Bernier, P., and Rubio, A., Elastic properties of C and $B_xC_yN_z$ composite nanotubes, Phys. Rev. Lett., 80:4502–4505, 1998.
13. Yakobson, B. I., Brabec, C. J., and Bernholc, J., Nanomechanics of carbon tubes: Instabilities beyond linear response, *Phys. Rev. Lett*., 76(14):2511–2514, 1996.
14. Harik, V. M., Ranges of Applicability for the Continuum-beam Model in the Constitutive Analysis of Carbon Nanotubes: Nanotubes or Nano-Beams?, NASA Langley Research Center, NASA/CR-2001-211013, ICASE Report No.2001-16, 2001.
15. Allen, M. P. and Tildesley, D. J., *Computer Simulation of Liquids*, Oxford: Clarendon Press, 1989.
16. Dewar, M. J. S. and Thiel, W., Ground states of molecules. The MNDO method. Approximations and parameters, *J. Am. Chem. Soc*., 99:4899–4907, 1977.
17. Nikitina, E. A., Computational modeling of surfaces and interphase layers of nanoobjects, *Mekh. Kompozit. Mater. Konstr*., 7(3):288–331, 2001.
18. Pople, J. A. and Beveridge, D. L., *Approximate Molecular Orbital Theory*, New York: McGraw-Hill, 1970.
19. Burstein, K. Y. and Isaev, A. N., MNDO calculations on hydrogen bonds. Modified function for core–core repulsion, *Theor. Chim. Acta*, 64:397–401, 1984.
20. Stewart, J. J. P., Optimization of parameters for semiempirical methods II. Applications, *J. Comp. Chem*., 10(2):221–264, 1989.
21. Lu, J. P., Elastic properties of carbon nanotubes and nanoropes, *Phys. Rev. Lett.*, 79:1297–1300, 1997.

International Journal of Nanomechanics. Science and Technology 1(1), 31–47 (2010)

SPECIAL FEATURES OF THE MECHANICAL BEHAVIOR OF POLYMER/ORGANOCLAY NANOCOMPOSITES

B. Zh. Dzhangurazov,[1] G. V. Kozlov,[2*]
G. E. Zaikov,[3] & A. K. Mikitaev[2]

[1]*CRR "TD PolyChemGroups", 18/19 Barklay Str., Moscow, 121309, Russia*

[2]*Kabardino-Balkarian State University, 173 Chernyshevskiy Str., Nalchik, 360004, Russia*

[3]*N. M. Emanuel Institute of Biochemical Physics, Russian Academy of Sciences, 4 Kosygin Str., Moscow, 119991, Russia*

[*]Address all correspondence to G. V. Kozlov E-mail: i_dolbin@mail.ru, Tel.: +7(8662)424144

The principal mechanical characteristics (elasticity modulus, yield stress, strain up to failure) of polymer/organoclay nanocomposites are studied. The quantitative relationships have been proposed, allowing one to correctly describe these characteristics with consideration for the interfacial adhesion (nanoadhesion) level and for the change in the polymer matrix molecular indicators due to nanofiller introduction. For this purpose, the modern physical concepts, namely, the cluster model of the amorphous state of the structure of polymers, fractal analysis, and the anharmonicity concept were used.

KEY WORDS: *nanocomposite, organoclay, mechanical characteristics, molecular indicators, interfacial adhesion, nanoadhesion, structure*

1947-5748/10/35.00

1. INTRODUCTION

Layered silicates, in particular, Na^+-montmorillonite (natural clay) are the promising natural materials for being used as nanofillers to obtain polymer nanocomposites [1, 2]. Usually, the introduction of small amounts of organoclay (up to 10 wt.%) into a polymer matrix results in substantial enchancement of the elasticity modulus of receiving nanocomposites. Although at the present time there are theoretical models for describing a change in the elasticity modulus of nanocomposites filled with organoclay which are based on the notion of the so-called "effective particles" [3], these models do not take account of two factors, which are most important for theoretical description of multiphase polymeric systems: the interfacial adhesion level and the molecular characteristics of a polymer matrix. The first factor has acquired a special importance after the discovery of the nanoadhesion effect, which assumes the availability of a much higher interfacial adhesion level in polymer nanocomposites in comparison with traditional composites filled with particles (fibers) of micron size [4]. Therefore, the purpose of the present paper is to study theoretically the basic mechanical characteristics (elasticity modulus, yield stress, strain at failure) of polymer/organoclay nanocomposites taking into account the indicated-above factors.

2. EXPERIMENTAL

For the nanocomposites based on polyimide (PI), Na^+-montmorillonite (MMT) with particles of average size of 50 μm was used as a nanofiller. The first series of organically modiefed MMT (MMT-16C) was prepared by ions change reaction in water with the use of concentrated hydrochloric acid, the second series (MMT-OM-m) was also obtained by a reaction in water with the use of N-[4-(4'-aminophenoxy)] phenylphthalimide. The PI/MMT-16C and PI/MMT-OM-m nanocomposites were prepared by polymerization *in situ*, the details of which are given in [5, 6]. The MMT content amounts to 1–3 wt.% in the PI/MMT-16C nanocomposites and 0.5–5.0 wt.% in the PI/MMT-OM-m nanocomposites.

The mechanical properties of PI/MMT nanocomposites were obtained with the use of the universal Instron tester of model 4465 at a temperature of 293 K and strain rate of $\sim 1.1 \times 10^{-3}$ s^{-1}. Dumbbell samples were prepared from films of thickness 0.1 mm, basic length of 75 mm, and width of 4 mm [5].

For nanocomposites based on polyethylene, linear low-density polyethylene (LDPE), of mark Dowlex 2032, having the melt flow index of 2.0 g/10 min and density of 0.926 g/cc, which corresponds to the crystallinity degree of 0.49, was used.

Modified Na^+-montmorillonite (MMT), obtained by the cation exchange reaction between MMT and quaternary ammonium ions, was used as a nanofiller [7].

The low-density polyethylene/montmorillonite (LDPE/MMT) nanocomposites were prepared by blending components in a melt using the Haake twin-screw extruder at a temperature of 473 K [7].

Tensile specimens were prepared by injection molding on Arburg Allrounder 305-210-700 molding machine at a temperature of 463 K and pressure of 35 MPa. Tensile tests were performed using the Instron tester of model 1137 with direct digital data acquisition at a temperature of 293 K and strain rate of $\sim 3.35 \times 10^{-3}$ s^{-1}. The average deviation in the determination of the elasticity modulus was 7% with the yield stress being equal to 2% [7].

The data of [8] were also used for nanocomposites based on isotactic polypropylene (PP) of industrial Shell Co. manufacture, filled with Na^+-montmorillonite with the weight content of the latter W_n = 2.5, 5.0, and 10.0 wt.%. Dioctadecildimethylammonium bromide (DODAB) plus the polyethyleneoxide-polyethylene (PEO-PE) block-copolymer (conventionally abbreviated as PP/MMT-1); PEO-PE (PP/MMT-2); DODAB plus PEO-PE with isobutylene (PP/MMT-3), and PEO-PE plus isobutylene (PP/MMT-4) were used as modifiers. The detailed description of the procedure of preparing specimens was given in [8].

Tensile tests of PP/MMT nanocomposites were carried out on film specimens (length 10 mm, width 3 mm, and thickness 0.2 mm) obtained by pressing from melt at a temperature of 473 K. Tensile tests were conducted at a temperature of 293 K and strain rate of 8.3×10^{-3} s^{-1} [8].

3. RESULTS AND DISCUSSION

3.1 The Reinforcement Degree of PI/MMT Nanocomposites

In [2], the relationship allowing one to connect the reinforcement degree of nanocomposites E_n / E_m with the molecular characteristics of a polymer matrix was obtained:

$$\frac{E_n}{E_m} = 1 + 0.19 W_n^{1/2} l_{st}, \quad (1)$$

here E_n and E_m are the elasticity moduli of the nanocomposite and polymer matrix, respectively, W_n is the nanofiller weight content (in wt.%), and l_{st} is the statistical segment length for the polymer matrix chain (in nm).

To estimate l_{st}, it is necessary to calculate the fractal (Hausdorff) dimension d_f of the nanocomposite structure, which can be made by the equation [9]

$$d_f = (d - 1)(1 + \nu), \tag{2}$$

where d is the dimension of the Euclidean space in which a fractal is considered (it is obvious that in our case $d = 3$), ν is the Poisson ratio estimated by the results of mechanical tests with the aid of the relationship [10]

$$\frac{\sigma_Y}{E_n} = \frac{1 - 2\nu}{6(1 + \nu)}, \tag{3}$$

where σ_Y is the yield stress of the nanocomposite.

The characteristic ratio C_∞, which is an indicator of the polymer chain statistical flexibility [11], is related to the structural characteristic d_f by the equation [12]

$$C_\infty = \frac{2d_f}{d(d - 1)(d - d_f)} + \frac{4}{3}. \tag{4}$$

Finally, the length of the statistical segment l_{st} can be determined by the formula [13]

$$l_{st} = l_0 C_\infty, \tag{5}$$

where l_0 is the length of the main chain skeletal bond which is equal to 2.05 Å for polyimide [14].

The calculation of the value of E_n/E_m according to Eqs. (1)–(5) yields understated values of this parameter: E_n/E_m = 1.15–1.59, since the experimental values of the reinforcement degree for the nanocomposites studied are within the range 1.11–3.65 [5, 6]. The cause of this discrepancy is obvious enough: Eq. (1) takes into account the polymer chain flexibility of the nanocomposite with the aid of the parameter l_{st}, but does not take into account the interfacial adhesion level. The accounting for the last factor can be achieved with the aid of the parameter b, which is used in heat expansion of composites and is determined according to the formula [15]

$$\alpha_n = \alpha_n^{\text{mix}} - b\left(\alpha_n^{\text{mix}} - \alpha_n^T\right), \tag{6}$$

where α_n, α_n^{mix}, and α_n^T are the values of the nanocomposite heat expansion coefficient, obtained experimentally and calculated according to the mixtures rule and Turner equation, respectively.

Since the calculation by the Turner equation gives a lower limiting value for the heat expansion coefficient, then it follows from Eq. (6) that $b = 1$ at $\alpha_n = \alpha_n^T$, i.e., when perfect adhesion is reached [15]. For a larger number of polymer composites with various polymer matrices and fillers the values of b were obtained within the range ~0.1–1.0 [15]. The nanoadhesion effect supposes much higher values of b in the nanocomposites case. So, for particulate-filled phenylone/aerosil nanocomposite the value of b can reach ~12, which corresponds to the condition $\alpha_n < \alpha_n^T$ [4]. The value of the parameter b or interfacial adhesion level, according to the results of mechanical tests, can be estimated as follows. It is known [2] that the reinforcement degree of polymer nanocomposites can be determined by the following percolation relationship:

$$\frac{E_n}{E_m} = 1 + 11\left(\varphi_n + \varphi_{if}\right)^{1.7}, \tag{7}$$

where φ_n and φ_{if} are the relative volume fractions of the nanofiller and interfacial regions, respectively.

The following relationship between φ_{if} and φ_n for exfoliated layered silicates was obtained [2]:

$$\varphi_{if} = 1.91\varphi_n b\,. \tag{8}$$

Thus, Eq. (8) demonstrates that in the nanoadhesion case the value of φ_{if} increases b times in comparison with the perfect adhesion for which $b = 1$. Equation (8) substituted into formula (7) gives the following relationship:

$$\frac{E_n}{E_m} = 1 + 11\left[\varphi_n\left(1 + 1.91b\right)\right]^{1.7}, \tag{9}$$

which takes into account the interfacial adhesion (nanoadhesion) level in determining the nanocomposites reinforcement degree.

Returning to Eq. (1), we note that the only parameter that can be influenced by the interfacial adhesion level in this equation is the statistical segment length. It can be supposed that the enhancement of the interfacial adhesion level, characterized by

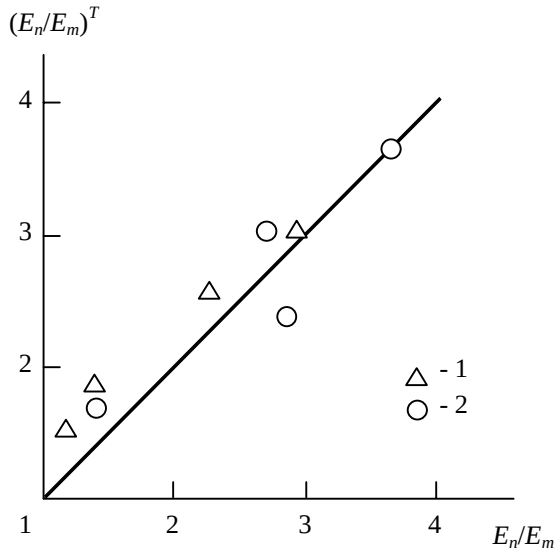

FIG. 1: A comparison of the experimental E_n/E_m and calculated from Eq. (11) values of the reinforcement degree $(E_n/E_m)^T$ for the PI/MMT-16C (1) and PI/MMT-OM-m (2) nanocomposites

the growth of the parameter b, or by the intensification of the polymer matrix with montmorillonite platelets surface interaction restricts the mobility of polymer chains in the interfacial layer and results in higher rigidity (straightening) of these chains in comparison with thebulk polymer matrix or increase in l_{st} [16], which can be expressed with the aid of the statistical segment effective length l_{st}^{eff}:

$$l_{st}^{\text{eff}} = l_0 C_\infty b \,. \tag{10}$$

Taking into account relationship (10), Eq. (1) can be written as follows:

$$\frac{E_n}{E_m} = 1 + 0.19 W_n^{1/2} l_{st} b \,. \tag{11}$$

The value of b can be calculated with the aid of Eq. (9) with the assumption that $\varphi_n = W_n$. These estimations have shown that for the nanocomposites studied the parameter b varies within the range 2.40–5.74, i.e., for the PI/MMT-16C and PI/MMT-OM-m nanocomposites the nanoadhesion effect ($b > 1$) is observed. Figure 1 presents

a comparison between the experimental ratio E_n/E_m and reinforcement degree values $(E_n/E_m)^T$ calculated by Eq. (11) for the polyimide/montmorillonite nanocomposites. As one can see, in this case there is a good correspondence between the theory and experiment: the $(E_n/E_m)^T$ value varies within the range 1.56–3.71 and its average discrepancy with experimental values of E_n/E_m amounts to about 16%.

3.2 Yield Stress of Low-Density Polyethylene/Montmorillonite Nanocomposites

As a rule, an introduction of layered silicates into a polymer matrix results in a substantial (up to 1.5 times) increase in the nanocomposites yield stress [2, 7, 8]. Such an effect is important from the practical point of view, since the attainment of the yield stress σ_Y restricts the exploitation range of polymer materials from above. The analysis of the yield process within the framework of the cluster model of the amorphous state structure of polymers [12, 18] shows that the attainment of the yielding point is connected with the decay of the densely-packed regions of the polymers structure, i.e., local order domains (clusters) and crystallites, in the applied mechanical stress field. An introduction of a nanofiller into a polymer matrix results in the complication of the nanocomposite structure obtained which requires account for the influence of the newly formed structural formations. Thus, in [19] it is shown by an example of the PP/MMT nanocomposites that the σ_Y value for these materials is determined by the crystallites and interfacial regions, and the latter were formed by epitaxial crystallization on the surface of the layered nanofiller platelets [2]. Therefore, below we will carry out a structural analysis of the yield process for low-density polyethylene/organoclay nanocomposites (LDPE/MMT) [7].

As is noted above, in polymer materials the attainment of the yield stress σ_Y (realization of the yield process) is connected with the decay of densely-packed regions [12, 18]. In the case of the LDPE/MMT nanocomposites, the crystallites, local order domains (clusters) in an amorphous phase, and interfacial regions with the relative fractions K, φ_{cl}, and φ_{if}, respectively, or any variant of the sum of these densely-packed regions represent such regions. The estimation of the indicated relative fractions of structural components can be performed as follows. The crystallinity degree K was calculated according to the equation [20]

$$K = 0.32C_\infty^{1/2}, \tag{12}$$

where the value of the characteristic ratio C_∞ was determined by Eq. (4).

It should be noted that estimations according to Eq. (12) yield the value of K within the range 0.47–0.54 which corresponds well to the calculation of K in terms of the density for the LDPE matrix, which is equal to 0.49. The relative fraction of clusters φ_{cl} was calculated with the aid of the equation [12]

$$d_f = 3 - 6\left(\frac{\varphi_{cl}}{C_\infty S}\right)^{1/2}, \tag{13}$$

where S is the cross-sectional area of the macromolecule, which is equal to 14.4 Å^2 for polyethylenes [21].

And finally, the relative fraction of the interfacial regions φ_{if} can be calculated with the aid of Eq. (7). Within the framework of the cluster model of the amorphous state structure of polymers, theoretical estimation of the yield stress σ_Y was performed according to the equation [12]

$$\sigma_Y = \frac{Gb_B \rho_d^{1/2}}{2\pi}, \tag{14}$$

where G is the shear modulus, b_B is the Burgers vector, and ρ_d is the density of structural linear defects, i.e., their total length per unit volume of polymer material.

The value of G was determined from the following fractal relationship [22]:

$$G = \frac{E_n}{d_f}. \tag{15}$$

For polymer materials the Burgers vector b_B is a function of polymer chain flexibility characterized by C_∞ and estimated as follows [12]:

$$b_B = \left(\frac{60.5}{C_\infty}\right)^{1/2}, \ \text{Å}. \tag{16}$$

The cluster model assumes that the segments of the polymer chains participating in the densely-packed regions of the polymer material are the linear defects of the structure [12]. Therefore the value of ρ_d can be calculated by the equation [12]

$$\rho_d = \frac{\varphi_{dens}}{S}, \tag{17}$$

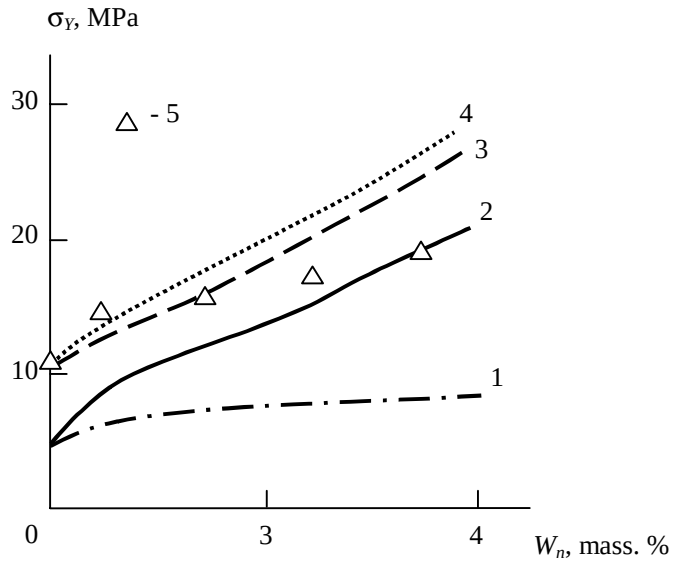

FIG. 2: The dependences of the yield stress σ_Y on the organoclay weight content W_n for the LDPE/MMT nanocomposites: 1–4) calculation by Eq. (14) at $\varphi_{dens} = \varphi_{cl}$ (1), $\varphi_{dens} = \varphi_{cl} + \varphi_{if}$ (2), $\varphi_{dens} = K$ (3), and $\varphi_{dens} = K + \varphi_{if}$ (4), respectively; 5) experimental data

where φ_{dens} is the relative fraction of the densely-packed regions.

As was noted above, for the LDPE/MMT nanocomposites K, φ_{cl} or φ_{if} or their sum in any possible variant can be accepted as φ_{dens}. In the present paper, to estimate ρ_d by Eq. (17), the following structural parameters were selected: φ_{cl}, K, $\varphi_{cl} + \varphi_{if}$, and $K + \varphi_{if}$. In Fig. 2, a comparison of the experimental dependences and those calculated according to Eq. (14) of the yield stress σ_Y on the nanofiller weight content W_n is presented. It is apparent from the data of Fig. 2 that the following structural parameters: σ_{if}, as giving the understated values of σ_Y, and also $K + \varphi_{cl}$ and $K + \varphi_{if}$, as giving obviously the overstated values of σ_Y, can be excluded from consideration. At small values of W_n, the value of σ_Y is checked by the crystalline phase and at $W_n \geq 5$ wt.% the transition to the case occurs where the yield process structural component is checked by the sum $(\varphi_{cl} + \varphi_{if})$. Such transition is due to the change in the crystalline phase deformation mechanism of the LDPE/MMT nanocomposites. In [23] it was supposed that the drawing occurred as a result of the straightening of the crystalline and amorphous molecular sequences, and, in this case, the limiting draw ratio λ_{lim} can be expressed in terms of the times number f, which is passed by the macromolecule through the same crystallite:

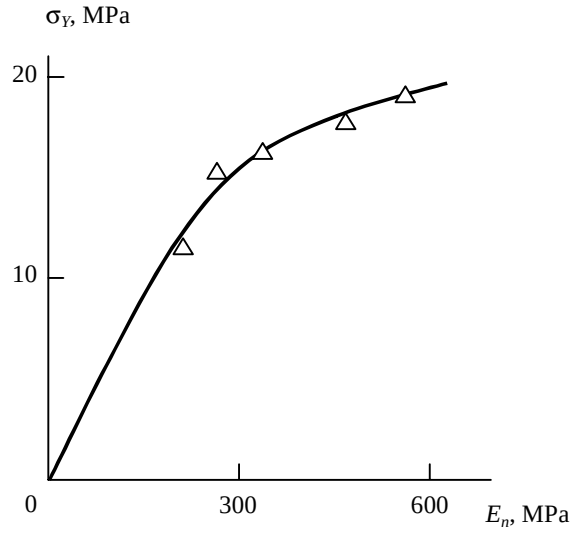

FIG. 3: The relation between the yield stress σ_Y and elasticity modulus E_n for the LDPE/MMT nanocomposites

$$\frac{1}{\lambda_{\text{lim}}} = \frac{K}{f} + \frac{(1 - K)^{1/2}}{n^{1/2}}, \tag{18}$$

where n is the number of equivalent statistical links between the nodes of macromolecular entanglements in a melt, further assumed equal to 300 [24].

It is obvious that the value of f determines the number of folds which are formed by the macromolecule in the folded chains of the crystallite [24]. The condition $f \geq 2$ is necessary for fulfillment of folds formation. The calculation by Eq. (18) with the use of experimental values of λ_{lim} [7] demonstrated that at W_n = 5 wt.% $f = 3.25$, i.e., somewhat higher than 2, and at W_n = 7 wt.% f = 1.90, i.e., in this case, $f < 2$. Thus, the reduction of f, i.e., the impossibility of the straightening of the crystalline molecular sequences [23], is the cause of the transition of the structural component of the checking yield process from crystallites to clusters and interfacial regions.

It was a widespread opinion that there was the proportionality between the elasticity modulus and yield stress for polymer materials [25]. In Fig. 3, the relation of σ_Y and E_n for the LDPE/MMT nanocomposites is given, which demonstrates the absence of the postulated proportionality: at E_n increasing 2.76 times the value of σ_Y increases only by a factor of 1.59. The cause of the disproportion in the change of

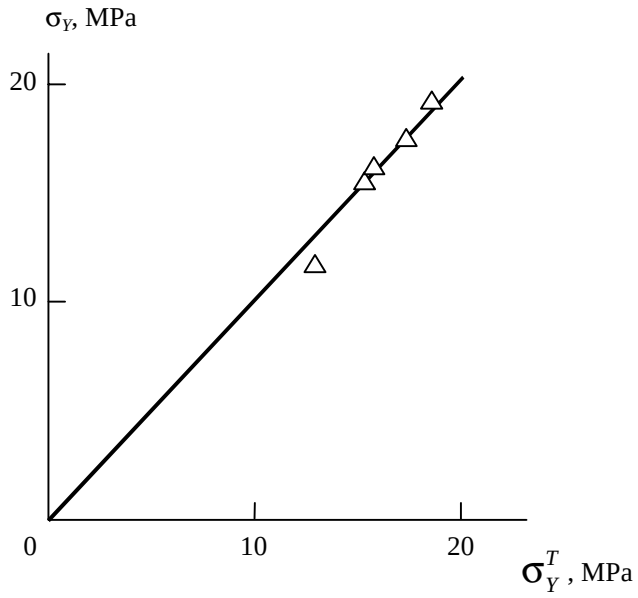

FIG. 4: The relation between the experimental σ_Y and calculated by Eq. (21) values of the yield stress σ_Y^T for the LDPE/MMT nanocomposites

E_n and σ_Y obvious from the plot of Fig. 3 follows from Eqs. (14) and (15): the proportionality postulated in [25] can be realized only at constant molecular and structural characteristics of polymer material [which are interrelated, see Eq. (4)], but this condition is not fulfilled for the LDPE/MMT nanocomposites, for which the dimension of d_f varies within the range 2.528–2.730 with W_n = 0–7 wt.%. Therefore, the relation between σ_Y and E_n must be written as follows [10]:

$$\sigma_Y = \frac{E_n}{6\gamma_L}, \tag{19}$$

where γ_L is the Grüneisen lattice parameter connected with the dimension d_f by the relationship [19]

$$\gamma_L = \frac{d_f}{2\,(d\,-\,d_f)}. \tag{20}$$

The combination of Eqs. (19) and (20) allows one to obtain the relation between σ_Y and E_n, with account for the change in the nanocomposites structure:

$$\sigma_Y = \frac{E_n (d - d_f)}{3d_f}. \tag{21}$$

In Fig. 4, the comparison of experimental σ_Y values and the σ_Y^T yield stress values calculated from Eq. (21) for the LDPE/MMT nanocomposites is presented. As one can see, in the case of the account for the change in the structure characterized by the dimension d_f, one obtains linear correlation between σ_Y and E_n.

3.3 Deformability of the PP/MMT Nanocomposites

As a rule, the introduction of small amounts of organoclay (up to 10 wt.%) reduces sharply the plasticity of nanocomposites, which can be characterized by the limiting strain up to failure ε_f, in comparison with the polymer matrix. So, in [8] the structure and deformation behavior of the PP/MMT nanocomposites were studied and the reduction in ε_f by two orders on introduction of 2.5–10 wt.% of organoclay was revealed. A similar effect was observed for a number of other nanocomposites with an amorphous glassy [26] and semicrystalline [7, 27] matrix. Such a rather strong and common effect requires more thorough investigation. Therefore, a structural analysis of the sharp reduction in plasticity on introduction of layered silicate will be performed below by an example of the PP/MMT nanocomposites.

A comparison between the results of the mechanical tests of the PP/MMT nanocomposites has shown that the increase in the reinforcement degree E_n/E_m was accompanied by the reduction in the plasticity of these materials characterized by the limiting strain up to failure ε_f. In Fig. 5, the relationship between the parameters E_n/E_m and ε_f in the logarithmic coordinates for the PP/MMT nanocomposites is given. From the data of this figure a sharp nonlinear reduction in ε_f on an increase in E_n/E_m follows and at $E_n/E_m \approx 3$ the value of ε_f is close to zero ($\varepsilon_f \approx 2.5\%$). The reinforcement degree of nanocomposites can be determined from the percolation relation (7), from which it follows that an increase in the solid-state component in the structure of nanocomposites defined by the sum $(\varphi_n + \varphi_{if})$ results in an increase in the reinforcement degree E_n/E_m and, hence, in the reduction of ε_f. This effect was shown in Fig. 6 in the diagram form, where the dependence of ε_f on $(\varphi_n + \varphi_{if})$ in the logarithmic coordinates is given for the PP/MMT nanocomposites.

Let us consider theoretically the empirical correlations given in Figs. 5 and 6. As is known [28], the limiting strain up to failure ε_f can be determined theoretically from the equation:

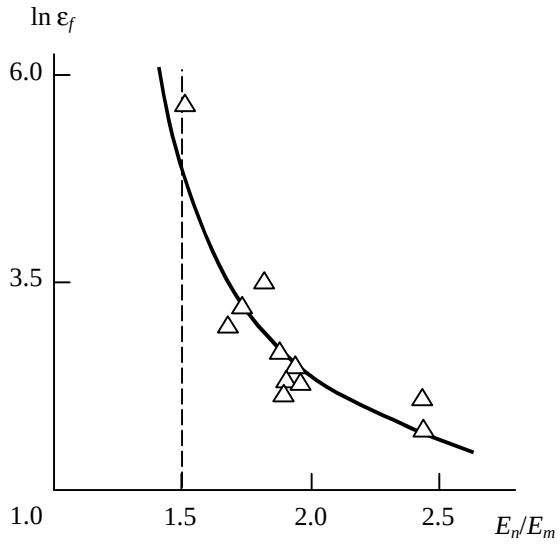

FIG. 5: The dependence of the limiting strain up to failure ε_f on the reinforcement degree E_n / E_m in the logarithmic coordinates for the PP/MMT nanocomposites. The vertical dashed lines in Figs. 5 and 6 correspond to the criterion $f = 2$

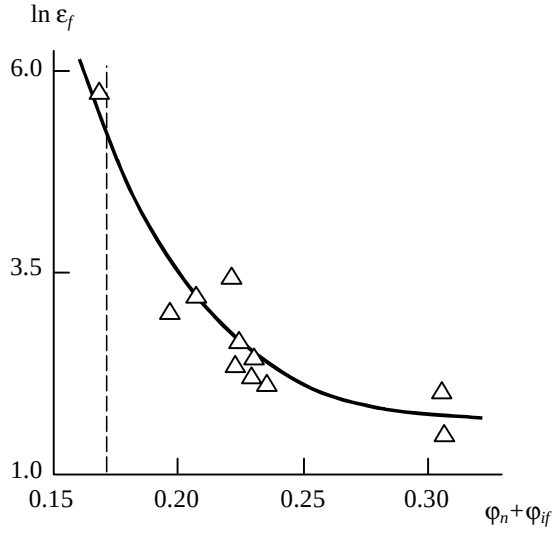

FIG. 6: The dependence of the limiting strain up to failure ε_f on the relative fractions of the sum of nanofiller φ_n and interfacial regions φ_{if} in the logarithmic coordinates for the PP/MMT nanocomposites

$$\varepsilon_f = C_\infty^{D_{ch}-1} - 1, \tag{22}$$

where D_{ch} is the fractal dimension of a part of the polymer chain between its fixation points (chemical cross-linking nodes, physical entanglements, local and long-range order, etc.), that characterize the molecular mobility extent of a polymer material [12, 18].

The estimation of the value of C_∞ was performed according to Eq. (4) and the dimension D_{ch} was calculated with the aid of the following formula [12]:

$$\frac{2}{\varphi_{dens}} = C_\infty^{D_{ch}}, \tag{23}$$

where the sum $(\varphi_{cl}^{red} + \varphi_n + \varphi_{if})$ was used as φ_{dens}. The reduced value of the clusters relative fraction φ_{cl}^{red} takes into account the availability of crystalline regions in the PP polymer matrix and is determined as follows [12]:

$$\varphi_{cl}^{red} = \varphi_{cl}(1 - K), \tag{24}$$

where K and φ_{cl} values were calculated from Eqs. (12) and (13), respectively.

A comparison of the experimental ε_f and ε_f^T calculated by Eq. (22) as the limiting strain up to failure values is given in Table 1. As one can see, a good enough correspondence of the theory and experiment is obtained, although in the majority of cases the condition $\varepsilon_f^T > \varepsilon_f$ is fulfilled. The latter observation is due to two factors. Firstly, the power dependence in Eq. (22) gives an increased error. Secondly, the theoretical value of ε_f^T is determined for an ideal defectless nanocomposite, whereas in real materials defects always exist, and this results in the reduction of ε_f in comparison with ε_f^T.

The only substantial discrepancy is observed for the PP/MMT-4 nanocomposite with the MMT content of 2.5 wt.% (ε_f = 345%, ε_f^T = 86%). We will consider the physical causes of this discrepancy, for which the Gent and Madan model [Eq. (18)] will be used [23]. In Table 1, the values of f for the PP/MMT nanocomposites, obtained from Eq. (18) using experimental values of λ_{lim}, are presented. As one can see, the condition $f \geq 2$ is fulfilled for the PP/MMT-4 nanocomposite with the MMT content of only 2.5 wt.%. In this case, the theoretical value of ε_f (ε_f^{fold}) can be estimated from the following equation:

TABLE 1: The values of the limiting strain up to failure ε_f, ε_f^T and of the folding parameter f for the PP/MMT nanocomposites

Nanocomposite	MMT content, wt.%	ε_f, %	ε_f^T, %	f
PP/MMT-1	5	8	12	0.64
	10	4	9	0.65
PP/MMT-2	2.5	11	23	0.61
	5	14	22	0.65
	10	9	18	0.63
PP/MMT-3	2.5	10	25	0.61
	5	8	19	0.61
	10	6	28	0.62
PP/MMT-4	2.5	345	86	2.80
	5	33	44	0.75
	10	23	29	0.70

$$\varepsilon_f^{fold} = \varepsilon_f^T f + \varepsilon_f^T = \varepsilon_f^T (f + 1). \quad (25)$$

The calculation by Eq. (25) gives ε_f^{fold} = 327%, which corresponds well to the experimental value ε_f = 345% for the indicated nanocomposite. In Figs. 5 and 6, the vertical dashed lines indicate the critical values of E_n/E_m and $(\varphi_n + \varphi_{if})$ corresponding to the criterion f = 2. This criterion demonstrates that at $E_n/E_m \geq 1.5$ or $(\varphi_n + \varphi_{if}) \geq 0.17$ in the PP/MMT nanocomposites the straightening of the crystalline molecular sequences from folded-chain crystallites of PP is suppressed, and only the drawing of chains in amorphous and interfacial regions with $f < 1$ is possible, which results in the sharp reduction of the plasticity of the indicated materials. Similar calculation for the PP matrix gave the following values of the parameters: ε_f^T = 127%, f = 8.7, ε_f^{fold} = 1232%, that correspond well to the value ε_f = 901% [8].

4. CONCLUSIONS

The results obtained in the present work have demonstrated a strong influence of the interfacial adhesion (nanoadhesion) level on the reinforcement degree of polyimide/montmorillonite nanocomposites. The intensification of the interaction between the nanofiller and the polymer matrix characterized by the parameter b results in a

substantial (by a factor of *b*) change in the flexibility of the polymer chains in the interfacial layer in comparison with the bulk polymer matrix. The proposed modified equation for the determination of the reinforcement degree of nanocomposites with account for both the polymer matrix molecular characteristics and interfacial adhesion (nanoadhesion) level gives a good correspondence to experiment.

The cluster model of the amorphous state structure of polymers coupled with the fractal analysis and anharmonicity concept provides a correct quantitative description of the yield process of the LDPE/MMT nanocomposites. The increase in the content of organoclay results in the reduction in the straightening number of the crystalline molecular sequences that defines the transition of the structural component of the checking yield process from crystallites to clusters and interfacial regions. Such a transition causes a decrease in the yield stress by 27%. The linear relationship between the yield stress and elasticity modulus of the LDPE/MMT nanocomposites can be obtained on allowing for their structural changes only in the case of the change in the organoclay content.

The enhancement of the reinforcement degree of nanocomposites, which is due to the growth of the total relative fraction of nanofiller and interfacial regions, results in the reduction of their plasticity characterized by the limiting strain up to failure. A theoretical analysis has revealed that this reduction is determined by a decrease or suppression of the straightening of the crystalline molecular sequences from folded-chain crystallites.

REFERENCES

1. Mikitaev, A. K., Kaladzhyan, A. A., Lednev, O. B., and Mikitaev, M. A., Nanocomposite polymeric materials on the basis of organoclays, *Plast. Massy*, 12:45–50, 2004.
2. Mikitaev, A. K., Kozlov, G. V., and Zaikov, G. E., *Polymer Nanocomposites: Variety of Structural Forms and Applications*, New York: Nova Science Publishers, Inc., 2008.
3. Sheng, N., Boyce, M. C., Parks, D. M., Rutledge, G. C., Abes, J. I., and Cohen, R. E. Multiscale micromechanical modeling of polymer/clay nanocomposites and the effective clay particle, *Polymer*, 45(2):487–506, 2004.
4. Kozlov, G. V., Burya, A. I., Yanovskiy, Yu. G., and Afashagova, Z. Kh., Nanoadhesion effect in particulate-filled nanocomposites phenylone/aerosil, *Nanotekhnika*, 1:81–85, 2008.
5. Liang, Z.-M., Yin, J., and Xu, H.-J., Polyimide/montmorillonite nanocomposites based on thermally stable rigid-rod aromatic amine modifiers, *Polymer*, 44(4):1391–1399, 2003.
6. Liang, Z.-M., Yin, J., Wu, J.-H., Qiu, Z.-X., and He, F.-F., Polyimide/montmorillonite nanocomposites with photolithographic properties, *Eur. Polymer J.*, 40(2):307–314, 2004.
7. Hotta, S. and Paul, D. R., Nanocomposites formed from linear low density polyethylenes and organoclays, *Polymer*, 45(21):7639–7654, 2004.

8. Antipov, E. M., Barannikov, A. A., Gerasin, V. A., Shklyaruk, B. F., Tsamalashvili, L. A., Fisher, H. R., and Razumovskaya, I. V., The structure and deformation behavior of nanocomposites based on polypropylene and modified clays, *Vysokomolek. Soed. A*, 45(11):1885–1899, 2003.
9. Balankin, A. S., Elastic properties of fractals and dynamics of brittle fracture of solids, *Fiz. Tverd. Tela*, 34(4):1245–1258, 1992.
10. Kozlov, G. V. and Sanditov, D. S., *Anharmonic Effects and Physical-Mechanical Properties of Polymers* [in Russian], Novosibirsk: Nauka Press, 1994.
11. Budtov, V. P., *Physical Chemistry of Polymer Solutions* [in Russian], St. Petersburg: Khimiya Press, 1992.
12. Kozlov, G. V. and Zaikov, G. E., *Structure of the Polymer Amorphous State*, Utrecht-Boston: Brill Academic Publishers, 2004.
13. Wu, S. J., Chain structure and entanglement, *Polymer Sci., Part B: Polymer Phys*., 27(4):723–741, 1989.
14. Aharoni, S. M., On entanglements of flexible and rod-like polymers, *Macromolecules*, 16(9):1722–1728, 1983.
15. Holliday, L. and Robinson, J. D., The heat expansion of polymeric composite materials, in M. O. W. Richardson, Ed., *Polymer Engineering Composites*, London: Applied Science Publishers LTD, pp. 241–283, 1978.
16. Pfeifer, P., The interactions between fractals: polystyrene adsorption on Al_2O_3 porous surface, in: L. Pietronero and E. Tozatti, Eds., *Fractals in Physics*, Amsterdam–Oxford–New York–Tokyo: North-Holland, pp. 72–81, 1986.
17. Malamatov, A. Kh., Kozlov, G. V., and Mikitaev, M. A., *The Reinforcement Mechanisms of Polymer Nanocomposites*, Moscow: Publishers of Mendeleev Russian Chemical-Technological University, 2006.
18. Kozlov, G. V. and Novikov, V. U., The cluster model of the amorphous state of polymers, *Usp. Fiz. Nauk*, 171(7):717–764, 2001.
19. Malamatov, A. Kh., Burya, A. I., Kozlov, G. V., and Kudina, E. F., Structural analysis of nanocomposites based on polypropylene yield process, *Mater. Tekhnol. Instrum*., 11(1):25–28, 2006.
20. Aloev, V. Z. and Kozlov, G. V., *Physics of Orientation Effects in Polymer Materials* [in Russian], Nalchik: Poligrafservis i T Press, 2002.
21. Aharoni, S. M., Correlations between chain parameters and failure characteristics of polymers below their glass transition temperature, *Macromolecules*, 18(12):2624–2630, 1985.
22. Balankin, A. S., *Synergetics of Deformable Body* [in Russian], Moscow: MO SSSR Press, 1991.
23. Gent, A. N. and Madan, S. J., Plastic yielding of partially crystalline polymers, *Polymer Sci., Part B: Polymer Phys*., 27(7):1529–1542, 1989.
24. Kozlov, G. V., Sanditov, D. S., and Serdyuk, V. D., Concerning the type of suprasegmental formations in the amorphous state of polymers, *Vysokomolek. Soed. B*, 35(12):2067–2069, 1993.
25. Brown, N., The relationship between yield point and modulus for glassy polymers, *Mater. Sci. Eng*., 8(1):69–73, 1971.
26. Yoon, P. J., Hunter, D. L., and Paul, D. R., Polycarbonate nanocomposites. Part 1. Effect of organoclay structure on morphology and properties, *Polymer*, 44(18):5323–5339, 2003.
27. Pegoretti, A., Dorigato, A., and Penati, A., Tensile mechanical response of polyethylene - clay nanocomposites, *EXPRESS Polymer Lett*., 1(3):123–131, 2007.
28. Kozlov, G. V., Serdyuk, V. D., and Dolbin, I. V., Chain fractal geometry and deformability of amorphous glassy polymers, *Materialovedenie*, 12:2–5, 2000.

International Journal of Nanomechanics. Science and Technology, 1(1), 49–97 (2010)

GAS FLOW AND DIFFUSION IN NANO-SIZED CAPILLARIES AND POROUS BODIES

V. M. Zhdanov[a] *& V. I. Roldughin*[b*]

[a]*Moscow Institute of Engineering Physics, 31 Kashirskoe Highway, 115409, Moscow*

[b]*A. N. Frumkin Institute of Physical Chemistry and Electrochemistry, Russian Academy of Sciences, 31 Leninskii Ave., 119991, Moscow*

[*]Address all correspondence to V. I. Roldughin
E-mail: roldugin@phyche.ac.ru

Kinetic effects related to flows of gases and gas mixtures in capillaries and porous bodies are discussed. The models of porous media and the methods for calculation of kinetic coefficients are described. Much attention has been paid to the dusty-gas model. Results of calculation of the kinetic coefficients for small and large values of the Knudsen number are presented with due account for incomplete accommodation of molecules on the surfaces of capillary walls. Special features of gas flows in ultra-fine channels and the effects related to the action of surface forces, surface diffusion, entrainment of gases by phonons and quasi-one-dimensionality of gas flows have been considered. The effects of the asymmetry of gas transport through multilayer membranes have been discussed.

KEY WORDS: *gas mixture flow, non-equilibrium thermodynamics, kinetic theory of gases, Knudsen regime, thermal slip, viscous slip, diffusion slip, capillary, porous media, dusty-gas model, diffusion pressure effect, gas mixture separation, thermomolecular pressure drop, asymmetry effect, surface forces, surface diffusion, surface fluxes, sieve effect.*

1. INTRODUCTION

Recently, the study of gas and liquid flows in ultra-fine channels and heat transfer processes in them has evoked much interest. The appearance of such studies is related

1947-5748/10/35.00

to minituarization of diverse devices, development of new materials and nanotechnologies. Such flows are encountered in various electronic devices, in development of liquid-crystal displays, jet printers, fuel elements, membranes and filters of new generation, and in a number of other technological processes [1–6]. A heavy growth of the number of publications on the processes of heat and mass transfer in ultra-fine channels resulted in development of an independent trend of investigations which has its own specifics, is called *microfluidics*, and the essence of which is well covered in some reviews [1–3].

We should note that gas flow in ultra-fine channels is assumed to be rather well studied since it occurs in the so-called free-molecular regime that is described thoroughly within the framework of the classical methods of the rarefied gas dynamics [7, 8]. Recent studies show, however, that this problem is far from being completed since a number of new factors have been found here which affect the flow of gases in nano-sized channels (see, e.g., [5, 9]). Even more far from being completed is the region of gas flow in the regime that is intermediate between the free-molecular and hydrodynamic flows, especially it refers to gas flows in channels of complex geometry which are usually used in real devices. Effects that are unusual for this region have been mentioned, in particular, in our reviews [10–12].

All said above can be referred to gas flows in a slip regime as well. In addition to different problems related to the analysis of flow in channels of complex geometry and combination of heat and mass fluxes [4], in this regime there virtually still remained unstudied effects caused by the action of surface forces which, as is shown in [13], can appreciably affect gas slip. We note that an account of gas slip can also play an important role in the description of the effect of slip of fluids, which is an integral part of microfluidics [3]. The possibility itself of fluid slip along a solid surface was apprehended rather long ago and on the phenomenological level its account under the boundary conditions was introduced, e.g., in the classical monograph by Happel and Brenner [14]. Fluid slip was revealed in special real experiments [15, 16] conducted with fluids not wetting the surface. Slip of a nonwetting fluid is explained by different reasons [3, 15, 17]. Along with a purely formal explanation, e.g., due to a decrease of viscosity in the boundary layers, this effect is treated [15] as a real slip caused by the presence of thin gas interlayers near the solid surface. This means that to describe slip of nonwetting fluids one should, strictly speaking, consider gas flows in ultra-thin layers.

In this review, we discuss, mainly, classical ways of describing the flow and diffusion of gases in capillaries and porous bodies. This is related to the fact that these methods are well substantiated and checked on a great number of real systems; there-

fore, they can be useful in solution of various practical problems. We shall also mention a number of new effects which were observed in flows of gases and gas mixtures in ultra-fine channels.

2. BASIC MODELS OF POROUS MEDIA

To the first model of porous media, which is still urgent, we can refer a model of cylindrical capillaries. Gas flow in a long cylindrical capillary was calculated at the beginning of the last century by Knudsen [18] and Smoluchowski [18] for a free-molecular flow that is characterized by a large value of the Knudsen number $\mathrm{Kn} = l/R >> 1$ (l is the free path, R is the characteristic radius of a pore or capillary). Then it was shown that in flow of gases and gas mixtures in capillaries and porous bodies various physical effects (diffusion pressure effect, separation of gas mixtures, thermomolecular pressure drop, etc.) manifest themselves under the action of gradients of pressure and temperature. These effects are determined to a great extent by a value of the Knudsen number, channel geometry, and structure of a porous medium. Due to this reason, along with solution of problems for channels of simple geometry, much attention was paid to search for models which allow analysis of flows in channels of more complex geometry that are much closer to real porous bodies. Among the works dealing with theoretical investigation of a free-molecular flow in a porous medium we should mention, first of all, the work by Derjaguin [20] where he calculated gas permeability of a porous body and found the relation between this parameter and the specific surface of a porous medium irrespective of its geometry. The results of this work were then confirmed by the methods of a numerical experiment [21].

Of particular interest is flow and diffusion of gas mixtures at intermediate Knudsen numbers ($\mathrm{Kn} \sim 1$), i.e., in the transition regime from free-molecular to viscous flow with slip. In a number of works, this problem for long channels of a regular geometric shape (plane channel, round cylindrical channel, etc.) was solved using the linearized kinetic equation with a model collision integral. For flows of a pure gas, a detailed review of this problem is given in [22], for a gas mixture, references to the corresponding works can be found in [23–25]. On a semi-phenomenological level, effects related to transition from the slip regime to a free-molecular flow, which were found in real experiments, are discussed in [26]. On the other hand, rather general results for mass and heat transfer in capillaries can be obtained based on the kinetic eqution with an exact collision integral [27–29].

Expressions for averaged fluxes in a capillary can be used for description of flow and diffusion in a porous medium if the latter is considered as a block formed from a set of long capillary tubes (a capillary model of a porous medium). At the same time, alternative models which allow one to consider a porous medium as an ensemble of particles rigidly fixed in space have been developed; in this case, gas–surface interaction is allowed for by treating the motionless particles as giant molecules that form one of the components of the gas mixture.

A general idea of such a model was suggested by Derjaguin and Bakanov [30, 31], Kagan [32, 33], and Evans, Watson and Mason [34–36] independently. A pseudomolecular (near-Knudsen) regime of gas flow in porous media was described by Derjaguin and Bakanov in 1957. Kagan developed the theory of diffusion, baro- and thermal diffusion of gas mixtures in porous media (1956–1957) on the basis of the model which he called the "wall gas" model. A that time, his works were of top secret since they were directly related to the problem of separation of uranium isotopes by the method of gas diffusion [37]. In works of American scientists (1961–1963), a similar model, called the "dusty-gas" model, was developed. Two approaches led to actually the same results since both of them were based on the equations of diffusion written in the Stefan–Maxwell form and obtained by the Chapman–Enskog method for a multicomponent gas mixture [38, 39]. Diffusion, viscosity, and heat transfer in multicomponent mixtures were then studied by Zhdanov, Kagan and Sazykin [40] on the basis of the 13-moment approximation of the Grad method [41] which allowed one to consider the influence of viscous momentum transfer on diffusion of the components and to obtain new results in calculation of barodiffusion in a viscous flow of mixture. In this case, the expression for thermal diffusion factor in a multicomponent gas mixture turns to be simpler than that in the known monograph by Hirschfelder et al. [38]. It should be noted that on the basis of the equations obtained in [40], Mason et al. [42] completed formulation of their "dusty-gas" model. During last years, alternative dusty-gas models have appeared, one of which [43] we consider in the present review.

A model of rectilinear capillaries and a dusty-gas model were used in considering a number of more complex, from the physical point of view, problems related to flow of vapor–gas mixtures through porous bodies. To them refer an analysis of the influence of phase conversions occurring on the inner surface of channels on the flow and diffusion of gases [44–46], account for force interaction of gas molecules with the surface of capillary walls [47, 48], gas transfer accompanied by adsorption of gas molecules [49–53], combined transport of gas in a capillary volume and over its surface in an adsorption layer [54], transfer of gases through multilayer mem-

branes [55], flows in membranes of complex geometry [56]. Flow of dense gases in rectilinear channels was analyzed in [57, 58]; in this case, in [57], the influence of dispersion interaction of molecules with the surface of capillary walls was taken into account. In what follows we show that a long-range part of the potential "gas/surface" exerts an appreciable effect on both isothermal and nonisothermal flows of gases and gas mixtures.

A gas flow in porous bodies with account for the effect of external forces, combined transfer of molecules in the vapor phase and film flow, and motion of menisci were considered within the framework of the capillary model. The monograph of Churaev [15] is devoted to the formulation of these problems and consideration of a number of other problems of transfer in porous bodies and thorough comparison of theoretical and experimental results. In the present paper, we do not treat the mentioned group of problem The review is aimed mainly at consideration of the methods and results of the calculation of diffusion and heat transfer in capillaries and porous media at arbitrary Knudsen numbers and at analysis of a number of interesting physical effects arising during flow of gas mixtures through them. Comparison of the results obtained for the dusty-gas model with the data of the strict kinetic theory describing diffusion of gases in capillaries allows one to find the limit of applicability of different models in practical calculations.

We emphasize one more aspect of the problems discussed in the present review. Most of the physical effects that will be considered in what follows allow a simple experimental verification. This refers, first of all, to such phenomena as thermomolecular pressure drop and diffusion pressure effect. The presence of substantiated theoretical results on flow and diffusion of gases in capillaries and porous bodies allows one to use comparison of experimental data with the theory for determining a number of kinetic parameters characterizing interaction of gas molecules with each other and with a wall (in particular, the coefficient of accommodation of the tangential momentum of molecules on a wall). We also touch upon the problems related to the flow of gases in nano-sized channels, the effective lateral dimension of which is commensurable with the size of molecules, when the character of the motion of molecules undergoes great changes and substantial modification of kinetic models is needed.

3. NONEQUILIBRIUM THERMODYNAMICS OF CHANNEL FLOWS

First we consider some general phenomenological relations that follow from the nonequilibrium thermodynamics of discontinuous systems [59]. An ordinary presentation

of such systems presupposes the presence of two large closed volumes connected by a narrow capillary tube, porous partition or membrane. Let the system be occupied by an *N*-component gas mixture with the differences (jumps) of the main variables of state (pressure, temperature, and concentration of components) being present between the volumes. The character of variation of the mixture parameters in the volumes is determined by the balance equations of substance and energy which are written with account for mass and heat transfer through the cross section of the connecting channel. The corresponding fluxes, averaged over the channel cross section, are written in quasi-stationary approximation by ordinary linear equations, relating these fluxes with the gradients of the main macroscopic parameters. The boundary conditions for these equations (at the inlet to and outlet from the channel) correspond to slowly changing values of the parameters in the volumes. The sidewalls of the channel are assumed adiabatically insulated and impermeable for the substance, so the transfer occurs only along the channel axis. More general relations of nonequilibrium thermodynamics which take into account the permeability of sidewalls of a channel for heat transfer were discussed in [60].

In [59], entropy production was calculated within the framework of hydrodynamic approximation. The obtained phenomenological equations of nonequilibrium thermodynamics were also used for the Knudsen regime of gas flow. At the same time, the possibility of applying the methods of nonequilibrium thermodynamics to description of gas flows in channels in the intermediate regime was argued for a long time. The first great success in overcoming these challenges was achieved in [61] where it is shown that kinetic entropy production in gas coincides with phenomenological one. In this case, however, it is necessary to take into account entropy production not only at the expense of intermolecular collisions, but also at the expense of collisions of molecules with the surface of channel walls. We show this in a rather general form without defining specifically the structure of a capillary or a capillary-porous body. First of all we note that, within the framework of the classical nonequilibrium thermodynamics of discontinuous systems [59], linear phenomenological expressions for flow can be obtained by averaging local fluxes of mass and energy over the channel cross section, which, in turn, are found from the ordinary expressions for entropy production in the gas mixture. The procedure of averaging affects only the redetermining of the phenomenological coefficients, for which, as previously, the Onsager relations are valid. The kinetic theory, based on the linearized Boltzmann eqution, allows not only substantiation of such linear relations between the fluxes and thermodynamic forces, but also determination of the explicit form of the kinetic coefficients

of the Onsager matrix. We give the deduction of the expression for entropy production with account for the effect of surface forces [9].

A nonequlibrium state of a multicomponent mixture in the steady-state case is described by a system of the linearized kinetic Boltzmann equations [9, 39]

$$\mathbf{v}_{\alpha\perp}\frac{\partial\Phi_\alpha}{\partial\mathbf{x}_\perp}+v_{\alpha z}\left[\left(\frac{m_\alpha v_\alpha^2}{2kT}-\frac{5}{2}\right)\frac{\nabla_z T}{T}+\frac{\nabla_z p}{p}+\frac{\nabla_z y_\alpha}{y_\alpha}+\frac{U_\alpha(\mathbf{x}_\perp)}{kT}\frac{\nabla_z T}{T}\right]$$
$$=\sum_\beta L_{\alpha\beta}(\Phi_\alpha,\ \Phi_\beta), \tag{3.1}$$

where Φ_α is the correction to the Maxwell distribution function $f_{\alpha 0}$ for the component α, $\mathbf{v}_\alpha$ is the velocity of molecules, p is the pressure, T is the gas temperature, $y_\alpha = n_\alpha / n$ is the molar concentration of the component α, ∇_z is the operator of the gradient along the channel axis (axis z), $\beta_\alpha = m_\alpha / kT$ (m_α is the mass of the component α, k is the Boltzmann constant), U_α ($\mathbf{x}_\perp$) is the potential of interaction of molecules with the surface of channel walls, $L_{\alpha\beta}$ is the Boltzmann linearized collision integral, and $\mathbf{x}_\perp$ is the coordinate in the channel cross section.

We now consider separate components of entropy production which can be obtained on the basis of the system of kinetic equations (3.1). The entropy production caused by intermolecular collisions is given by the following expression [9, 39]:

$$\Delta S_m = -k\sum_\alpha\sum_\beta\int\Phi_\alpha L_{\alpha\beta}(\Phi_\alpha,\Phi_\beta)\,f_{\alpha 0}\,d\mathbf{v}_\alpha = -k[\Phi, L(\Phi)]. \tag{3.2}$$

Replacing $L(\Phi)$ by the left-hand side of the kinetic equation (3.1), integrating with respect to velocities, and averaging over the channel cross section, we obtain

$$<\Delta S_m> = -[<J'_{qz}> + <J_\alpha U_\alpha>]\frac{\nabla_z T}{T^2} - <u_z>\frac{\nabla_z p}{T}$$
$$-\frac{p}{T}\sum_\beta <w_{\beta z}>\, d_{\beta z} - \frac{k}{2\Sigma_c}\oint\,[v_\perp, \Phi^2(l)]dl. \tag{3.3}$$

with integration being done with respect to the perimeter of the channel cross section. Here Σ_c is the cross-sectional area, $v_\perp$ is the component of the velocity of molecules normal to the channel surface, the designation $\langle ... \rangle$ corresponds to the averaging over

the channel cross section. In this case, $u = \sum_{\alpha} C_\alpha u_\alpha$ is the mass-averaged velocity of the mixture, $w_\alpha = u_\alpha - u$ is the diffusion velocity (where u_α is the macroscopic velocity of the component), $C_\alpha = \rho_\alpha / \rho$ is the mass concentration of the component α, $\rho_\alpha = m_\alpha n_\alpha$ is the mass density of the component α, $\rho = \sum_{\alpha} \rho_\alpha$, $J_q' = J_q - \frac{5}{2} \sum_{\alpha=1}^{2} p_\alpha w_\alpha$ is the reduced heat flux, J_q is the heat-flux density, J_α is the flux density of the number of particles of the component α, and p_α is the partial pressure. The quantity d_α is determined as

$$d_\alpha = \nabla y_\alpha - (y_\alpha - C_\alpha) \nabla \ln p . \tag{3.4}$$

The expression for entropy production (3.3) differs form the classical one by the last term on the right-hand side. This term disappears in the limit of both small and large Knudsen numbers. This fact was likely the basis for arguments against the applicability of nonequilibrium thermodynamics at intermediate Knudsen numbers. In [61], however, it was noted that the entropy production (3.3) is not the total entropy production in a gas, since it does not take into account collision of gas molecules with the bounding walls. In the case of adiabatic walls, entropy production in collision of gas molecules with the walls is equal to an inverse flow of entropy from the gas phase to the wall. Calculation of this flux is not complex. The density of the entropy flux calculated by the known formulas of the kinetic theory is [61]

$$J^s = \frac{k}{2} [v , \Phi^2 (R)] + \frac{J_q'}{T} . \tag{3.5}$$

Hence we find the entropy production on the surface of channel walls normalized to the channel cross section

$$< \Delta S_\sigma >= \frac{k}{2\Sigma_{\tilde{n}}} \oint [v_\perp, \Phi^2 (l)] dl \quad . \tag{3.6}$$

As a result, for complete entropy production $\langle \Delta S \rangle = \langle \Delta S_m \rangle + \langle \Delta S_\sigma \rangle$ we have the expression

$$< \Delta S_m >= -[< J'_{qz} > + < J_\alpha U_\alpha >] \frac{\nabla_z T}{T_0^2} - < u_z > \frac{\nabla_z p}{T_0}$$
$$- \frac{p_0}{T_0} \sum_{\beta=1}^{N-1} (< w_{\beta z} > - < w_{Nz} >) d_{\beta z} \ . \qquad (3.7)$$

In the absence of potential interaction of molecules with a wall, expression (3.7) changes over to the well-known result

$$< \Delta S_m >= - < J'_{qz} > \frac{\nabla_z T}{T_0^2} - < u_z > \frac{\nabla_z p}{T_0}$$
$$- \frac{p_0}{T_0} \sum_{\beta=1}^{N-1} (< w_{\beta z} > - < w_{N_z} >) d_{\beta z} \ . \qquad (3.7a)$$

For channels of regular geometry, the kinetic theory allows also distinguishing of one more part of entropy production — surface entropy production. It may have its own phenomenological equations of nonequilibrium thermodynamics. We consider these equations in one of the sections below.

According to the principles of nonequilibrium thermodynamics, based on the expression for entropy production (3.7) we can write the relationships between the fluxes averaged over the cross sections of capillaries or a porous body and the gradients of thermodynamics parameters of a binary gas mixture in the presence or absence of surface forces as [59]

$$\begin{matrix} < u_z > \\ < u_{1z} > - < u_{2z} > \\ < J'_{qz} > + < J_\alpha U_\alpha > \end{matrix} = - \begin{pmatrix} \lambda_{mm} & \lambda_{m1} & \lambda_{mq} \\ \lambda_{1m} & \lambda_{11} & \lambda_{1q} \\ \lambda_{qm} & \lambda_{q1} & \lambda_{qq} \end{pmatrix} \begin{pmatrix} T^{-1} \nabla_z p \\ p T^{-1} d_{1z} \\ T^{-2} \nabla_z T \end{pmatrix} . \qquad (3.8)$$

The effect of surface forces must be taken into account for rather fine channels. Such fluxes will be considered at the end of the present review. Now we focus our attention on the situation when the effect of surface forces can be neglected (though generalization of the given relations to this case does not offers difficulties). In this case, we have

$$\begin{matrix} < u_z > \\ < u_{1z} > - < u_{2z} > \\ < J'_{qz} > \end{matrix} = - \begin{pmatrix} \lambda_{mm} & \lambda_{m1} & \lambda_{mq} \\ \lambda_{1m} & \lambda_{11} & \lambda_{1q} \\ \lambda_{qm} & \lambda_{q1} & \lambda_{qq} \end{pmatrix} \begin{pmatrix} T^{-1} \nabla_z p \\ p T^{-1} d_{1z} \\ T^{-2} \nabla_z T \end{pmatrix}. \tag{3.8a}$$

We transform expression (3.8a) since sometimes it is convenient to use the molar-averaged velocity $u_m = \sum_\alpha y_\alpha u_\alpha$ instead of the mass-averaged velocity of the gas mixture. For a binary mixture of gases it is easy to establish the equality

$$\langle u \rangle = \langle u_m \rangle + \frac{m_1 - m_2}{\rho} n y_1 y_2 (\langle u_1 \rangle - \langle u_2 \rangle). \tag{3.9}$$

Taking into account that

$$d_{1z} = \nabla_z y_1 + \frac{m_2 - m_1}{m_1 y_1 + m_2 y_2} y_1 y_2 \frac{\nabla_z p}{p}, \tag{3.10}$$

we can write the system of phenomenological equations for $\langle u_{mz} \rangle$, $\langle u_{1z} \rangle - \langle u_{2z} \rangle$, and $\langle J'_{qz} \rangle$ in the form [25, 59]

$$\begin{matrix} < u_{mz} > \\ < u_{1z} > - < u_{2z} > \\ < J'_{qz} > \end{matrix} = - \begin{pmatrix} \Lambda_{mm} & \Lambda_{m1} & \Lambda_{mq} \\ \Lambda_{1m} & \Lambda_{11} & \Lambda_{1q} \\ \Lambda_{qm} & \Lambda_{q1} & \Lambda_{qq} \end{pmatrix} \begin{pmatrix} T^{-1} \nabla_z p \\ p T^{-1} \nabla_z y_1 \\ T^{-2} \nabla_z T \end{pmatrix}. \tag{3.11}$$

The kinetic coefficients Λ_{ij} (as well as λ_{ik}) satisfy the Onsager reciprocity relations ($\Lambda_{ij} = \Lambda_{ji}$).

We introduce the flux of the component α, $J_{\alpha D}$, in the system of coordinates, where $\langle u_m \rangle = 0$; in the case of a binary mixture, we have

$$J_{1D} = J_1 - J_m y_1 = n y_1 y_2 [\langle u_1 \rangle - \langle u_2 \rangle], \tag{3.12}$$

where $J_\alpha = n_\alpha \langle u_\alpha \rangle$ and $J_m = n \langle u_m \rangle$.

In the general case, the expression for the diffusion flux of the first component can be written in the form

$$J_{1D} = -nD\left[\nabla\, y_1 + \alpha_p y_1 y_2 \frac{\nabla p}{p} + \alpha_T y_1 y_2 \frac{\nabla T}{T}\right]. \tag{3.13}$$

Here D is the coefficient of diffusion, α_p and α_T are the baro- and thermal diffusion factors of a binary gas mixture.

Comparison of Eqs. (3.13) and (3.11) gives

$$\Lambda_{11} = \frac{T}{py_1y_2} D\,, \quad \Lambda_{1m} = \frac{T}{p} D\alpha_p\,, \quad \Lambda_{1q} = TD\alpha_T\,. \tag{3.14}$$

According to the above-given definition, the total heat flux for a binary mixture is determined by the expression

$$J_q = J_q' + \frac{5}{2} p \sum_{\alpha=1}^{2} y_\alpha < w_\alpha >= J_q' + \frac{5}{2}\frac{p}{\rho}(m_2 - m_1) J_{1D}\,, \tag{3.15}$$

where $p = nkT$.

The second term on the right-hand side of expression (3.15) appears due to the fact that the total heat flux is determined relative to the mass-averaged velocity of the mixture, i.e., in the reference frame, where $\langle u \rangle = 0$. In the reference frame, where the molar-averaged velocity of the mixture is zero ($\langle u_m \rangle = 0$), this term disappears, therefore for the heat flux J_q^m in this reference frame the condition $J_q^m = J_q^{'}$ takes place.

The main aim of the following presentation is to discuss the existing methods and results of calculation of the coefficients Λ_{ij} and application of relations (3.9) and (3.12) in analysis of the kinetic phenomena arising in diffusion of gas mixtures in capillaries and porous media. In the general case, these coefficients are complex functions of effective Knudsen numbers, molar concentrations, masses of the components, effective collision cross sections, and coefficients of accommodation for scattering of molecules on the surface.

The symmetry of the coefficients of the Onsager matrix in the expressions for total fluxes (3.8) and (3.11) can be proved both within the framework of statistical presentation of nonequilibrium thermodynamics and on the level of a purely kinetic approach, if we use the symmetry of the kernel of the collision operator and the kernel

of the operator of scattering of gas molecules by the surface. For flows of a pure gas and binary mixtures, the symmetry of the coefficients Λ_{ik} and λ_{ik} was proved in [28, 29, 62–65]. As is known, in both hydrodinamics and electrodynamics there exist common relations named as the reciprocity theorems [14, 66] which follow directly from the main equations and can be successfully used in specific calculations. Such a situation is also observed in the kinetic theory of gases, where application of the reciprocity relations allows substantial simplification of calculations in solution of specific problems. Besides, the reciprocity theorems make it possible to draw certain conclusions on the properties of the symmetry of kinetic coefficients [14, 67, 68]. The proofs based on the reciprocity theorems do not need use of the concepts of nonequilibrium thermodynamics, therefore they may be treated as an independent confirmation of the Onsager reciprocity relations.

In the kinetic theory, the reciprocity relations were first formulated and used in the works of Waldmann [69–71]. As applied to the problem of a pure gas flow in a capillary they were obtained in [72], and in [73–78] they were used to prove the symmetry of the kinetic coefficients related to external gas flows past solid bodies.

For the case of flow of a multicomponent mixture under the action of differences of pressure Δp and temperature ΔT in a capillary connecting two vessels, the reciprocity theorem takes the form [71, 78]

$$\sum_{\alpha} \int_{\Sigma_w} (\Phi_{\alpha P} I v_{\alpha\perp} \Phi_{\alpha T})\, d\Sigma_w = 0\,, \tag{3.16}$$

where $\Phi_{\alpha P}$ and $\Phi_{\alpha T}$ are the corrections to the Maxwell distributions which correspond to gas mixture flows under the effect of the gradients of pressure and temperature, respectively, and integration is made over the wall surfaces of capillaries and vessels bounding the gas, and I is the operator of inversion in the space of velocities. The reciprocity theorems have a similar form for other cases where, for example, a flow under the action of the concentration gradient is treated as one of the pairs. To write them we only need to substitute Φ_P or Φ_T by the corresponding corrections.

In the considered case of flow of a multicomponent mixture under the action of the differences of pressure Δp and temperature ΔT in a capillary connecting two vessels, integration in (3.16) gives [62]

$$[\langle u_{mT} \rangle\, \Delta p / T_0 - \langle J'_{qP} \rangle\, \Delta T / T_0^2]\, \Sigma_c = 0\,, \tag{3.17}$$

where $\langle u_{mT} \rangle$ and $\langle J'_{qP} \rangle$ are, respectively, the molar velocity of the mixture caused by the temperature gradient and the reduced heat flux due to the pressure gradient — both are mean over the capillary cross section Σ_c.

It can be proved by the reciprocity theorems [72] that integral fluxes are determined by the differences of hydrodynamic parameters at the ends of the capillary and are independent of the character of distribution of these parameters along the capillary length. These theorems, as has already been mentioned, are convenient for proving the symmetry of kinetic coefficients. Thus, using (3.8) and (3.11) we can write

$$\langle u_{mT} \rangle = \Lambda_{mq} \frac{1}{T^2} \frac{\Delta T}{L}, \quad \langle J'_{qp} \rangle = \Lambda_{qm} \frac{1}{T} \frac{\Delta p}{L},$$

where L is the capillary length. Substituting these expressions into (3.17) and taking into account that the differences of temperature and pressure are independent parameters, we come to the condition of symmetry of the kinetic coefficients $\Lambda_{qm} = \Lambda_{mq}$.

4. THE KNUDSEN REGIME (Kn >> 1)

We consider the procedure of calculation of the coefficients in the free-molecular regime for a gas mixture flow in a long cylindrical capillary. It is convenient to use a well-known expression for a number of molecules dn_A which cross the surface element dA per time unit along the line forming the angle φ with the normal to the surface and having the velocity in the range from v to $v + dv$ within the spherical angle $d\omega$

$$dn_A = n (\beta / \pi)^{3/2} \exp(-\beta v^2) v^3 \cos\varphi d\omega dv dA . \tag{4.1}$$

Here n is the number density of molecules, $\beta = m / 2kT$, m is the molecule mass, and k is the Boltzmann constant.

For the flow of energy transferred by the same molecules we have

$$d\varepsilon_A = \frac{mv^2}{2} dn_A . \tag{4.2}$$

Integration of equalities (4.1) and (4.2) with respect to velocities gives total fluxes of particles and energy through the surface dA within the spherical angle $d\omega$

$$dN_A = \frac{n}{4\pi} \langle v \rangle \cos\varphi d\omega dA ,$$
$$dE_A = 2kTdN_A , \tag{4.3}$$

where $\langle v \rangle = (8kT/\pi m)^{1/2}$ is the mean thermal velocity of gas molecules.

Let dA be the surface element of the cross section of a long cylindrical tube. For small gradients of density and temperature for two cross sections lying at a distance z from each other we approximately have

$$n'(T')^{1/2} \approx nT^{1/2} + z\nabla_z (nT^{1/2}) ,$$
$$n'(T')^{3/2} \approx nT^{3/2} + z\nabla_z (nT^{3/2}) . \tag{4.4}$$

Following the well-known procedure of calculation of the number of molecules crossing dA after the last collision of them with the surface element of the tube at a distance z from the given cross section [35], we can find the expression for the fluxes of the component α and of its energy through the surface unit of the capillary cross section of the following form:

$$J_\alpha = n_\alpha \langle u_\alpha \rangle = -D_{\alpha K} T^{-1/2} \nabla_z (n_\alpha T^{1/2}) ,$$
$$J_{E\alpha} = -2kD_{\alpha K} T^{-1/2} \nabla_z (n_\alpha T^{1/2}) . \tag{4.5}$$

Here $D_{\alpha K}$ is the so-called Knudsen coefficient of diffusion of the component α. For a cylindrical capillary of radius R we have [79]

$$D_{\alpha K} = \frac{2}{3} R \langle v_\alpha \rangle b_\alpha , \tag{4.6}$$

where $\langle v_\alpha \rangle = (8kT/\pi m_\alpha)^{1/2}$ and $b_\alpha = (2-\kappa_\alpha)/\kappa_\alpha$, κ_α is the fraction of molecules diffusely reflected by a capillary wall (the coefficient of accommodation of the tangential momentum).

It is convenient to rewrite Eq. (4.5) in the form

$$J_\alpha = -\frac{D_{\alpha K}}{kT}\left(p\nabla_z y_\alpha + y_\alpha \nabla_z p - \frac{1}{2} y_\alpha \frac{p}{T}\nabla_z T \right),$$
$$J_{E\alpha} = -2D_{\alpha K}\left(p\nabla_z y_\alpha + y_\alpha \nabla_z p - \frac{1}{2} y_\alpha \frac{p}{T}\nabla_z T \right). \tag{4.7}$$

Using Eqs. (4.7) for determination of the reduced heat flux, $\langle J_q' \rangle = \sum_\alpha J_{E\alpha} - \frac{5}{2} kTJ_m$ and the values of $\langle u_m \rangle$ and $\langle u_1 \rangle - \langle u_2 \rangle$, in the case of a binary gas mixture ($\alpha = 1.2$) we have

$$\Lambda_{mm} = \frac{T}{p}(D_{1K} y_1 + D_{2K} y_2), \qquad \Lambda_{11} = \frac{T}{p y_1 y_2}(D_{1K} y_2 + D_{2K} y_1),$$
$$\Lambda_{1m} = \Lambda_{m1} = \frac{T}{p}(D_{1K} - D_{2K}), \qquad \Lambda_{1q} = \Lambda_{q1} = -\frac{1}{2} p\Lambda_{1m},$$
$$\Lambda_{qm} = \Lambda_{mq} = -\frac{1}{2} p\Lambda_{mm}, \qquad \Lambda_{qq} = \frac{9}{4} p^2 \Lambda_{mm}. \tag{4.8}$$

For the coefficients in the expression for the diffusion fluxes of component 1 (3.14) we find

$$D = D_{12}^K = D_{1K} y_2 + D_{2K} y_1 = \frac{y_1 y_2 p}{T}\Lambda_{11},$$
$$\alpha_p^K = \frac{D_{1K} - D_{2K}}{D_{12}^K} = \frac{m_2^{1/2} b_1 - m_1^{1/2} b_2}{(m^{1/2} b)_y}, \quad \alpha_T^K = -\frac{1}{2}\alpha_p^K, \tag{4.9}$$

where

$$(m^{1/2} b)_y = m_1^{1/2} b_2 y_1 + m_2^{1/2} b_1 y_2 .$$

In contrast to the ordinary diffusion in the opposite limit (Kn << 1), the coefficient of Knudsen diffusion does not depend on pressure, it is proportional to the capillary radius and depends on the coefficient of accommodation κ_α. It is also important that in the Knudsen regime the barodiffusion and thermal diffusion factors are related by a simple expression $\alpha_T^K = -(1/2)\,\alpha_p^K$. All obtained relations hold also for homogeneous and isotropic porous media. In this case [80],

$$D_{\alpha K} = \frac{4}{3} K_0 \langle v_\alpha \rangle , \tag{4.10}$$

where K_0 is the constant characterizing a porous medium. A value of K_0 can be obtained from measurements of the gas permeability of a porous medium in the Knudsen flow regime.

5. DIFFUSION AND HEAT TRANSFER IN A VISCOUS MIXTURE FLOW

To analyze diffusion transfer in a gas mixture at small Knudsen numbers (a viscous flow regime) we use the equations of momentum transfer (the equation of motion) for the component α [40, 81]

$$\rho_\alpha \frac{d_\alpha u_\alpha}{dt} + \nabla p_\alpha + div\hat{\pi}_\alpha - n_\alpha F_\alpha = R_\alpha , \tag{5.1}$$

where $d_\alpha / dt \equiv \partial / \partial t + (u_\alpha \nabla)$, $p_\alpha = n_\alpha kT$ is the partial pressure, $(div\hat{\pi}_\alpha)_i = \partial \pi_{\alpha ij} / \partial x_j$ corresponds to the i-th component of the "viscous friction force" acting on the component α in the volume unit, and F_α is the external force acting on the molecule of species α.

The partial tensor of viscous stresses is expressed in terms of the derivatives of the mass-averaged velocity

$$\pi_{\alpha ij} = -\eta_\alpha W_{ij} , \tag{5.2}$$

where $W_{ij} = \partial u_i / \partial x_j + \partial u_j / \partial x_i - (2/3)\, \delta_{ij} \partial u_l / \partial x_l$ and η_α is the partial coefficient of viscosity (not to be mixed with the viscosity of a pure component) that is determined such that the mixture viscosity $\eta = \sum_\alpha \eta_\alpha$. The term R_α on the right-hand side of (5.1) expresses the mean variation of the momentum of molecules of species α in intermolecular collisions ("diffusion force of friction").

In the simplest approximation of the kinetic theory [79] R_α is given by the expression

$$R_\alpha = -\sum_\beta \frac{n_\alpha n_\beta kT}{n [D_{\alpha\beta}]_1} (u_\alpha - u_\beta) , \tag{5.3}$$

where $[D_{\alpha\beta}]_1$ is the coefficient of the binary diffusion of the components α and β in the first approximation of the Chapman–Cowling theory [82].

For the case of slow stationary flows, we can drop the first (inertia) term on the left-hand side of the equation of motion (5.1) and write this equation with account for (5.2) in the form

$$\frac{\partial p_\alpha}{\partial x_i} - \eta_\alpha \frac{\partial W_{ij}}{\partial x_j} - n_\alpha F_{\alpha i} = R_{\alpha i}. \tag{5.4}$$

Thanks to the condition $\sum_\alpha R_\alpha = 0$, summation of (5.4) over all mixture components yields

$$\eta \frac{\partial W_{ij}}{\partial x_j} = \frac{\partial p}{\partial x_i} - \sum_\alpha n_\alpha F_{\alpha i}. \tag{5.5}$$

Substituting (5.5) into (5.4), we find

$$\sum_\beta \frac{n_\alpha n_\beta kT}{n[D_{\alpha\beta}]_1}(u_{\alpha i} - u_{\beta i}) = -\left(\frac{\partial p_\alpha}{\partial x_i} - \frac{\eta_\alpha}{\eta}\frac{\partial p}{\partial x_i}\right) + \left(n_\alpha F_{\alpha i} - \frac{\eta_\alpha}{\eta}\sum_\alpha n_\alpha F_{\alpha i}\right). \tag{5.6}$$

Equation (5.6) was obtained for the first time in [40] within the framework of the 10-moment Grad approximation. More general equations of the 13-moment approximation [40, 81] involve the thermal diffusion terms and corrections of the second approximation to the coefficients of diffusion and barodiffusion. Account of thermal diffusion corresponds to the appearance of the following term on the right-hand side of Eq. (5.6):

$$-\sum_\beta y_\alpha y_\beta \alpha^T_{\alpha\beta} \partial \ln T / \partial x_i,$$

where $\alpha^T_{\alpha\beta}$ is the generalized thermal diffusion factors for a multicomponent mixture. The expression for $\alpha^T_{\alpha\beta}$ can be presented as [81]

$$\alpha^T_{\alpha\beta} = \frac{\mu_{\alpha\beta} T}{[D_{\alpha\beta}]_1}\left(\frac{6}{5}C^*_{\alpha\beta} - 1\right)\left(\frac{\lambda_\beta}{m_\beta y_\beta} - \frac{\lambda_\alpha}{m_\alpha y_\alpha}\right). \tag{5.7}$$

Here $\mu_{\alpha\beta} = m_\alpha m_\beta / (m_\alpha + m_\beta)$ is the reduced mass of particles of species α and β, $C^*_{\alpha\beta}$ is the coefficient greatly dependent on the character of intermolecular interaction [39], and λ_α is the partial thermal conductivity determined such that $\lambda = \sum_\alpha \lambda_\alpha$ is the total thermal conductivity of mixture. We consider diffusion transfer along z in a binary gas mixture. In the absence of external forces, the expression for the diffusion flux J^{as}_{1D} takes the form

$$J^{as}_{1D} = -n[D_{12}]_1 \left(\nabla y_1 + [\alpha^v_p] y_1 y_2 \nabla \ln p + [\alpha_T] y_1 y_2 \nabla \ln T \right), \tag{5.8}$$

where $[\alpha_T]_1 = \alpha^T_{12}$ and for $[\alpha^v_p]_1$ we have [40]

$$[\alpha^v_p]_1 = \frac{1}{\eta} \left(\frac{\eta_2}{y_1} - \frac{\eta_1}{y_2} \right). \tag{5.9}$$

The supercript "as" indicates that corresponding fluxes are determined in the gas volume at a distance from the wall, i.e., without account for the Knudsen layer on the wall (see below). The expressions for partial viscosity and thermal conductivity, which are necessary for the calculation of α^v_p and α_T, can be found in [40, 81].

We also present the expression for the total heat flux in a viscous flow for the case of a binary mixture, which is obtained in the 13-moment approximation [9, 40]

$$J^{as}_q = -\lambda \nabla T + \frac{5}{2} kT(n_1 w_1 + n_2 w_2) + kT[\alpha_T]_1 J_{1D} + \frac{2}{5} \sum_{\alpha=1}^{2} \frac{\eta_\alpha \lambda_\alpha}{\eta p_\alpha} \nabla p \tag{5.10}$$

Here λ and $[\alpha_T]_1$ are, respectively, the thermal conductivity and the thermal diffusion factor of a binary mixture, the expressions for which can be found in [39, 81]. The last term on the right-hand side of (5.10) corresponds to the Burnett contribution which can also be obtained within the framework of an ordinary Chapman–Enskog procedure [9, 81].

We note that the modified expression for the barodiffusion factor in a viscous flow $[\alpha^v_p]_1$ turns to be much more complex than the known expression:

$$\alpha_p = (m_2 - m_1) / (m)_y, \quad (m)_y = m_1 y_1 + m_2 y_2, \tag{5.11}$$

Table 1: Barodiffusion factor of gas mixtures

Mixture	α_p^k	α_p	$[\alpha_p^v]_1$	$[\overline{\alpha}_p]_1$
H_2–Ar	1.2686	1.8092	1.3399	1.3043
He–Ar	1.0383	1.6357	0.9004	0.9694
N_2–Ar	0.1770	0.3512	0.2425	0.2098
H_2–N_2	1.1566	1.7335	1.1863	1.1715
D_2–He	0.0003	0.0006	0.1865	0.0934
Ar–CO_2	0.0484	0.0968	–0.1326	–0.0421
N_2–C_2H_4	0.0002	0.0004	–0.2215	–0.1106
Ne–C_2H_4	0.1638	0.3254	–0.3275	–0.0818

that follows form an ordinary (Burnett) approximation of the Chapman–Enskog theory [81]. In the general case, α_p^v appears to be the function of not only the masses of molecules and relative concentrations of components, but also of the ratios of effective cross sections of scattering of molecules.

Table 1 gives the values of the coefficients α_p^k, α_p^v, and α_p, which are calculated for some specific gas mixtures using the parameters of interaction of the Lennard-Jones potential and are borrowed from [38]. Concentrations of the components are assumed to be the same ($y_1 = 0.5$), the component with the subscript 1 correspond to lighter molecules. The last column gives the values of the barodiffusion factor in a capillary $\overline{\alpha}_p$ calculated with account for contribution of Knudsen layers (see expression (6.20) in Section 6). An appreciable difference in the masses of molecules is characteristic for the first four mixtures in the table which provides a relative closeness of the values of α_p^K, α_p^v, and $\overline{\alpha}_p$. The next four mixtures are characterized by both a relative closeness of masses and the difference in the effective cross sections of scattering of molecules. This leads to a noticeable difference of α_p^v and $\overline{\alpha}_p$ from α_p^K and α_p and even to the change in the sign of these quantities. It is just these mixtures for which accurate results of the kinetic theory become substantial.

It is also useful to give approximate expressions for a mixture with a small relative difference of masses and effective cross sections of scattering of molecules of the components that are obtained by expansion of the general expressions into a series with respect to small parameters. The barodiffusion factors α_p^K and α_p in this case are

$$\alpha_p^K \cong \frac{m_2 - m_1}{m_2 + m_1}, \quad \alpha_p \cong 2\frac{m_2 - m_1}{m_2 + m_1}. \tag{5.12}$$

The use of the model of molecules–hard spheres with diameters d_1 and d_2 — in calculation of α_p^v gives

$$[\alpha_p^v]_1 \cong 1.13\,(m_2 - m_1)/(m_2 + m_1) - 1.50\,(d_2 - d_1)/(d_2 + d_1) \tag{5.13}$$

An account for corrections of the second approximation to the barodiffusion factor α_p^v substitutes the numerical coefficients 1.13 and 1.50 for 1.41 and 1.26.

6. TRANSFER PHENOMENA IN A CAPILLARY AT INTERMEDIATE KNUDSEN NUMBERS

Calculation of the coefficients Λ_{ik} at arbitrary Knudsen numbers for channels of different geometry (a plane channel, a long cylindrical channel, etc.) is usually based on the use of the linearized kinetic Boltzmann equation with assignment of the corresponding boundary conditions for the distribution function on channel walls. In this case, the model presentation of the collision integral (the BGK model [5] or *S*-model [83] for a pure gas, the Hamel–Oguchi model [84] or the McCormak model [75] for a gas mixture) is used as a rule. A review of different methods of solution of the linearized Boltzmann equation, which are used for determining the fluxes of mass and energy (averaged over the channel cross section) in the case of a pure gas, can be found in [22].

For the case of an isothermal gas-mixture flow ($\nabla_z T = 0$) the expressions for averaged fluxes of mixture components in a round cylindrical channel were obtained in [86, 87] using the model collision integral in the Hamel–Oguchi form. In this case, for solution of the system of integral equations obtained from the model kinetic equations by integration with respect to the characteristics [5, 87] and written for longitudinal velocities of the components, the variational method [7] (or the Bubnov–Galerkin method [88]) is used. The choice of the trial function for distribution of velocities over the channel cross section in the form of the constant provides transition to exact solutions within a free-molecular mixture flow (Kn >> 1). To obtain satisfactory results in the other limiting region (Kn << 1) it suffices to use the quadratic trial function.

Unfortunately, the BGK model (or the Hamel–Oguchi model for a gas mixture) does not guarantee simultaneous correct description of mass and heat transfer in a gas and, in particular, does not allow for the effects of thermal diffusion in a mixture. In this case, more suitable is the McCormak model [85] (or the generalized Gross–Jackson model [89]) that is based on the equivalency of the N-th order moments from the accurate and model collision integrals. The use of this model allows one to obtain rather correct expressions for diffusion and heat transfer within a hydrodynamic limit. For the case of an isothermal gas flow in plane and cylindrical channels on the basis of the McCormak model the effects of viscous slip, diffusion slip, and barodiffusion in a mixture at small Knudsen numbers were studied by the method of total momenta [23]. The same model (or the 3-rd order Gross–Jackson model) was used in [24] for calculation of macroscopic velocities of the mixture components in an isothermal flow in a capillary at intermediate Knudsen numbers by a numerical method of solution of the system of integral equations. The expressions for all coefficients Λ_{ik} at arbitrary Knudsen numbers are obtained in [90] for the case of a nonisothermal motion of mixture on the basis of solution of the system of integral-moment equations by the Bubnov–Galerkin method.

In [91, 92], these coefficients were calculated for a flow of some specific mixtures of inert gases in plane and cylindrical channels by applying the method of discrete velocities to the solution of the linearized kinetic equation by the McCormak model.

The expressions obtained in [90] are the complex functionals of the well-known Abramowitz functions [93] and a thorough analysis of their dependence on the parameters of mixture molecules, relative concentration of components, and the Knudsen number turns to be rather laborious in a general case. In what follows, we consider more illustrative expressions obtained within the limit of relatively small Knudsen numbers corresponding to a viscous regime of the flow with a slip.

In the hydrodynamic limit (Kn << 1), a mass-averaged velocity of the gas mixture in a round cylindrical channel of radius R is determined by the expression [94]

$$u_{hz}(r) = -\frac{1}{4\eta}(R^2 - r^2)\nabla_z p + u_z^{as}(R), \tag{6.1}$$

where an ordinary sticking condition ($u_{hz}(R) = 0$) is substituted by the condition which envisages the difference of the tangential velocity of gas on the wall from zero. Actually, the case in point is some dummy velocity of gas on the wall (slip velocity) the assignment of which provides a correct limiting transition to the values of the velocity at a distance from the wall and which is determined by an ordinary

Navier–Stokes equation [5]. The slip velocity on the wall was determined in a great number of works using different methods of solution of the linearized kinetic Boltzmann equation with model and exact collision integrals. For a binary gas mixture, the general expression for the slip velocity takes the form [22, 23]

$$u_\tau^{as} = A_p \frac{\partial u_\tau^{as}}{\partial x_n} + A_T \frac{\partial T}{\partial x_\tau} - \sigma_{12}^{(v)} y_1 y_2 (u_{1\tau}^{as} - u_{2\tau}^{as}), \tag{6.2}$$

where the derivatives are taken along the normal (x_n) and tangential (x_τ) coordinates to the surface and the difference of velocities corresponds to asymptotic values, i.e., to the solution at a distance from the wall ($x \to \infty$). The coefficients A_p, A_T, and $\sigma_{12}^{(v)}$ are called the coefficients of viscous, thermal, and diffusion slip. In the general case, there also exists a "second-order slip" related to the non-zero second derivative of velocity along the normal coordinate. In addition to the second-order slip, when allowing for the corresponding corrections to the Knudsen number for the cylindrical channel, we should take into account the dependence of the coefficients A_p, A_T, and $\sigma_{12}^{(v)}$ on the surface curvature [95–98].

For the mass-averaged velocity of the mixture (averaged over the capillary cross section) we have

$$< u_{hz} >= -\frac{1}{\eta}\left(\frac{R^2}{8} + A_p \frac{R}{2}\right)\nabla_z p + A_T \nabla_z T - \frac{\sigma_{12}^{(v)}}{n} < J_{1D}^{as} > , \tag{6.3}$$

where

$$\langle J_{1D}^{as} \rangle = n y_1 y_2 (u_{1\tau}^{as} - u_{2\tau}^{as})$$

is determined by expression (5.8).

When writing (6.3), we used the relation

$$\frac{\partial u_\tau^{as}}{\partial x_n} = -\left.\frac{\partial u_{hz}}{\partial r}\right|_{r=R} = \frac{1}{2\eta} R \nabla_z p . \tag{6.4}$$

Often, it turns to be more convenient to use expressions for the molar-averaged velocity of mixture in a channel. By virtue of condition (3.9) relating u and u_m, for

the molar-averaged velocity $\langle u_{mz} \rangle$ in a capillary with account for determination of the diffusion flux (5.8) we have

$$< u_{mz} >= -\frac{1}{\eta}\left(\frac{R^2}{8} + A_p \frac{R}{2}\right)\nabla_z p + A_T \nabla_z T + \sigma_{12} D_{12} \times [\nabla_z y_1 + \alpha_p^{v} y_1 y_2 \nabla \ln p + \alpha_T y_1 y_2 \nabla \ln T], \tag{6.5}$$

where

$$\sigma_{12} = \sigma_{12}^{(v)} + \frac{m_1 - m_2}{(m)_y}.$$

The coefficients A_p, A_T, and $\sigma_{12}D_{12}$ are proportional to the effective mean free path of molecules l, since their calculation is closely related to the account for the behavior of the distribution function in a thin Knudsen layer with a thickness of several free paths. In the case of a pure gas, it is convenient to define l by the expression

$$l = \frac{\sqrt{\pi}}{2}\frac{\eta}{p}\left(\frac{2kT}{m}\right)^{1/2}, \tag{6.6}$$

where η is the gas viscosity, and to introduce the dimensionless slip coefficients [22]

$$\sigma_p = \frac{\sqrt{\pi}}{2l} A_p, \quad \sigma_T = \frac{1}{l}\left(\frac{\pi m T}{2k}\right)^{1/2} A_T. \tag{6.7}$$

A review of the methods and results of calculation of the coefficients σ_p and σ_T can be found in [22, 99].

The simplest result is obtained when the Maxwell method is used and when it is assumed that the distribution function of molecules falling on the wall remains the same as that at a distance from the wall. In the case of completely diffuse reflection of molecules from the wall, when the coefficient of accommodation of the momentum of molecules $\kappa = 1$, we have

$$\sigma_p = \frac{\sqrt{\pi}}{2} = 0.8862, \quad \sigma_T = 0.75,$$

More exact expressions which allow for variation of the distribution function in the Knudsen layer can be obtained using the variational method of solution of the linearized Boltzmann equation [7, 100]. The simplest choice of the trial function in this method (equivalent to the use of the generalized Maxwell method or the approximate Loyalka method [101]) in the case of a pure gas and for the specular-diffuse model of scattering of molecules on a wall ($\kappa \neq 1$) leads to the results [102]

$$\sigma_p = \frac{2 - \kappa}{\kappa} 0.8862\,(1 + 0.1366\kappa)\,, \quad \sigma_T = 0.75\,(1 + 0.5\kappa)\,. \tag{6.8}$$

For $\kappa = 1$ we have

$$\sigma_p = 1.007\,, \quad \sigma_T = 1.125\,.$$

These values turn to be close to exact values obtained by the numerical methods for the BGK model [7]

$$\sigma_p = 1.016\,, \quad \sigma_T = 1.149\,.$$

For the model of molecules–hard spheres the numerical methods of integration of the kinetic equation give [103]

$$\sigma_p = 0.985\,, \quad \sigma_T = 1.015\,.$$

The results of calculation of the slip coefficients for a pure gas by other methods (the method of elementary solutions, method of half-space moments, etc.) can be found in [7, 22, 99].

We also present the results for A_p and A_T for the case of a binary gas mixture. Here the use of the ordinary Maxwell method gives [104, 105]

$$A_p = \left(\frac{\pi kT}{2}\right)^{1/2} \frac{1}{(m^{1/2})_y} \frac{\eta}{p}\,, \quad A_T = \frac{1}{5} \frac{(m^{3/2})_y}{(m^{1/2})_y\,(m)_y} \frac{\lambda}{p}\,, \tag{6.9}$$

where η and λ are, respectively, the viscosity and thermal conductivity of the gas mixture.

More accurate results obtained by the variational method for the case of the specular-diffuse and more general models of scattering of molecules on a wall can be found in [106, 107].

Of special interest are the expressions for the coefficient of diffusion slip σ_{12} that was calculated by different methods in a number of works. The idea of diffusion slip was first presented by Kramers and Kistemaker [108]. The elementary considerations equivalent to the Maxwell method lead to the result

$$\sigma_{12} = \frac{m_1^{1/2} - m_2^{1/2}}{(m^{1/2})_y}. \tag{6.10}$$

The verified expressions obtained by the Grad 13-moment approximation for the distribution function at a distance from the wall were considered in [104, 105]. More acceptable, however, are the expressions obtained by the variational method [106, 107] (or by the approximate Loyalka method [101, 109]) or by the method of full and half-space moments [23, 110, 111]. In [112], the coefficient of diffusion slip was calculated on the basis of the direct numerical integration of the linearized kinetic equation for the model of molecules–hard spheres.

In what follows, we present a value of σ_{12} obtained by the variational method [106] for the case of fully diffuse scattering of molecules on the wall (neglecting the corrections of the second approximation to the kinetic coefficients)

$$\sigma_{12} = \frac{1}{2}\left[\frac{m_1^{1/2} - m_2^{1/2}}{(m^{1/2})_y} + \frac{1}{\eta}\left(\frac{\eta_1}{y_1} - \frac{\eta_2}{y_2}\right)\right]. \tag{6.11}$$

General expressions for the coefficient of diffusion slip with an arbitrary character of scattering of molecules on the wall can be found in [106, 109, 111, 113].

We now consider the problem of obtaining the expression for the diffusion flux in the mixture (averaged over the capillary cross section) with account for the boundary condition on the channel wall. For this sake we use Eq. (5.1). For a stationary isothermal flow in the cylindrical channel in the absence of external forces Eq. (5.1) can be rewritten in the form

$$\nabla_z p + \frac{1}{r}\frac{\partial}{\partial r}(r\pi_{\alpha rz}) = \sum_{\beta=1}^{N} \frac{n_\alpha n_\beta kT}{n[D_{\alpha\beta}]_1}(u_{\alpha z} - u_{\beta z}). \tag{6.12}$$

Integration of (6.12) for r going from 0 to R leads, in the case of a binary mixture, to the following expression for the averaged diffusion flux

$$< J_{1D} >= -n[D_{12}]_1 \left[\nabla_z y_1 + \frac{y_1}{p}\nabla_z p + \frac{2}{pR}\pi_{1rz}(R)\right] . \tag{6.13}$$

A value of the partial tensor of viscous stresses on the inner surface of the capillary differs from its value at a distance from the wall. The latter is given by the expression

$$\pi_{1rz}^{as} = -\frac{r}{2}\frac{\eta_1}{\eta}\nabla_z p .$$

Calculation of $\pi_{1rz}(R)$ with account for variation of the distribution function in the Knudsen layer on the basis of the modified Maxwell method at $\kappa_1 = \kappa_2 = 1$ gives [114]

$$\pi_{1rz}(R) = -\frac{R}{4}\left[\frac{m_1^{1/2} y_1}{(m^{1/2})_y} + \frac{\eta_1}{\eta}\right] + \frac{1}{4} n \left(\frac{8kT}{\pi}\right)^{1/2} \frac{m_1^{1/2} m_2^{1/2}}{(m^{1/2})_y}(u_{1z}^{as} - u_{2z}^{as}) . \tag{6.14}$$

Substittion of (6.14) into (6.13) leads to the result

$$J_{1D} = -n\,[D_{12}]_1 \left(\nabla_z y_1 + [\bar{\alpha}_p]_1 y_1 y_2 \frac{1}{p}\nabla_z p\right), \tag{6.15}$$

where

$$[\bar{\alpha}_p]_1 = \frac{1}{2}\left([\alpha_p^K]_1 + [\alpha_p^v]_1\right). \tag{6.16}$$

This expression was obtained by another method in [28]. Comparison of (6.16) and (6.11) shows that the equality $[\bar{\alpha}_p]_1 = -\sigma_{12}$ takes place. Thus, the fulfillment of the reciprocity Onsager relations $\Lambda_{1m} = \Lambda_{m1}$ is confirmed by direct kinetic calculation.

As for the thermal diffusion term in the expression for $\langle J_{1D}\rangle$, it remains unchanged in the considered approximation during averaging. If we also take into account the second-approximation corrections to the kinetic coefficients, then instead of (6.15) we have [113]

$$< J_{1D} >= -n[D_{12}]_2 \left(\nabla_z y_1 + [\bar{\alpha}_p]_2 y_1 y_2 \frac{1}{p} \nabla_z p + [\alpha_T]_1 y_1 y_2 \frac{1}{T} \nabla_z T \right) . \tag{6.17}$$

In this case, for the barodiffusion factor there still holds expression (6.16) where $[\alpha_p^v]_1$ must be replaced by $[\alpha_p^v]_2$ [23] and $[\alpha_p^K]_1$ by $[\alpha_p^K]_2 - \delta$, where δ is the correction to the coefficient of diffusion slip which was calculated in [105].

For the case of mixture with slightly differing masses and effective diameters of molecules of the components and also with a small difference of the coefficients of accommodation, using the model of molecules–hard spheres we have [113, 115]

$$[\bar{\alpha}_p]_2 = (1.1441 + 0.1303\bar{\kappa}) \frac{m_2 - m_1}{m_1 + m_2} + (0.0678 - 0.6653\bar{\kappa}) \frac{d_2 - d_1}{d_2 + d_1}$$
$$+ (1.9322 - 0.0339\bar{\kappa}) \frac{\kappa_2 - \kappa_1}{\kappa_2 + \kappa_1}. \tag{6.18}$$

For $\kappa_2 = \kappa_1 = 1$ we obtain

$$[\bar{\alpha}_p]_2 = 1.274 \frac{m_2 - m_1}{m_1 + m_2} - 0.5975 \frac{d_2 - d_1}{d_2 + d_1}. \tag{6.18a}$$

Comparison of $[\alpha_p^v]_2$ and $[\bar{\alpha}_p]_2$ shows a close dependence of these parameters on the difference of masses of molecules and a twice smaller dependence on the difference in cross sizes of scattering of molecules.

The expressions for $\langle u_{mz} \rangle$ and $\langle J_{1D} \rangle$ obtained above allow one to find a form of the coefficients Λ_{ik} in the capillary for the viscous flow regime with a slip. Comparison with (3.8) gives

$$\Lambda_{11} = \frac{T}{p y_1 y_2} D_{12} , \quad \Lambda_{1q} = T \alpha_T D_{12},$$
$$\Lambda_{1m} = \frac{T}{p} \bar{\alpha}_p D_{12}, \qquad \Lambda_{m1} = -\frac{T}{p} \sigma_{12} D_{12}, \tag{6.19}$$
$$\Lambda_{mm} = T \left[\frac{1}{\eta} \left(\frac{R^2}{8} + A_p \frac{R}{2} \right) - \sigma_{12} \alpha_p^v D_{12} \frac{y_1 y_2}{p} \right].$$

The above analysis of the terms related to slip effects turns to be incomplete. It was shown in [27–29] that the boundary conditions to the equations of motion of a mixture in a capillary include, along with the slip velocity, the so-called Burnett

terms and flows localized in the Knudsen layer. The latter represent some moments of the Knudsen part of the distribution function (i.e., differences between the true distribution function and the distribution function at a distance from the wall) that are calculated directly on the channel wall. An example of such simultaneous account for the Barnett terms and contribution of the Knudsen layer to diffusion transfer in the channel (calculation of $\pi_{1rz}(R)$ on the wall) was demonstrated above in calculation of the averaged diffusion flow (6.17). In the general case, expressions for the mass-aversged velocity $\langle u_z \rangle$, diffusion flow $\langle J_{1D} \rangle$, and heat flux in a binary mixture $\langle q_z \rangle$ — all averaged over the cross section of the cylindrical capillary — can be presented in the form [27, 29]

$$\begin{aligned} < u_z > &= -\frac{R^2}{8\eta} + u_z^{as}(R) + \frac{1}{\rho} j_m \ , \\ < J_{1D} > &= J_{1D}^{as} + n y_1 y_2 \left(\frac{j_{w1}}{n_1} - \frac{j_{w2}}{n_1} \right) , \\ < J_{qz} > &= J_{qz}^{as} + j_q \ . \end{aligned} \tag{6.20}$$

We note that contribution of Burnett terms has already been taken into account in the expressions for J_{1D}^{as} (5.8) and J_{qz}^{as} (5.10). As for j_m, $j_{w\alpha}$, and j_q, they are determined with the help of the Knudsen part of the distribution function $f_{0\alpha}\varphi_\alpha$ by the expressions [29]

$$\begin{aligned} \frac{j_m}{\rho} &= \frac{kT}{\eta} \frac{1}{R} [v_z \Phi_B v_r \varphi(R)] = \frac{1}{\Sigma_c} \int\limits_{\Sigma_c} d\Sigma_c \int \sum_\alpha \frac{m_\alpha}{\rho} v_{\alpha z} f_{\alpha 0} \varphi_\alpha dv \ , \\ \frac{j_{w\alpha}}{n_\alpha} &= \frac{2}{\eta} \frac{1}{R} [v_z \Phi_d^\alpha v_r \varphi(R)] = \frac{1}{\Sigma_c} \int\limits_{\Sigma_c} d\Sigma_c \int \frac{1}{n} \sum_\beta \frac{n}{n_\beta} (\delta_{\beta\alpha} - \frac{\rho_\alpha}{\rho}) v_{\beta z} f_{\beta 0} \varphi_\beta dv_\beta \ , \\ \frac{j_q}{kT} &= \frac{2}{R} [v_z \Phi_t v_r \varphi(R)] = \frac{1}{\Sigma_c} \int\limits_{\Sigma_c} d\Sigma_c \int \sum_\alpha \left(\frac{m_\alpha v_\alpha^2}{2kT} - \frac{5}{2} \right) v_{\alpha z} f_{\alpha 0} \varphi_\alpha dv \ , \end{aligned} \tag{6.21}$$

where in the expressions including [...] integration is fulfilled only with respect to velocities and a value of the Knudsen distribution function on the surface of capillary walls is taken, and on the right-hand side of subsequent expressions integration is made over the capillary cross section. In this case, Φ_t and Φ_d^α are the Chapman–Enskog solutions for the problem of heat conduction and diffusion of a gas mixture,

Φ_B is the Burnett solution of the kinetic problem for the Poiseuille flow. In expressions (6.21), only near-wall layers make contribution to the fluxes j_m, j_{w_α}, and j_q, since the Knudsen function $f_{0_\alpha}\varphi_\alpha$ differs from zero at distances of the order of free path l from the surface of capillary walls.

The moments of the distribution function on the channel wall or fluxes that are localized in the Knudsen layer were calculated in a number of works [23, 28, 63, 113–116]. First we consider a pure gas. In this case, relations (3.8) take the form

$$\langle u_z \rangle = -\Lambda_{mm} \frac{\nabla_z p}{T} - \Lambda_{mq} \frac{\nabla_z T}{T^2},$$

$$\langle J_{qz} \rangle = -\Lambda_{qm} \frac{\nabla_z p}{T} - \Lambda_{qq} \frac{\nabla_z T}{T^2}. \tag{6.22}$$

We present the expressions for Λ_{ik} that follow from (6.20) and (6.21) and that are calculated by the variational method [63, 113]

$$\Lambda_{mm} = \frac{R^2 T}{8\eta}\left(1 + 4\sigma_p \,\mathrm{Kn} + 2\kappa\,\mathrm{Kn}^2 - \frac{20}{3\sqrt{\pi}}\mathrm{Kn}^3\right),$$

$$\Lambda_{mq} = -\frac{\eta T}{\rho}\sigma_T\left[1 - \frac{4}{\sqrt{\pi}}\frac{1}{1+0.5\kappa}\mathrm{Kn}\right],$$

$$\Lambda_{qm} = -\frac{1}{5}\frac{\lambda T^2}{p}\left[1 + 0.5\kappa - \frac{4}{\sqrt{\pi}}\mathrm{Kn}\right],$$

$$\Lambda_{qq} = \lambda T\left(1 - \frac{9}{5}\frac{\kappa}{\sqrt{\pi}}\mathrm{Kn}\right). \tag{6.23}$$

Here $\lambda = (15/4)(k/m)\eta$ is the gas thermal conductivity; the Knudsen number is determined as $\mathrm{Kn} = (m/2kT)^{1/2}\eta/pR = (2/\sqrt{\pi})\, l/R$.

Each coefficient of the Onsager matrix contains a number of terms over the powers of Kn to the terms quadratic by the Knudsen number being included (we recall that $\eta \sim \mathrm{Kn}$ and $\lambda \sim \mathrm{Kn}$). Most obvious is the structure of the coefficient Λ_{mm}. In this case, the parabolic profile gives the term $(-R^2/8\eta)\nabla_z p$ and slip effects related to the first and second derivatives of the hydrodynamic velocity (viscous slip of the first and second order, respectively) make contribution of the order of Kn and Kn^2.

Moreover, there is contribution to z caused by distortions of the profile of gas flow velocity in the Knudsen layer and specified by the terms of the order of Kn^2 and Kn^3.

For the heat flux caused by the temperature gradient, the contribution of the Knudsen layer amounts to a value of the order of Kn relative to the bulk term corresponding to heat transfer via an ordinary mechanism of heat conduction.

A curious situation is realized in the case of cross phenomena, i.e., mass transfer due to the temperature gradient and isothermal heat transfer under the effect of the pressure gradient. As would be expected the Onsager relations ($\Lambda_{mq} = \Lambda_{qm}$) hold. However, the nature of some contributions to each of these coefficients turns to be different. So, in the first order over the Knudsen number in the expression for $\langle u_z \rangle$ the main term is that related to the coefficient $\sigma_T = 0.75\,(1 + 0.5\kappa)$ that describes thermal slip. The correction to this term of the order of Kn is determined by the distortion in the boundary layer of the velocity profile. As for the isothermal heat flux, fulfillment of the Onsager relations in the first order over the Knudsen number is provided by the account of two terms, namely, the bulk (Burnett) flow $\sim (2/5)\,(\lambda T \nabla_z p/p)$ and the Knudsen heat flux that makes contribution of the same order as the bulk term. The next over the order of Kn term is generated by distortion in the Knudsen layer of the isothermal bulk heat flux that is uniform over the cross section.

General expressions for the coefficients Λ_{ik} in the plane and cylindrical channels in the case of a gas mixture have a rather complex form [113, 115]. As a simpler example we present the expressions for the coefficients Λ_{11}, Λ_{1m}, and Λ_{1q} in the case of mixture with a small relative difference of masses and effective diameters of molecules of the components calculated for the model of molecules–solid spheres [115]

$$\Lambda_{11} = \frac{T}{p y_1 y_2}[D_{12}]_2 (1 - 0.652 Kn),$$

$$\Lambda_{1m} = \frac{T}{p}[D_{12}]_2 \left[(1.274 - 1.235 Kn)\frac{m_2 - m_1}{m_2 + m_1} - (0.598 - 1.712 Kn)\frac{d_2 - d_1}{d_2 + d_1} \right],$$

$$\Lambda_{1q} = -T[D_{12}]_2 \left[(0.890 - 1.111 Kn)\frac{m_2 - m_1}{m_2 + m_1} + (0.339 - 0.309 Kn)\frac{d_2 - d_1}{d_2 + d_1} \right]. \qquad (6.24)$$

In solving the problem of gas flow in capillaries at small Knudsen numbers by the methods of nonequilibrium thermodynamics, along with the integral equations of transfer (3.8) and (3.11) we can introduce the so-called local equations for the kinetic coefficients of which the eigen relations of the Onsager symmetry hold [63, 117–120]. These relations also include fluxes (6.21) and asymptotic velocities of gas slip on the channel walls.

Total entropy production in gas flow in a capillary is given by expression (3.6) We now consider that part of entropy production which is determined by the bulk distribution function

$$\Delta S_b = -k\,[\Phi_b\,,\ L\,(\Phi_b)]\,, \tag{6.25}$$

where Φ_{b_α} are the bulk (or asymptotic) Chapman–Enskog solutions for a nonequilibrium multicomponent mixture [82].

Using the known solutions for Φ_{b_α} [82, 120] we find the bulk entropy production that is averaged over the cross section of a cylindrical capillary

$$\begin{aligned} <\Delta S_b> = -<J'^{b}_{qz}>\frac{\nabla_z T}{T_0^2} - <u_{bz}>\frac{\nabla_z p}{T_0} \\ -\frac{p_0}{T_0}\sum_{\beta=1}^{N-1}(<w^{b}_{\beta z}> - <w^{b}_{Nz}>)d_{\beta z} - \frac{k}{R}[v_z, \Phi_b^2(R)], \end{aligned} \tag{6.26}$$

where the bulk components of the corresponding fluxes and velocities are labeled by the index b (this is, for example, expression (6.1) for a mass-averaged gas velocity).

Subtracting the entropy production $\langle \Delta S_b \rangle$ from (3.6), we obtain the so-called boundary entropy production

$$\begin{aligned} \Delta S_\Sigma = -\left(j_q - \frac{5}{2}kT\sum_\alpha j_{w\alpha}\right)\frac{\nabla_z T}{T_0^2} - j_m\frac{\nabla_z p}{\rho T_0} \\ -\frac{p_0}{T_0}\sum_{\beta=1}^{N-1}\left(\frac{j_{w\beta}}{n_\beta} - \frac{j_{wN}}{n_N}\right) d_{\beta z} + \frac{k}{R}[v_r, \Phi_b^2(R)], \end{aligned} \tag{6.27}$$

where the boundary fluxes are determined by expressions (6.21).

The last term in (6.27) can be calculated using the bulk distribution function [120]. As a result, for a cylindrical capillary we have [120]

$$\begin{aligned} \frac{k}{R}[v_r, \Phi_b^2(R)] = -\frac{2}{r}ku'_h(R) \\ \times\left[\frac{\eta}{kT_0}u_h(R) + a_B\frac{\nabla_z T}{T_0} + c_B\frac{\nabla_z p}{\eta} + \sum_\alpha n b_\alpha d_{\alpha z}\right], \end{aligned} \tag{6.28}$$

where

$$c_B = -[v_r^2 v_z^2 \Phi_p,\ \Phi_b],$$

$$a_B = -[v_r^2 v_z^2 \Phi_p,\ \Phi_t].$$

Here Φ_p is the Chapman–Enskog solution for the gas mixture viscosity.

The system of phenomenological equations corresponding to the entropy production ΔS_Σ with account for (6.28) can be written in the form

$$\begin{aligned}
&\frac{2}{R}k\left[\frac{\eta}{kT_0}u_h(R) - a_B\frac{\nabla_z T}{T_0} - c_B\frac{\nabla_z p}{\eta} - \sum_\alpha n b_\alpha d_{\alpha z}\right] \\
&= \tilde{\Lambda}_{00}u_h'(R) + \sum_{\beta=1}^{N-1}\tilde{\Lambda}_{0\beta}d_{\beta z} + \tilde{\Lambda}_{0N}\frac{\nabla_z T}{T_0^2} + \tilde{\Lambda}_{0,N+1}\frac{\nabla_z p}{T_0}, \\
nk\left(\frac{j_{w\alpha}}{n_\alpha} - \frac{j_{wN}}{n_N}\right) &= \tilde{\Lambda}_{\alpha 0}u_h'(R) - \sum_{\beta=1}^{N-1}\tilde{\Lambda}_{\alpha\beta}d_{\beta z} + \tilde{\Lambda}_{\alpha N}\frac{\nabla_z T}{T_0^2} + \tilde{\Lambda}_{\alpha,N+1}\frac{\nabla_z p}{T_0}, \\
j_q - \frac{5}{2}kT\sum_\alpha j_{w\alpha} &= \tilde{\Lambda}_{N0}u_h'(R) - \sum_{\beta=1}^{N-1}\tilde{\Lambda}_{N\beta}d_{\beta z} + \tilde{\Lambda}_{NN}\frac{\nabla_z T}{T_0^2} + \tilde{\Lambda}_{N,N+1}\frac{\nabla_z p}{T_0}, \\
\frac{j_m}{\rho} &= \tilde{\Lambda}_{N+1,0}u_h'(R) - \sum_{\beta=1}^{N-1}\tilde{\Lambda}_{N+1,\beta}d_{\beta z} + \tilde{\Lambda}_{N+1,N}\frac{\nabla_z T}{T_0^2} + \tilde{\Lambda}_{N+1,N+1}\frac{\nabla_z p}{T_0}.
\end{aligned} \tag{6.29}$$

For small Knudsen numbers (Kn << 1) when the Knudsen part of the distribution function $f_{0_\alpha}\varphi_\alpha$ is localized in a thin boundary layer near the wall, the first equation of (6.29) describes the effects of viscous, diffusion, and thermal slip, and baroslip. The next three equations characterize diffusion and heat and mass transfer in boundary layers. In this case, Eqs. (6.29) supplement expressions for fluxes (3.8) and (3.11) servings as if the system of boundary conditions for multicomponent mixture flow in a channel.

At intermediate and large Knudsen numbers separation of system (6.29) has a formal character and its interpretation is difficult. In these regimes of mixture flow, system (6.29) indicates only the possibility of separation of certain parts, that are calculated by the Knudsen distribution function, from total fluxes (3.8) and (3.11).

In the case of a simple gas, the system of equations (6.29) has a simpler form

$$\frac{2}{R}k\left[\frac{\eta}{kT_0}u_h(R) - a_B\frac{\nabla_z T}{T_0} - c_B\frac{\nabla_z p}{\eta}\right]$$

$$= \tilde{\Lambda}_{00} u_h'(R) + \tilde{\Lambda}_{01} \frac{\nabla_z T}{T_0^2} + \tilde{\Lambda}_{0,2} \frac{\nabla_z p}{T_0},$$

$$j_q = \tilde{\Lambda}_{10} u_h'(R) + \tilde{\Lambda}_{11} \frac{\nabla_z T}{T_0^2} + \tilde{\Lambda}_{12} \frac{\nabla_z p}{T_0},$$

$$\frac{j_m}{\rho} = \tilde{\Lambda}_{20} u_h'(R) + \tilde{\Lambda}_{21} \frac{\nabla_z T}{T_0^2} + \tilde{\Lambda}_{22} \frac{\nabla_z p}{T_0}. \tag{6.30}$$

For the kinetic coefficients, in Eqs. (6.29) and (6.30) we can also establish the validity of the Onsager symmetry relations [115]. They were calculated in a number of works [63, 97, 116–119, 121]. Their values can also be obtained by subtracting the corresponding bulk contributions from the kinetic coefficients (6.24). These coefficients and the corresponding boundary conditions (6.29) play an important role in the problems of external rarefied gas flows past a body. For flows in capillaries and porous bodies they play and auxiliary role and allow one to give physical interpretation of different contributions into kinetic coefficients (6.24).

7. THE DUSTY-GAS MODEL

The dusty (or wall) gas model was developed in order to describe, on the unified basis, the flow and diffusion of a gas mixture in a porous body within the entire range of characteristic Knudsen numbers in the range from the free-molecular to viscous regime of flow. The model is based on a number of basic concepts [33, 42, 80]:

1) dust particles (porous medium) represent one of components of a gas mixture. They are motionless and are uniformly distributed in space, i.e., $u_d = 0$ and $\nabla_z n_d = 0$, where the subscript d refers to the dusty component;
2) in the presence of the pressure gradient in a gas some external force acts on dust particles ensuring their immobility;
3) diffusion and viscous motions in a gas mixture are independent, therefore

$$u_\alpha = u_\alpha^D + u_v, \tag{7.1}$$

where the viscous component of the flow velocity u_v does not cause relative motion of mixture components.

Condition 2) is the decisive one for the dusty-gas model. We can show [63] that a force necessary for keeping particles of species d at rest is equal to

$$n_d F_d = \nabla_z p \,. \tag{7.2}$$

Considering dust particles as molecules with a very large mass, we can use the known results of the kinetic theory for gas mixtures [38–40]. In this case, for the interdiffusion coefficient of particles of an ordinary gas and dust particles $D_{\alpha d}$ the expression that relates it with the Knudsen coefficient of diffusion under determination $D_{\alpha K}$ is introduced.

If the above-mentioned conditions along with a number of obvious assumptions [80] are met, then equation of diffusion (5.6), that has a form of the Stefan–Maxwell relations, takes the form

$$\frac{n_\alpha kT}{D_{\alpha K}}(u_\alpha - u_v) + \sum_{\beta=1}^{N} \frac{n_\alpha n_\beta kT}{n[D_{\alpha\beta}]_1}(u_\alpha - u_\beta) = -\nabla_z p_\alpha \,. \tag{7.3}$$

Here, for simplicity, external forces that can act on gas particles are disregarded. At the same time, the presence of force (7.2) leads to the fact that terms related to viscous transfer of momentum are cancelled in the equations.

Equations (7.3) describe transfer of gas mixture components in the reference frame where viscous transfer of gas as a whole is absent ($u_v = 0$). Actually, u_v is the velocity of viscous flow, averaged over the cross section, $\langle u_v \rangle$. For porous bodies [80]

$$\langle u_v \rangle = -\frac{B_0}{\eta} \nabla_z p \,, \tag{7.4}$$

where B_0 is some geometric characteristic (the Darcy constant) which is found empirically. In the case under consideration, $n_\alpha u_\alpha = n_\alpha \langle u_\alpha \rangle$ is also the flow of component α averaged over the cross section. It is necessary to somewhat modify the expression for the coefficient of diffusion in order to take into account the effect of the medium porosity ε and pore tortuosity q on it:

$$D_{\alpha\beta} = (\varepsilon / q)\,[D_{\alpha\beta}]_1 \,. \tag{7.5}$$

We note that equations similar to (7.3) were obtained first by Present and de Bethune [122] for a round cylindrical capillary by elementary considerations based on the method of momentum balance. In this case, $B_0 = R^2/8$, $D_{\alpha\beta} = [D_{\alpha\beta}]_1$, and $D_{\alpha K}$ is given by equality (4.6).

In the context of the method of momentum balance Eqs. (7.3) can be interpreted as follows: the first and second terms on the left-hand side of the equation are, respectively, mean variation of the momentum of molecules of component α during their collision with the capillary walls or a porous medium and during collision with molecules of other species. The Knudsen and diffusion "friction forces" related to these variations are counterbalanced together with the gradients of partial pressure of the components.

Equations (7.3) are written in the approximation that corresponds to the first Chapman–Cowling approximation without regard for thermodiffusion [39] or to the 10-moment approximation of the Grad method [40]. The expressions, which allow for thermal difusion and corrections of the second approximation, can be obtained from the equations of the 13-moment approximation of the Grad method. In the dusty-gas model this leads to the possibility of describing thermotranspiration and thermal diffusion in a porous medium. Here we omit consideration of these problems due to the complexity of the corresponding expressions (see [80]).

Equations (7.3) can be easily solved relative to molar fluxes of the components which gives the expression for $J_\alpha = n_\alpha \langle u_\alpha \rangle$. A useful relation for fluxes follows immediately from summation of Eqs. (7.3) over α, since the sum of the terms corresponding to diffusion forces of friction vanishes. The relation takes the form

$$\sum_{\alpha=1}^{N} \frac{J_\alpha}{D_{\alpha K}} = -\frac{1}{kT} \nabla_z p \left(1 + \frac{B_0}{\eta} p \sum_{\alpha=1}^{N} \frac{y_\alpha}{D_{\alpha K}} \right). \tag{7.6}$$

In the absence of the pressure gradient for a binary mixture it follows from this equation that

$$-\frac{J_1}{J_2} = \frac{D_{2K}}{D_{1K}} = \left(\frac{m_1}{m_2} \right)^{1/2} \frac{b_2}{b_1}, \tag{7.7}$$

which at $b_1 = b_2$ corresponds to the known Graham law of diffusion [80].

In the general case, instead of expressions for fluxes J_1 and J_2 it is more convenient to deal with the total molar fluxes of the mixture $J_m = J_1 + J_2$ and diffusion flow $J_{1D} = y_2 J_1 - y_1 J_2$. Then, by definition

$$J_1 = y_1 J_m + J_{1D}, \quad J_2 = y_2 J_m - J_{1D}. \tag{7.8}$$

The expressions for J_m and J_{1D} obtained as a result of solution of Eqs. (7.3) have the form

$$J_m = J_v - \frac{D_{1K}D_{2K}}{D_{12}^K}\nabla_z p + \frac{D_{1k} - D_{2K}}{D_{12}^K} J_{1D},$$

$$J_{1D} = -nD_{\text{eff}}\left[\nabla_z y_1 + \alpha_p^K y_1 y_2 \frac{1}{p}\nabla_z p\right], \tag{7.9}$$

where $J_v = n\langle u_v\rangle$ and D_{eff} is the ffective coefficient of diffusion, determined as

$$\frac{1}{D_{\text{eff}}} = \frac{1}{D_{12}^K} + \frac{1}{D_{12}}. \tag{7.10}$$

For the coefficients D_{12}^K and α_p^K formulas (4.9) hold.

Comparison of Eqs. (7.9) and (3.8) gives

$$\Lambda_{11} = \frac{T}{py_1y_2} D_{\text{eff}},$$

$$\Lambda_{1m} = \Lambda_{m1} = \frac{T}{p} D_{\text{eff}}\,\alpha_p^K,$$

$$\Lambda_{1D} = \frac{T}{p}\left[B\frac{0}{\eta}p + \frac{D_{1K}D_{2K}}{D_{12}^K} + (\alpha_p^K)^2 D_{\text{eff}} y_1 y_2\right]. \tag{7.11}$$

In the limit Kn >> 1 we have $J_v \to 0$, $D_{\text{eff}} \to D_{12}^K$, and expressions for Λ_{ik} coincide with those presented in (4.8). In the other limiting case (Kn << 1), the coefficient of diffusion D_{eff} tends to D_{12}, but α_p is not equal to α_p^v but coincides with the constant of barodiffusion in the Knudsen regime α_p^K. We note that in the considered dusty-gas model the barodiffusion factor remains the same within the entire range of variation of the Knudsen number. This is not unexpected since the viscous friction force is not a part of Eq. (7.3). In fact, this force acts differently on the components of a gas mixture in a viscous flow. Moreover, as follows from the results of the previous section, a value of the constant of barodiffusion (in lengthy channels of regular geometry) is also appreciably affected by the account of the behavior of the distribution function of molecules in a thin Knudsen layer near the wall.

We note that for a pure gas it follows from (7.6) that

$$J_m = -\frac{1}{kT}\left(D_K + \frac{B_0}{\eta}p\right)\nabla_z p\,. \tag{7.12}$$

The additivity of the diffusion (Knudsen and viscous flows is confirmed by measurements of the permeability of porous media [45, 123]; however, for capillaries, as is known there is an ill-defined minimum of permeability in the region close to the free-molecular regime of flow, which can be explained, taking into account correction of the second approximation of the theory [80].

It is easily seen that the term $D_{1K}D_{2K}/D_{12}^K$ in the expression for Λ_{mm} in the region of small Knudsen numbers can be interpreted as correction due to viscous slip. In the case of a capillary model of a porous medium, with account for (4.6) and (4.9) we have

$$\frac{D_{1K}D_{2K}}{D_{12}^K} = \frac{2}{8}\left(\frac{8kT}{\pi}\right)^{1/2} R\,\frac{1}{(m^{1/2})_y}\,,$$

and this correction is in full conformity with the coefficient of viscous slip A_p (6.9) obtained by the Maxwell method. The effective coefficient of diffusion D_{eff} in the expression for diffusion flux is written in the form which, for a mixture with close masses of molecules of the components, was first suggested by Bosanquet and Pollard and Present [124]. Applying in this case a value of the coefficient of binary diffusion $[D_{12}]_1$ to the model of hard spheres, we can present the expression for Λ_{11} in the region of small Knudsen numbers in the form

$$\Lambda_{11} = \frac{T}{py_1y_2}[D_{12}]_1\,(1 - 0.797\,\text{Kn})\,, \tag{7.13}$$

which is in satisfactory agreement with the behavior of Λ_{11} following from the strict kinetic theory for a round cylindrical capillary [see formula (6.24)].

We now refer to one of alternative models of a porous medium (binary friction model) which has been recently suggested by Kerkhof [43]. The idea of the model originates from the possibility (mentioned in [80]) of transformation of the equations of diffusion (7.3) such that the term responsible for viscous transfer was included in the terms describing diffusion of the components and thus the Stefan–Maxwell equations with the "generalized" coefficients of diffusion were obtained. To do this, Eq. (7.6) is solved relative to $\nabla_z p$ that is substituted into (7.3). In [43], it is suggested to

include the terms responsible for viscous transfer of momentum in each component of the mixture to the diffusion term along with the Knudsen coefficient of diffusion. As a result, the equations of diffusion in a porous medium for the considered model take the form

$$f_{\alpha K} n_\alpha u_\alpha + \sum_{\beta=1}^{N} \frac{n_\alpha n_\beta}{n\,[D_{\alpha\beta}]_1}(u_\alpha - u_\beta) = -\frac{1}{kT}\nabla_z p_\alpha\,, \tag{7.14}$$

where $f_{\alpha K}$ is the coefficient of "friction" of component α with the wall, that is determined as

$$f_{\alpha K}^{-1} = A_{\alpha K} = D_{\alpha K} + \frac{B_0 p}{\eta_\alpha} y_\alpha\,. \tag{7.15}$$

Here η_α is the partial viscosity of component α with $\eta = \Sigma\eta_\alpha$ being the total viscosity of the mixture.

It is easy to note that the expressions for fluxes of the components or fluxes J_m and $J_{\alpha D}$ obtained in these equations retain the previous structure of expressions (7.9) in which the viscous fluxes J_v must be omitted and the coefficients $D_{\alpha K}$ must be replaced by new coefficients $A_{\alpha K}$. For a pure gas, an ordinary expression for fluxes (7.12) follows from the suggested model. Of highest interest in this case is the expression for the diffusion fluxes in a binary mixture, which follows from (7.14)

$$J_{1D} = -A_{12\,\mathrm{eff}}\left[\nabla y_1 + \frac{A_{1K} - A_{2K}}{A_{12}^K} y_1 y_2 \frac{\nabla p}{p}\right]. \tag{7.16}$$

Here

$$A_{12}^K = A_{1K} y_1 + A_{2K} y_1\,,\quad A_{12\,\mathrm{eff}}^{-1} = (A_{12}^K)^{-1} + [D_{12}]_1^{-1}\,. \tag{7.17}$$

The most important result following from the considered model is the fact that in the region of small Knudsen numbers this model provides the limiting transition to the barodiffusion factor in a viscous flow α_p^v (5.9), and in the region of a free-molecular flow it leads to an ordinary Knudsen quantity α_p^K (4.9). As in the traditional dusty-gas model, the issue on the account of the effect of Knudsen layers at small Knudsen numbers remains open.

It should be noted however that behavior of the effective coefficient of diffusion at intermediate Knudsen numbers somewhat differs from that predicted by the Bosanquet and Pollard and Present formula (7.10). To estimate the observed dependence of D_{eff} on the Knudsen number we consider, as usually, the case of a mixture of molecules with close masses and cross sizes of scattering. For the model of molecules–hard spheres the corresponding estimates give

$$A^K = D_K (1 + 0.166\,\text{Kn}^{-1}), \quad \frac{D_{12}}{D_K} = 0.796\,\text{Kn}.$$

As a result

$$D_{\text{eff}} = \frac{D_{12}}{1 + 0.796\,\text{Kn}^2/(0.166 + \text{Kn})}.$$

Thus, only when $\text{Kn} >> 0.17$ the behavior of D_{eff} corresponds to ordinary results predicted by the dusty-gas model. On the contrary, when $\text{Kn} << 0.17$ we have $D_{\text{eff}} = D_{12}(1 - 4.8\,\text{Kn}^2)$ which gives a much quicker tendency of D_{eff} to D_{12}, since their difference decreases in proportion to the square of the Knudsen number, rather than the first power of this number, as follows from the ordinary theory and which is confirmed by more accurate calculations for capillaries [see formula (6.24)].

8. SOME KINETIC EFFECTS

Linear phenomenological relations for a total molar flux J_m, diffusion flux J_{1D}, and heat flux J_q, which follow from (3.8), in combination with the expressions for the coefficients Λ_{ij}, which were discussed in the previous sections, can serve as a basis for analysis of a number of kinetic effects in a gas mixture that arise in its flow and diffusion in a capillary or porous medium. To them, in particular, refer the Graham law of diffusion at a constant gas pressure [80] and the effects of time-variation of gas parameters (pressure, temperature, concentration of mixture components) in volumes connected by a packet of capillary tubes or porous medium, if at the initial instant of time there exists some fixed difference of values of one of these parameters at the inlet to and outlet from the channels. Mass flows arising in this case in capillaries or a porous medium due to the gradients of pressure, concentration, and temperature can, under certain conditions, compensate each other and lead to establishment of some dy-

namic equilibrium in the system, which is characterized by the difference in macroscopic parameters of the mixture in the volume. We consider some of these effects in more detail.

8.1 Cross Diffusion at Constant Pressure

One of classical experiments on gas diffusion in capillaries or porous media is in independent measurement of cross fluxes of the mixture components J_1 and J_2 at a constant pressure in the system, when the packet of capillaries and porous medium are washed from two sides by two different gases. The condition of the absence of the pressure gradient in the system means vanishing of the mass-aversged velocity of mixture u. In this case, an ordinary hydrodynamic approach leads to the relation

$$\frac{J_1}{J_2} = -\frac{m_2}{m_1}. \tag{8.1}$$

Among other things, in the experiments of Graham [80], which were conducted at the end of the previous century and which were confirmed in subsequent measurements made much later [125–128], the "square root" law was established which is valid for any flow regime in a channel — from the Knudsen regime to the viscous slip regime:

$$\frac{J_1}{J_2} = -\left(\frac{m_2}{m_1}\right)^{1/2}. \tag{8.2}$$

As has already been mentioned in the previous section, relation (8.2) obviously follows from the equations of the dusty-gas model if we assume diffuse scattering of molecules on the wall being absolutely completed. For an alternative Kerkhof model [43] this law is fulfilled in the region close to a free-molecular mode of regime flow, and in the other limiting region ($\mathrm{Kn} << 1$) it takes the form

$$\frac{J_1}{J_2} = -\frac{\eta_2}{\eta_1}\frac{y_1}{y_2}. \tag{8.3}$$

In the slip flow regime, the equations for total and diffusion fluxes through a capillary in the absence of the pressure gradient are written as

TABLE 2: Ratio of fluxes ($-J_1 / J_2$) for different mixtures

Mixture	Eq. (7.2)	Eq. (7.3)	Eq. (7.4)
H_2–Ar	4.469	6.0551	4.747
He–Ar	3.160	2.630	2.880
N_2–Ar	1.194	1.276	1.234
H_2–N_2	3.742	3.915	3.760
D_2–He	1.000	1.205	1.096
Ar–CO_2	1.049	0.875	0.958
N_2–C_2H_4	1.000	0.801	0.895
Ne–C_2H_4	1.178	0.719	0.923

$$J_m = -\sigma_{12} J_{1D}, \quad J_{1D} = -nD_{12}\nabla_z y_1 .$$

Then, allowing for (7.8) we obtain

$$\frac{J_1}{J_2} = -\frac{1 - y_1\sigma_{12}}{1 + y_2\sigma_{12}}. \tag{8.4}$$

When the elementary formula (6.10) is used for the coefficient of diffusion slip σ_{12}, the ordinary Graham law (8.2) follows from (8.4). In a more general case, the ratio of the diffusion fluxes depends not only on the ratio of masses of molecules but also on their effective cross sizes of scattering. Table 2 gives the values of the ratio of the flows ($-J_1 / J_2$) taken with the opposite sign and calculated by formulas (8.2)–(8.4) for pairs of gases which has been considered in Table 1. We note that the data of the last column in Table 2 are obtained using the coefficient $\sigma_{12} = -\alpha_p$ calculated by the variational method [formula (6.16)]. In this case, it was taken that $y_1 = y_2 = 0.5$ and $\kappa_1 = \kappa_2 = 1$.

The comparison with the experimental data of [125–128] made in [110] shows that there is a somewhat better agreement between the theory and experiment when the data from the third column of Table 2 are used. At the same time, for mixtures the molecules of which strongly differ by masses, with account for the available accuracy of flow measurements any theoretical expression is, in principle, admissible.

So, for example, for He–Ar mixture, results of different measurements give for the flow ratio the values of 3.18 [126] and 3.75 [128] which appeared to be more close

to the square root law. It is probably necessary to make more precise measurements of flux in order to draw a conclusion on the advantages of one or another theory. This note is of special importance for mixtures of molecules with close masses where the account of differences in the coefficients of accommodation of molecules on the channel wall becomes significant [110].

8.2 Diffusion Pressure Effect

This effect is observed in the system consisting of two closed volumes V_1 and V_2 connected by a packet of narrow capillaries or a porous medium. If at the initial instant of time the pressure at all points is the same and concentrations of the mixture components in volumes V_1 and V_2 differ (e.g., if at the initial instant the volumes are occupied by different gases), then the available difference in the velocity of diffusion of components in channels leads to appearance of the pressure difference between the volumes ("diffusion pressure effect"). The character of the dependence of Δp on time is determined by the ratio of diffusion and hydrodynamic flows through the connecting channels, and the difference of pressures attains a maximum, when the total molar flow of the mixture vanishes, i.e., when diffusion transfer is fully compensated by ordinary hydrodynamic transfer due to the pressure gradient. The theory of diffusion pressure effect was considered from different points of view in [106, 129–131], experimental measurements were conducted in [129, 130, 133].

The pressure difference and variation of the concentration of components in the volumes can be found from the consideration of the balance of the number of particles of each mixture component in the volumes with due regard for flows of components from one volume to another. In particular, the equation for determination of the pressure difference arising between the volumes takes the form

$$\frac{d}{dt}\Delta p = \frac{kT}{V} s J_m . \tag{8.5}$$

Here $V = V_1 V_2 (V_1 + V_2)$ and s is the total cross-sectional area of the connecting channels. To completely solve the problem, the flow must be expressed in terms of the differences of pressures and concentrations in the volumes and Eq. (8.5) must be supplemented by the equations for variation of concentrations which follow from the balance equations.

In the Knudsen regime (Kn >> 1), the times of relaxation for the difference of concentrations and pressure have the same order of magnitude, therefore $\Delta p(t)$ reaches a

maximum and then rather quickly decreases to zero. In this case, the expression for $\Delta p(t)$ is found from the balance condition for each component with account for the expressions for flows given by equalities (4.7). For a maximum pressure difference $\Delta p_{\max}$ between the volumes the corresponding result can be presented in the form

$$\frac{\Delta p_{\max}}{p_0} = (\Delta y_1)_0 \left[\exp\left(\frac{-\gamma \ln \gamma}{\gamma - 1}\right) - \exp\left(-\frac{\ln \gamma}{\gamma - 1}\right)\right], \tag{8.6}$$

where $(y_1)_0 = y_1(0) - y_1(L)$ and $\gamma = (m_2 b_1 / m_1 b_2)^{1/2}$ at the instant of time $t = 0$. Here it is assumed that $\kappa_1 = \kappa_2 = 1$.

In the other limiting region (Kn << 1), the values of concentrations in the volumes change much slower than the pressure; therefore, the established maximum difference of pressures decreases to zero very slowly. In this case, a good approximation for determining $\Delta p_{\max}$ is the use of the condition of vanishing of the total molar mixture flow under the assumption that the difference of concentrations in the volumes remains equal to its initial value. Thus, from the condition $\langle u_m \rangle = 0$ there follows the relation

$$\nabla_z p = -\frac{\Lambda_{m1}}{\Lambda_{mm}} p \nabla_z y_1 , \tag{8.7}$$

which, in the case of a round cylindrical capillary and without account for correction to viscous slip, can be rewritten as

$$dp = (8\eta / R^2)\, \sigma_{12} D_{12} dy_1 . \tag{8.8}$$

Integration of relation (8.8) along the channel length gives

$$\Delta p_{\max} = (8 D_{12} / R^2) \int_{y_1(0)}^{y_2(0)} \sigma_{12} \eta \, dy_1 . \tag{8.9}$$

For a gas mixture with $(m_2 - m_1)/(m_1 + m_2) << 1$ and $(d_2 - d_1)/(d_2 + d_1) << 1$ the use of equations (6.18a) leads to the result

$$\frac{\Delta p_{\max}}{p} = 4.8 Kn^2 \left(1.274 \frac{m_2 - m_1}{m_2 + m_1} - 0.598 \frac{d_2 - d_1}{d_2 + d_1}\right) \Delta y_1 , \tag{8.10}$$

TABLE 3: Coefficient of diffusion slip

Mixture	$-(\sigma_{12})_{exp}$ [111]	$-(\sigma_{12})_{eff}$	Mixture	$-(\sigma_{12})_{exp}$ [115]	$-(\sigma_{12})_{eff}$
H_2–N_2	1.10	1.21	H_2–N_2	1.08	1.23
N_2–Ar	0.21	0.21	N_2–Ar	0.25	0.21
N_2–CO_2	0.18	0.18	C_2H_4–Ne	0.033	0.031
N_2–O_2	0.082	0.091			
N_2–C_2H_4	0.04	0.10			
Ar–CO_2	0.026	0.030			

where $\Delta y_1 = y_1(0) - y_1(L)$.

It follows from (8.10) that diffusion pressure effect for such mixtures greatly depends not only on the difference of masses of molecules but also on the difference in the effective cross sizes of scattering (and also on the difference of the coefficients of accommodation of molecules on the wall) and can therefore have any sign.

To compare the theory with the experiment it is useful to introduce the effective coefficient of diffusion slip; thus

$$\Delta p_{max} = (8D_{12}/R^2)(\sigma_{12})_{eff}\,\eta dy_1, \tag{8.11}$$

whence it follows

$$\sigma_{12max} = \frac{\int_{y_1(0)}^{y_1(L)} \sigma_{12}\eta dy_1}{\bar{\eta}\Delta y_1},$$

where $\bar{\eta}$ is determined at $y_1 = y_2 = 0.6$.

Table 3, composed on the basis of the data from [110], gives the values of $(\sigma_{12})_{eff}$ calculated by the results of measurements [129, 133] in comparison with the theoretical values of $[\sigma_{12}]_2 = -[\alpha_p]_2$ calculated by the variational method [107] for fully diffuse scattering of molecules on the wall. In this case, only those results of measurements on the packet of capillaries of radius R are used, which correspond to

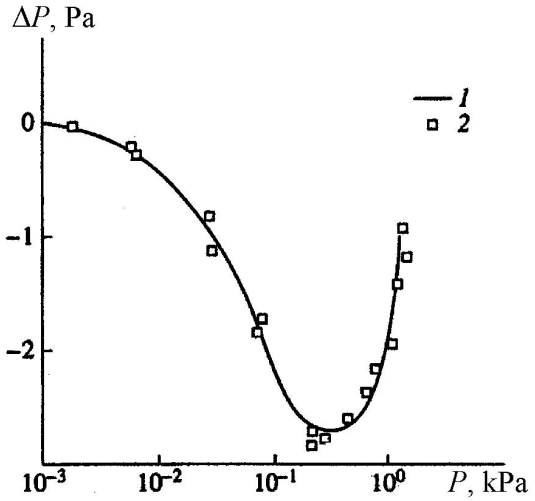

FIG. 1: Theoretical (1) and experimental (2) dependences of the diffusion pressure effect on total pressure for CO_2–Ar mixture

the region of small values of the Knudsen number. The minus sign for the coefficients of diffusion slip is stipulated by the fact that a lighter molecule in each considered pair of gases is taken as component 1. As is seen from the table, quite satisfactory agreement between the experimental and theoretical results is observed.

A thorough calculation of the diffusion pressure effect for a system consisting of equal volumes connected by a packet of capillaries has recently been conducted in [24] for the whole range of the Knudsen number on the basis of the linearized model of the third-order collision integral. The results of calculations show a satisfactory agreement with the data of experiments [133] for the mixtures H_2–N_2, Ar–CO_2, N_2–Ar, and Ne–C_2H_4 at arbitrary Knudsen numbers. Figures 1 and 2 present the results of calculations and experimental dependences for two pairs of gases for which an anomalous behavior of the diffusion pressure effect was observed in the experiments. Especially impressive is the explanation (obtained on the basis of the kinetic theory) of a sign of the effect for the Ar–CO_2 mixture, which is opposite to the ordinary one and change of the sign of the effect with variation of the Knudsen number for the Ne–C_2H_4 mixture. We note that for other systems which do not show anomalies the agreement between the theory and experiment is much better from the quantitative point of view: within the limit of experimental accuracy the theory reproduces the observed dependences.

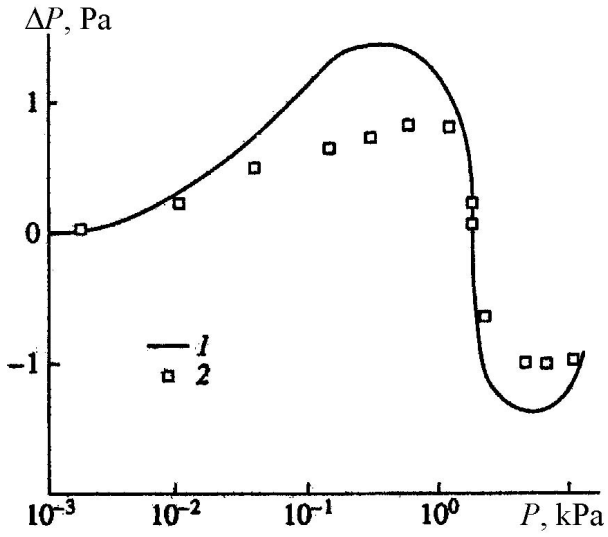

FIG. 2: Theoretical (1) and experimental (2) dependences of the diffusion pressure effect on total pressure for C_2H_4–Ne mixture

8.3 Separation of Gas Mixture

An effect, which in a certain sense is opposite to a previous one, is the appearance of the difference of concentrations in the volumes separated by a packet of capillaries or a porous medium, if a constant pressure gradient is maintained between the volumes ("effect of separation"). The existence of this effect forms the basis for the industrial diffusion method of separation of gas mixtures, which played an important role in solution of the problem of separation of uranium isotopes [134].

Specifying a value of the stationary difference of pressures at the ends of the channels $\Delta p = p(0) - p(L)$, we can, taking into consideration the condition $J_1 = J_m y_1(L)$, find the difference $\Delta y_1 = y_1(L) - y_1(0)$, which indicates the absence of the diffusion flux at the outlet from the channels. Using relation (3.12) we can write

$$J_m [y_1 (L) - y_1] = J_1 (1 - y_1) - J_2 y_1 . \tag{8.12}$$

As a result, with account for specific expressions for fluxes J_m and J_α we come to the linear differential equation for y_1 the solution of which allows one to find the

distribution of concentration along the channel length and, consequently, a value of the difference of concentrations Δy_1 [106, 130, 134].

In the Knudsen regime of flow, the solution has the form

$$\Delta y_1 = \alpha_p^K y_1(L)\, y_2(L)\, \frac{\Delta p}{p_0}, \tag{8.13}$$

where the Knudsen constant of barodiffusion α_p^K from (4.9) is determined by a value of $y_1(L)$ at the outlet from the channels.

In the limit of the viscous slip flow ($\mathrm{Kn} \ll 1$) for the case of mixture with $(m_2 - m_1)/(m_2 + m_1) \ll 1$ and $(d_2 - d_1)/(d_2 + d_1) \ll 1$, substitution of J_m and J_{1D} into (8.12) leads to the equation

$$\frac{dy_1}{dp} + ap\,[y_1 - y_1(L)] + \bar{\alpha}_p y_1(0)\, y_2(0)\, \frac{1}{p} = 0, \tag{8.14}$$

where $a = R^2/8\eta(pD_{12})$ and $\bar{\alpha}_p$ is given by expression (6.18).

Solution of such equation has the form [25]

$$\Delta y_1 = \bar{\alpha}_p y_1(0) y_2(0) \int_{p(L)}^{p(0)} \frac{1}{p} \exp\left[-\frac{a}{2}(p^2(0) - p^2 dp\right]. \tag{8.15}$$

If $\Delta p/p_0 \ll 1$ and $\kappa_1 = \kappa_2 = 1$, we approximately have

$$\Delta y_1 = 4.8 Kn^2 \left(1.247\frac{m_2 - m_1}{m_2 + m_1} - 0.598\frac{d_2 - d_1}{d_2 + d_1}\right)\left[1 - \exp\left(-\frac{0.208}{Kn^2}\frac{\Delta p}{p(0)}\right)\right]. \tag{8.16}$$

A review of some theoretical methods of analysis of the separation effect can be found in the paper of Masignone [134]. A comparatively small number of works [135–137] is devoted to experimental investigation of the separation effect. The change of sign in the separation effect was observed in the mixtures Ar–CO_2 and Ne–C_2H_4. For the ratio of masses of molecules close to unity the effect of mixture separation in the Knudsen regime of flow can be determined by the difference in the coefficient of accommodation of molecules on the wall. In the other limiting region, the experimentally observed negative effect is predicted by expression (8.16).

8.4 Thermomolecular Pressure Drop and Thermal Diffusion Mixture Separation

We now consider the effects arising in the case when a stationary fixed difference of temperatures $\Delta T = T(0) - T(L)$ is maintained between the volumes. In this case, the effect of thermomolecular pressure drop (TPD) for a pure gas is studied rather well [30]. The corresponding expressions for the pressure difference Δp arising between the volumes were obtained and analyzed both for the limiting cases of flows and at arbitrary Knudsen numbers. A review of the results on TPD for a pure gas can be found in [22].

In the case of a binary gas mixture, a stationary state is attained when both an averaged total molar flux of mixture and diffusion fluxes vanish. Then, using Eqs. (3.11), we find

$$\frac{\Delta p}{\Delta T} = -\frac{1}{T}\frac{\Lambda_{11}\Lambda_{mq} - \Lambda_{m1}\Lambda_{1q}}{\Lambda_{11}\Lambda_{mm} - \Lambda_{m1}\Lambda_{1m}}. \tag{8.17}$$

In the Knudsen regime, substitution of expressions for Λ_{ij} from (4.8) into (8.17) leads to the known result

$$\frac{\Delta p}{\Delta T} = \frac{1}{2}\frac{p}{T}, \tag{8.18}$$

which is obtained in the case of a pure gas. In the limit of small Knudsen numbers and for a gas mixture with $(m_2 - m_1)/(m_2 + m_1) << 1$ and $(d_2 - d_1)/(d_2 + d_1) << 1$, we have

$$\frac{\Delta p}{\Delta T} = 4.5\frac{p}{T}\mathrm{Kn}^2\frac{1 - 1.50\,\mathrm{Kn}}{1 + 4.03\,\mathrm{Kn}}. \tag{8.19}$$

The presence of the stationary temperature gradient in the channel also leads to the effect of thermal diffusion mixture separation. The arising difference of concentrations between the volumes $\Delta y_1 = y_1(0) - y_1(L)$ can be found in this case from the condition $J_{1D} = 0$ and relation (8.17) between Δp and ΔT. Then

$$\Delta y_1 = -\frac{1}{p}\left(\Lambda_{1q} + \frac{1}{2}\Lambda_{1m}p\right)\frac{1}{\Lambda_{11}}\frac{\Delta T}{T}. \tag{8.20}$$

It is interesting to note that $\Delta y_1 = 0$ in the Knudsen regime, although in the region of intermediate Knudsen numbers $\Delta y_1 \neq 0$. In particular, for $\mathrm{Kn} << 1$ we have

$$\Delta y_1 = -\left(\alpha_T + \frac{1}{2}\bar{\alpha}_p\right) y_1(0)\, y_2(0)\, \frac{\Delta T}{T} \tag{8.21}$$

and for a gas mixture with $(m_2 - m_1)/(m_2 + m_1) << 1$ and $(d_2 - d_1)/(d_2 + d_1) << 1$

$$\Delta y_1 = -\left(0.153\frac{m_2 - m_1}{m_2 + m_1} + -0.176\frac{d_2 - d_1}{d_2 + d_1}\right) y_1(0) y_2(0) \frac{\Delta T}{T} \ . \tag{8.22}$$

In the steady state, an ordinary effect of separation due to thermal diffusion in a mixture is partially compensated by an opposite effect related to barodiffusion. As a result, the total effect of separation decreases and in the Knudsen regime it even vanishes (to be continued).